APPLICATION OF NUCLEAR ANALYTICAL TECHNIQUES IN MANGANESE ORE EVALUATION

BY

ONOJAH, AUDU

A DISSERTATION SUBMITTED TO THE POSTGRADUATE SCHOOL
AHMADU BELLO UNIVERSITY ZARIA,
IN PARTIAL FULFILLMENT OF THE REQUIREMENTS FOR THE AWARD
OF THE DEGREE OF DOCTOR OF PHILOSOPHY IN PHYSICS

DEPARTMENT OF PHYSICS,
FACULTY OF SCIENCE,
AHMADU BELLO UNIVERSITY,
ZARIA, NIGERIA.

JANUARY, 1995.

DEDICATION

THIS THESIS IS DEDICATED TO MY

MOTHER

DECLARATION

I hereby declare that:

(i) the report presented in this Thesis is the result of my original research;
(ii) this thesis has not been submitted to any other institution, for any award other than Ahmadu Bello University Zaria;
(iii) all inclusions from works other than this have been duly referenced and acknowledged.

Onojah Audu

30th May 1995
Date

CERTIFICATION

This thesis entitled **APPLICATION OF NUCLEAR ANALYTICAL TECHNIQUES IN MANGANESE ORE EVALUATION** by A. Onojah, meets the regulation governing the award of the degree of Doctor of Philosophy in Physics of Ahmadu Bello University Zaria, and is approved for its contribution to knowledge and literary presentation.

Prof. S. B. Elegba
Chairman, Supervisory committee — Date: 10-06-95

Dr. I. M. Umar
Member Supervisory Committee — Date

Prof S. B. Ojo
Head, Department of Physics — Date: 04/03/96

Dean, Postgraduate School — Date: 24/3/96

ACKNOWLEDGEMENT

I wish to express my sincere gratitude to my major Supervisor Professor S. B. Elegba who suggested the topic of research, and the members of the supervisory Committee, Dr. I. M. Umar and Dr. I. I. Funtua for their vital contributions to the successful execution of this project.

I am grateful to many of the CERT workers especially, the Sectional Heads: Dr. L. A. Dim and Dr. B. W. Jimba and the other Senior workers: Dr M. O. A. Oladipo, Dr T. C. Akpa, Mr Kabiru Usman, Dr. T. Ige, Mr. A. Mustapha, Mr D. A. Yesufu, Mr D. Barak Dr G. I. Balogun and Mr. Y. Musa for their numerous contributions and assistances in the work.

I would like to express my gratitude to the Head of Department of Physics, Professor S. B. Ojo and the other senior members of the department especialy Dr I. B. Osazuwa and Dr. N. Hariharan for their encouragement and contributions to the success of the work.

My thanks also go to Professor H. A. Das of the Netherlands Energy Research Foundation for the extensive discussions and interest in the neutron irradiation set-up at CERT during the IAEA expert mission here.

My gratitude goes to the University of Agriculture Makurdi for the study leave and the financial support granted me during the period of the work.

ABSTRACT

A paraffin thermal neutron irradiating unit has been designed to provide reproducible geometry and handle large samples. The system, cast from commercial paraffin, has six large irradiation holes that can take up to 63 grams of powdered rock samples (average density=l.8g/cm^3) each and central hole for a 5Ci ^{241}Am-Be source. Using neutron activation analysis, the unit was characterized and on the basis of the neutron flux, detection limits measured, the system was found useful for routine non destructive determination of Mn, Al, As, V, W, Mo, I, Br, and Na at concentration above 2% by weight or at their ore levels.

As a typical application, manganese ores from North Western Nigeria were analyzed by instrumental neutron activation analysis and the results compared and complimented with an established X-ray fluorescence analysis technique. The two results agreed fairly well. Some of the manganese ores analyzed have shown considerable level of Mn concentration, up to 45% by weight.

For a complete evaluation of these Mn ores, XRD was used to determine the mineralogy. This analysis has confirmed most of the Mn minerals identified by other workers in some of the of the localities and has resulted in the determination of pyrolusite for the first time in the Nigerian deposit.

TABLE OF CONTENTS

Contents		page
Title		i
Dedication		ii
Declaration		iii
Certification		iv
Acknowledgement		v
Abstract		vi
Table Of Contents		vii
List of Tables		xi
List of Figures		xiii
List of Plates		xvi
List of Appendices		xvii
Abbreviations		xviii
	CHAPTER ONE	
1	INTRODUCTION	1
	CHAPTER TWO	
2	THEORETICAL ASPECTS	7
2.1	NEUTRON ACTIVATION ANALYSIS (NAA)	7
2.1.1	Introduction	7
2.1.2	Neutron Sources	9
2.1.3	Am-Be Neutron Source	10
2.1.4	Neutron Moderation	11
2.1.5	Thermal Neutrons	15
2.1.6	Principle of NAA	16

2.1.6.1	Activation and Decay	16
2.1.6.2	Gamma Ray interaction with Matter	20
2.1.7	Photoelectric Absorption	20
2.1.8	Compton Scattering	22
2.1.9	Pair Production	23
2.2	**X-RAY FLUORESCENCE ANALYSIS (XRF)**	26
2.2.1	Introduction	26
2.2.2	Principle	27
2.2.3	Semiconductor Detectors in XRF	30
2.2.4	Radioisotope in XRF	31
2.2.5	Matrix Absorption in X-Ray Analysis	32
2.3	**X-RAY DIFFRACTION ANALYSIS (XRD)**	35
2.3.1	Introduction	35
2.3.2	Principle	37

CHAPTER THREE

3.0	**MANGANESE OCCURRENCES, CLASSIFICATION AND SAMPLE COLLECTION**	41
3.1	Geology of N. W. Nigeria	41
3.2	Classification of Mn Ores and Minerals	45
3.3	Field Work and Sample Collection	47

CHAPTER FOUR

MATERIALS AND METHODS

4.1	**Neutron Activation Analysis**	48
4.1.1	The Design of the Paraffin Moderator	48
4.1.2	Safety Consideration	51
4.1.3	Preparation of Standards for NAA	54

4.1.3.1	Standards for Mn Minerals	54
4.1.3.2	Standards for Al, As, W, V, Mo, Br, I, and Na	55
4.1.4	Irradiation	56
4.1.5	Gamma ray Spectroscopy	59
4.1.6	Measurements	63
4.1.7	Detection Limits	65
4.1.8	Mn Concentration in the Ores	66
4.1.9	Precision and Accuracy of NAA	68
4.2	**X Ray Fluorescence Analysis**	70
4.2.1	Instrumentation	70
4.2.2	Measurements	71
4.2.3	Precision and Accuracy for XRF	73
4.3	**X Ray Diffraction Analysis**	73
4.3.1	Instrumentation	73
4.3.2	Sample Preparation for XRD	76
4.3.3	Measurements	77
4.3.4	Interpretation	77

CHAPTER SIX

5.0	**RESULTS AND DISCUSSION**	79
5.1	Thermal and Epithermal Flux Measurement	79
5.2	Detection limits for Al, V, Mo, Mn, As Br, Mo, I, and W	86
5.3	Mn Ore Samples Concentration by NAA	86
5.4	XRF Measurements	100
5.5	Results for the XRD	111

CHAPTER SIX

6.0	**CONCLUSION AND RECOMMENDATIONS**	**113**
6.1	Conclusion	113
6.2	Recommendations	114
	REFERENCES	116
	APPENDICES	123

LIST OF TABLES

4.1	Nuclear Data of 10 Elements of High Thermal Neutron Cross Section.	60
5.1	Thermal/Epithermal Flux for the Six Irradiation Positions	79
5.2	The Directional Dependence of the Count Rates in the Irradiation Position 3	82
5.3	The Flux Values at Different Heights of Irradiation (position 3)	82
5.4	Detection Limits for Nine Elements	87
5.5	Count Rates/Mn Concentration at the Six Positions of Irradiation (Powder)	90
5.6	Count Rates/Mn Concentration at the Six Positions of Irradiation (15Ml $KMnO_4$ Solution)	90
5.7	Count Rates/Mn Concentration at all Positions Counted Together (Powder-$KMno_4$)	91
5.8	Count Rates/ Mn Concentration at all Positions Counted Together	91
5.9	The Concentration of Mn in the Rock Samples	96
5.10	Mn K_α Intensity and Compton Peak	

	Ratio	101
5.11	Fe K_β Intensity and Peak Intensity Ratio	101
5.12	Ca K_α Intensity and Compton Peak Ratio	102
5.13	Si K_α Intensity and Peak Intensity Ratio	102
5.14	The Evaluation of the Effect of Mn in 12.1% Fe	102
5.15	Evaluation of Peak Intensities and Peak Intensity Ratios for the Ores	107
5.16	Mn, Fe, Si, and Ca Concentration in Mn Ores by XRF.	108
5.17	Equivalent Oxides in the Ores	109
5.18	Comparison of NAA and XRF Results of Mn Concentration for the Ores Samples	111
5.19	The Distribution of the Minerals with Localities of Mn Occurrences	112

LIST OF FIGURES

2.1	Am-Be Spectrum (Vijaya and Kumar, 1973)	12
2.2	Differential Compton Scattering Cross Section as Function of Scattering Angle	25
2.3	Attenuation Coefficients in NaI.	25
2.4	Attenuation Processes and the Analytical Applications	27
2.5	Diffraction Cone Formation in Powder Method	39
3.1	Geographical and Geological Setting of Mn Occurrences (Mucke and Okujeni, 1984)	43
3.2	Geological Map and Section of Mn Occurrence at Tudun Kudu (Monome *et al.*,1982)	43
3.3	Typical Mn Minerals and their Environments (Chapman, 1985)	46
4.1	Illustration of the NAA Irradiation Set-up	53
4.2	Arrangement for Foil Activation	58
4.3	The Cadmium Box used for Epithermal Activation.	58
4.4	NAA Counting Set-up at CERT	61

4.5	XRF Set-up at CERT	70
5.1	Thermal/Epithermal Activity Versus Position of Irradiation with Indium Foil.	81
5.2	Directional Dependence of Activity at Position 3 with Indium Foil in Open-Cd Box	81
5.3	Height Dependence of Activity in I rradiation Position 3	84
5.4	Calibration Curves for W, Br, V, I, Na, As, Mo, and Al.	88
5.5	Mn Calibration Curves for the Six Irradiation Positions (Powder-$KMnO_4$)	92
5.6	Mn Calibration Curves for the Six Irradiation Positions (15ml $KMnO_4$-Solution)	93
5.7	Comparison of Calibration Curves for Mn at the Six Irradiation Positions	94
5.8	Calibration Curves for Mn at all Six Positions Counted Together (100g powder)	95
5.9	Calibration Curves for Mn at all Six Positions Counted Together (90ml $KMnO_4$ Solution)	95

5.10	XRF Calibration Curves for Mn, Fe, Si, and Ca	104
5.11	Variation of Peak Intensity and Peak Intensity Ratios with Concentration of Mn with Concentration of Mn, Ca, Si, and Fe	105
5.12	Effect of Mn on 12.1 (Wt %) Fe	106
5.13	Comparison of Peak Ratios for Mn Standard and Mn Ores	106
5.14	The Plot of MnO_2 Versus Fe_2O_3 in the ore Samples	110
5.15	The Plot of MnO_2 Versus SiO_2 in Ore Samples	110
5.16	Relation between MnO_2 and Fe_2O_3 + SiO_2 in the Ore Samples	110

LIST OF PLATES

4.1	Photographs of the NAA Irradiation Set-up.	52
4.2	Photographs of the Philips Diffractometer	75

LIST OF APPENDICES

1.	Efficiency Calculation for the 7.6 by 7.6cm NaI(Tl) Detector	123
2.	Calculation of the Detection Limits	125
3.	Neutron Flux Calculation	126
4.	Calculation of the Errors in the Measured Mn Concentration	127
5.	The Calculated Flux at 25cm from the Neutron Source in Paraffin	129
6.	XRD Diffractograms	130
7.	Typical Outputs from the NaI(Tl) Counting Set-up	140
8.	The Manufacturer s specifications for the 5Ci Am-Be Neutron Source	142

ABBREVIATIONS

ACA	American Crystallographic Association.
ACS	American Chemical Society.
ASTM	American Society for Testing and Materials.
CERT	Centre for Energy, Research and Training, Zaria.
FWHM	Full Width at Half Maximum.
IAEA	International Atomic Energy Agency.
IISI	International Iron and Steel Institute.
MCA	Multichannel Analyzer.
NAA	Neutron Activation Analysis.
PCA	Personal Computer Analyzer.
PHA	Pulse Height Analysis.
SCA	Single Channel Analyzer.
XRD	X-Ray Diffraction.
XRF	X-Ray Fluorescence

CHAPTER ONE

INTRODUCTION

Manganese (Mn), the element number 25, is the twelfth commonest element in the earth crust, with crustal abundance of about 1000ppm (0.1%) (Chapman, 1985). Mn isotopes include ^{51}Mn, ^{52}Mn, ^{54}Mn, ^{55}Mn, and ^{56}Mn, but ^{55}Mn is the only stable one. It can exist in several valency states but natural occurrences are chiefly in the divalent and tetravalent forms. The most common natural sources of Mn are the minerals pyrolusite and psilomelane.

The Mn resources of the world are dominated overwhelmingly by South Africa,the bulk of whose reserves is in the Kalahari field. The reserve in this field is estimated to be 3285 x 10^6 metric tones. The next largest reserves are found in the former Soviet Union (USSR) whose reserve is estimated to be 147 x 10^6 metric tonnes (De Young *et al.*, 1984). Other countries that have substantial reserves includes Australia, Brazil, China, Mexico, Ghana, India and Hungary.

Mn is virtually never incorporated in manufactured articles in a pure unalloyed state but it is indispensable in the production of steel as an alloy. More than 90% of the world's consumption of Mn is related directly to production of steel (Myhre, 1985). In molten steel, it can act as a scavenger for oxygen and sulphur, thus eliminating the principal causes of embrittlement. In certain steel it is

used as an alloying element to improve the strength, toughness and heat treating characteristics of structural and engineering steel. At low temperature Mn improves the ductility of iron, its effect is to redistribute grain-boundary carbides to the intragranular sites and to spheroidize embrittling grain boundary sulfides (Allen *et al.*,1953). Complex ferro-manganese containing elements like Ce, Ti,and Ni are used to increase plasticity, impact toughness, and wear resistance of an alloy steel (Svidunovich *et al.*, 1987). High Mn (12-23 wt%) steel are used to achieve desirable properties of melt flowabilty, impact abrasion resistance (Tichonovic *et al.*, 1987), corrosion-resistance (Huang, 1987) and cold toughness, fatique srtrength (Kisutsyn, 1987).

The usage of Mn in the steel industry is extensive. For example, in 1982, the Mn ore exports of alloy grade ore for every ton of steel produced by member countries of the International Iron and Steel Institute (IIST) amounted to 13.5Kg/t (Robert-Tissot, 1985).

The Mn ores that are used by the steel industry can be separated broadly into two types. The lower grade (30-35% MnO_2) ore are used to add small quantities of Mn in the production of pig iron. The high grade ore (35-50% MnO_2) is used in Mn containing flux mixtures for converter steel making (Myhre, 1985)

The bulk of Mn ore is used for the production of Mn alloys, the most important of which is ferromanganese. This alloy is produced in the blast or electric furnace, charged with MnO_2, C and Fe. Another important Mn alloy is the silicon Mn (65-70% Mn and 15-20% Si) (Robert-Tissot, 1985). These alloys are used in the ladle or in the final trimming of the Mn content in the carbon steel, stainless steel and alloy steels.

Another important use of Mn is in the aluminum (Al) industry. Al consumes about 53-57% of the electrolytically produced Mn (Robert-Tissot, 1985). This Mn produced as cathode flakes is alloyed (1.5% Mn) with Al mainly for manufacture of beverage cans, utensils, and building sheet. The metal may be added as flakes, in combination with Al as master alloys or briquettes or in the form of coarse powder that is injected into the molten Al with the aid of an inert carrier gas.

Other metallurgical uses of Mn are in the production of Mn bronzes, super alloys, bimetallic strips, powder metallurgy and as pure metal flux in welding electrodes. Mn metal powder in the core flux electrodes and coated welding rods ensures the correct weld metal composition when high quality welding electrodes are needed. Welding electrodes use about 7-8% electrolytic Mn produced.

Mn equally plays vital roles in the non-metallurgical industries as an efficient depolarizer in Lechlenche dry cell battery. It is widely used for decolourizing glass in the furnace and finds several uses in the Pharmaceuticals and chemicals. It is used as fertilizer for certain soils.

No real economic deposit of Mn had been found in Nigeria. This fact together with its industrial importance especially the critical role it plays in steel production may make the Nation's Steel Industries vulnerable to interruption of supply since it has to be obtained from restricted number of foreign countries.

The Exploration and Mining Division of the Nigerian National Steel Council could have perceived Mn as a strategic metal to have started the search for it in 1979 in the Oban Hills of Cross River State where its occurrence had been reported in the Annual Report of the Geological Survey of Nigeria; 1955-1956 (Moneme, *et al.*,1982). The Mn ores found in the Oban Hill were in the form of spessartite garnet, and of no commercial value. Interest later shifted to Northern Nigeria where Wright and McCurry (1970) reported the gondite type Mn mineralization. Field trials which covered over 500km^2 were conducted in 1980 around Zaria and Maska (Moneme *et al.*, 1982)

The main occurrences of the Mn mineralization are:

Tudun Kudu and Farin Ruwa in Kaduna State, Ruwan Dorawa and Maraba hills in Sokoto State. All these occurrences, on the basis of field observations, thin section and microscopic investigation by Mucke *et al.* (1984) are reportedly rich in spessartite/almandine quartz and secondary Mn minerals like cryptomelane, lithiophorite, pseudorutile etc.

The studies of these occurrences have mainly been done using conventional geological techniques (Wright and McCurry, 1970; Moneme *et al.*, 1982; Mucke *et al.*, 1984). The only occurrence whose elemental composition is available in the literature is the Tudun Kudu locality, where Moneme *et al.* 1982, determined the elemental concentration by X-ray Fluorescence analysis. The present work partly addresses the problem of inadequate data on the elemental composition of these occurrences by examining the use of three complementary analytical techniques: Neutron activation analysis (NAA), X-ray fluorescence (XRF) and X-ray diffraction (XRD).

This study was initiated with the following objectives:

(1) Optimization of an ^{241}Am-Be isotope source by way of its neutron spectrum moderation.

(2) Establishment of a thermal neutron activation analysis facility for routine analysis of Mn, Al, As, V, W, Mo, I, Br and Na,

(3) Measurement of the Mn concentration of the Nigerian Mn ore by thermal neutron activation analysis using the facility (2) and X-ray Fluorescence analytical techniques.

(4) Determination of the mineralogy of the Mn ore by X-ray diffraction analysis.

Many workers have determined Mn in its ore by using relatively low thermal neutron flux because of Mn high neutron capture cross section (13.6 barns). Some early works were by Naskidashvili *et al.* (1963), who determined Mn in ore using Po-Be source (source strength=$2x10^7$ n/s) in paraffin moderator with an accuracy equal to chemical analysis; Berres (1966), activated a large mass (38 grams) of Mn powdered rocks with a 7.3 Ci Po-Be neutron source and measured the Mn concentration to an accuracy meeting industrial requirements. Cardoso *et al.* (1976) determined Mn in pyrolusite, rhodonite and ore blend used in dry batteries using thermal neutron flux of 10^6n/s/cm^2 from ^{252}Cf.

CHAPTER TWO

2.0 THEORETICAL ASPECTS OF NAA, XRF AND XRD

2.1 Neutron Activation Analysis (NAA)

2.1.1 Introduction

NAA is a method of quantitative analysis in experimental nuclear spectroscopy first introduced by G.Von Havesy and H. Levy in 1936 (Op De Beek, 1986) four years after the discovery of neutron by Chadwick in 1932. It is a method of quantitative analysis in which a sample is exposed to a flux of ionizing particles, usually slow neutrons from a reactor or fast neutrons from an isotope source or neutron generator. The isotope of the element to be determined is thereby converted into a radioactive isotope of the same element if it is by slow neutron activation -(n,γ) reaction or radioactive isotope of a different element for fast neutron activation *i.e.*(n,p), or (n,α) reactions. The resulting radioactivity is assayed by usual counting methods. Quantitative determination is made by comparison with standard containing known amount of element(s) or by the method of absolute gamma measurement. The identity of the element(s) is established by determining energies corresponding to the photopeaks, and then comparing them against known standards and/or checking them with data tables.

Neutron activation using fast neutrons from a reactor or generator are less convectional and of considerably less

application than thermal neutron activation (Lyon, 1967). In order to obtain a flux of thermal neutrons in situations where a reactor is not available, accelerator or isotope sources must be used and the neutron thermalized by surrounding the same with a quantity of moderating material like water, graphite, paraffin and many hydrogenous materials. Neutron moderation was first reported by Fermi *et. al.* in 1932 (Feld, 1952). They observed that neutron induced radioactivity in Ag can be significantly increased by interposing between the source of fast neutrons and the silver detector a slab of paraffin.

The application of activation analysis using low isotopic neutron sources is restricted to a few elements of high thermal neutron cross section, high isotopic abundance, more efficient detecting system and preferably short half life of the product nuclide (Garg and Batra, 1986).

An isotopic neutron source (^{241}Am-Be) manufactured in China was used for this work. The source was supplied by the IAEA under a Technical Cooperation Project with CERT. The source strength, quoted on 18th February 1989 was 1.29×10^7 n/s and its half life 433yrs. At the time of this work (four years later) it was expected to have decayed to 99.3% of its initial specification value. A typical ^{241}Am-Be source produces a wide spectrum of neutron energy with most established peak at 4.3Mev (Lorch, 1973). The moderating system that was used to thermalize this source was cast from

commercial paraffin, obtained from the Kaduna Refinery and Petrochemical Company. Paraffin was chosen as the moderator because of the ease with which the material can be handled.

2.1.2 Neutron sources

Neutron fields cover a wide range of energies; cold or sub-thermal (0 - 0.005ev), thermal (0.005- 0.5ev) epithermal (0.5-1kev), intermediate (1kev- 100kev) and fast (>100kev). (Burger and Schwartz, 1988). These energy ranges are generally available through: Radioactive sources, Nuclear reactors and particle accelerators.

There are three categories of radiative neutron sources: (α,n) sources, employing one of the actinide isotope as an alpha emitter; (τ,n) sources, using a radioisotope as gamma ray emitter; and spontaneous fission sources.

A common source of neutron in the (α,n) category is a mixture of an alpha-emitting radiative nuclide with a light element such as lithium, beryllium, boron or fluorine. Only the lightest elements can be combined with the alpha emitting isotopes to make practical neutron sources since the energy of the alpha particles is sufficient only to penetrate the potential barriers of the light element.

The most commonly used neutron sources are: (^{210}Po-B),

(^{210}Po-Be), (^{139}Pu-Be), (^{241}Am-Be) and (^{226}Ra-Be). Of these, radium is the least desirable because of its gamma ray emission and the potential hazard from leakage of radon gas, this was very prevalent in the older sources (Suschny, 1968). ^{241}Am also emits significant amounts of gamma radiation, but at much lower energies and intensities than radium. ^{210}Po, because of its high specific activity, produces a large quantity of neutrons from a small size source but its half-life of only 140 days makes frequent replacement necessary.

2.1.3 Am-Be neutron source

The ^{241}Am is a widely used α-emitter in neutron sources; its main advantages over the other a-emitters are convenient half life (433yr) and simple decay correction because of the very long half life (2.2×10^6yr) of the daughter nucleus, ^{237}Np. ^{9}Be is the most common target material since it has the highest yield (Breen *et. al.*, 1965). In an isotopic neutron source with beryllium as the target material, neutrons are produced by the ^{9}Be (a,n) ^{12}C reaction or

$$^{9}_{4}\mathrm{Be} + {}^{4}_{2}\mathrm{He} \longrightarrow {}^{12}_{6}\mathrm{C} + {}^{1}_{0}\mathrm{n} \qquad 2.1$$

This reaction is exoergic (Jordan *et al.*, 1964) with Q value of 5.703Mev. In addition, the kinetic energy of the α-particle is on the average 5.47Mev for ^{241}Am. The total energy for this reaction is therefore, approximately 11Mev,

which appears as excitation and recoil energy of the C^{12} product nucleus and as kinetic energy of the emitted neutron. The τ-radiation associated with an isotopic neutron source originates from de-excitation of the product nucleus formed in the (α,n) reaction. Am-241 decays by emission of predominant 60kev τ-ray. The maximum yield for ^{241}Am-Be is 70 ± 2 neutrons per 10^6 alphas (Jordan *et al.*, 1964). A typical Am-Be has well established peaks at 3.3Mev, 4.3Mev, 5.0Mev (Thompson *et al.*, 1965). The spectral features are dependent on the source construction and especially on the particulate size of the AmO_2 and Be powder (Van DerZwan, 1968). The energy of neutrons produced depends on the angle of scatter and is quite spread out (Garg and Batra, 1986). In mixed sources there is a smearing of the alpha particle spectrum due to energy loss so that a large smearing in neutron energy results and also Doppler broadening amounts to as much as 2Mev spread (Leo, 1985). All these account for the wide spectrum of the ^{241}Am-Be source. A typical spectrum of an ^{241}Am-Be is shown in figure 2.1.

2.1.4 Neutron moderation

Neutrons lose energy through inelastic collisions with medium of heavy nuclei and through elastic collisions with light nuclei. If the capture cross section is small compared to the scattering cross section (as it is in the intermediate and fast neutron ranges for most materials, especially light elements), the neutrons continue to loose

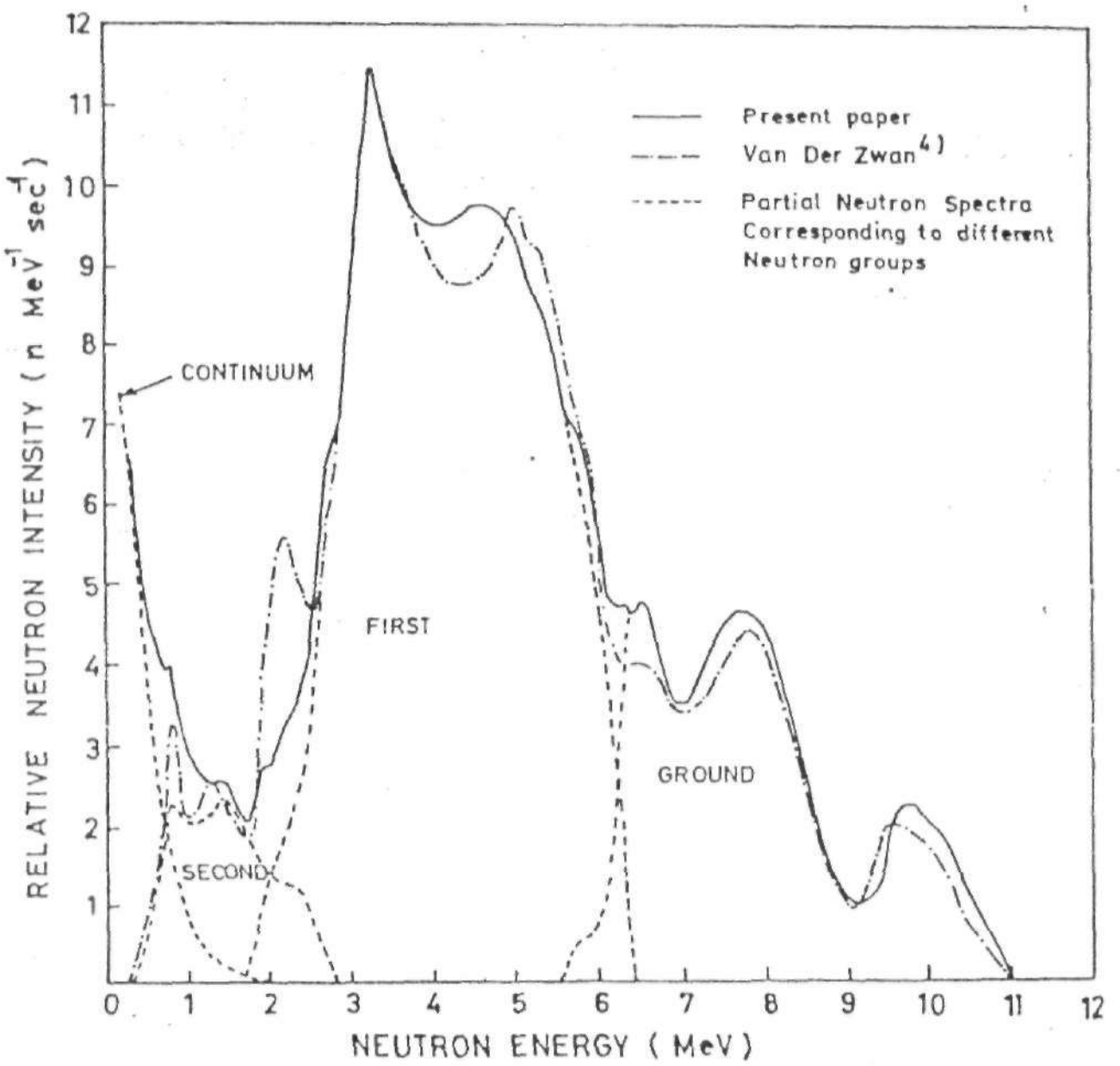


Fig 2.1 ^{241}Am-Be Spectrum (Vijaya and Kumar, 1973)

energy until their energy is comparable to the energy of the thermal agitation of the nuclei in the material. Under this condition, the neutrons are said to be thermallized.

In a moderating material, neutrons follow a complex trajectory during the slowing down process. The average number $\bar{n}$ of collisions needed to slow down the maximum number of neutrons from an initial energy E_o to a certain energy E is given (Mukhin, 1987) by:

$$\bar{n} = (1/\epsilon)\ln(E_o/ E) \qquad 2.2$$

$\ln(E_o/E)$ is called the lethargy of neutrons and $\epsilon = \ln(E_i/E_j)$ is the logarithmic loss of energy per collision. E_i and E_j are the neutron energies before and after collision. The spatial distribution of neutrons of energy E which have slowed down from a point source of energy E_o is of the form:

$$F(r) \quad \alpha \quad \exp(-r^2 /4t) \qquad 2.3$$

where t is referred to as Fermi Age and is the mean square distance a neutron migrates in slowing down from E_o to E. It is given by :

$$t = \int_E^{E_o} \frac{DdE}{E\epsilon\Sigma_s} \qquad 2.4$$

Where D is the diffusion coefficient and Σ_s is scattering cross section. ϵ is an important charateristic of a moderator, it is related to the mass number A by:

$$\epsilon = 1 + ((A-1)^2/2A)\ln((A-1)/(A+1)) \qquad 2.5$$

It can be seen that the higher the value of ϵ (lighter materials) the better the moderator. This is why hydrogen $_1H^1$ is the most efficient attenuator of fast neutrons (Amaldi, 1959). Its presence in a fast neutron moderation is therefore most desirable. The role of hydrogen in moderating material is to obtain high thermal neutrons densities with smaller quantities of the material for a given source strength. Another important nuclei for neutron thermalisation is carbon, it has a considerably smaller capture cross section than hydrogen, so that it is possible to obtain purer thermal neutron by making observations at greater distances from the fast neutron source.

The ideal moderator material should have a negligible neutron capture cross section throughout the significant energy range and a high neutron scattering cross section. It should have low mass in order to thermalize the neutrons in a minimum number of collisions. In addition, ready availability, cheapness, ease of handling, and freedom from toxicity or other undesirable characteristics. The most frequently used moderating media are water, paraffin or

graphite. Other useful but expensive moderators are:- heavy water, beryllium and beryllium oxide.

2.1.5 Thermal neutrons

When neutrons reach thermal equilibrium with the moderator, their energies are determined by the thermal energy distribution of the moderator atoms. The energy of neutrons in the thermal equilibrium is in many respect similar to that of the molecules of gas at the temperature of the medium, closely approximated by Maxwell distribution function: (Moteff, 1970).

$$n(v) = n_{th} 4\pi \left| m/2\pi kT \right|^{2/3} v^2 . \exp(-mv^2/2kT) \qquad 2.6$$

where T = the absolute temperature,

m = the mass of neutron,

k = Boltzmann constant,

v = the neutron velocity and

n_{th}= is the total neutron density given by

$$n_{th} = \int_0^\infty n(v)dv \qquad 2.7$$

The most probable velocity is given by :

$$V_p = \left[\frac{2kT}{m} \right]^{\frac{1}{2}} = 2200 m/s \text{ (at } 20.44^{\circ}C) \qquad 2.8$$

this is equivalent to E = kT = 1/40 eV or 0.0253eV.

To achieve Maxwell distribution, neutrons are emitted into the medium with the Maxwellan energy distribution and the absorption cross section obeys the 1/V law. A real

moderated spectrum is composed of slow down neutrons in thermal equilibrium with the medium. The spectrum is regarded as superposition of two components: the thermal energy range (0.005-0.5ev) and the epithermal range (0.5ev-1Kev)

2.1.6 Principle of NAA

NAA is based on three related processes:- radioisotope formation by activation, decay of this radioactive species and the interaction of radiation from decaying nuclei with matter. The first two are opposite reactions taking place: build up of radioisotope determined by cross section and neutron flux and its concurrent disintegration or decay as expressed by its half-life or its decay constant. The last is the basis of gamma ray spectroscopy.

Activation and decay. When a sample is exposed to a uniform flux of neutrons, the rate of growth of the isotope is the difference between the production rate, P and the decay rate given by:

$$dN/dt = P - XN \qquad 2.9$$

where X = the decay constant,

N = the number of exposed nuclei that are able to form radionuclide

If the nuclide is produced at a constant rate, then the solution to the equation 2.9 is

$$N(t) = P/X(1-e^{-Xt}) + N(o)e^{-Xt} \qquad 2.10$$

where N(o) is the radioactive atoms present at time t=0 and can be ignored for sample not radioactive at this instant.

The activity at any time is therefore

$$A(t) = XN(t) = P(1-e^{-Xt}) \qquad 2.11$$

At large t, the saturated activity A is attained

$$A = N.\Phi.\sigma \qquad 2.12$$

Φ is the neutron flux (neutrons/cm sec) and

σ is the activation cross section in barn/nucleus

N is also given as (Vose, 1980)

$$N = (m/M).E.(6.02x10^{23}) \qquad 2.13$$

m is mass of the element,

M is the atomic weight of the element,

E is the fractional abundance of the target isotope in the natural element and

$6.02x10^{23}$ is the Avogadro's constant.

by combining equations 2.11, 2.12, 2.13 the general equation for activity results.

$$A(t) \equiv \frac{m\Phi\sigma(6.02x1023)(1-e^{-Xt})E}{M} \qquad 2.14$$

This equation is useful in the determination of the amount of the element being determined if the direct method is being used and for calculating neutron flux when pure samples like Au and In foils are used. Generally this same mathematical expression with different values of nuclear constants and time parameter is used for activation problems, flux monitoring and radioisotope production in reactors and accelerators. The modified form of equation 2.14 used for thermal flux determination, (Droulers, 1970) is:

$$\Phi = \frac{M.F_{CD}.A(t)}{m\sigma.(6.02x10^{23})(1-e^{-Xt})e^{-Xtd}(1-e^{-Xtc})E} \qquad 2.15$$

Where t = irradiation time (seconds)

t_d = delay time (seconds)

t_c = Counting time (seconds)

F_{CD} = the Cadmium factor, defined in the following expression:

$$(A_{tot} - A_{epi}) = A_{tot}.(R_{CD}-1)/R_{CD} = A_{tot}F_{CD} \qquad 2.16$$

where A_{tot} = total activity without cadmium,

A_{epi} = the epicadmium activity,

R_{CD} is called the cadmium ratio:

$$R_{CD} = A_{tot}/A_{epi} \qquad 2.17$$

$$F_{CD} = (R_{CD}-1)/R_{CD} \qquad 2.18$$

If a sample is irradiated in a reactor or a moderated isotopic neutron source, the induced activity will be caused by both thermal and the epithermal neutrons. Cadmium cover is usually used to distinguish between these two as the absorption cross section for cadmium depends in such a way on neutron energy that at a certain thickness of cadmium (about 0.75mm) nearly all neutrons below a cut off energy E_{CD} (about 0.5eV) are absorbed, while nearly all neutrons above this energy pass the cadmium without appreciable capture (Zijp, 1970)

The flux measurement for epithermal neutrons is much more complicated than for thermal neutrons as the cross section varies inversely proportional to the neutron velocity and the presence of narrow peaks called resonance peaks, for example, the first resonance peak for indium is at (1.54ev) and for gold, it is at 4.8ev. The resonance integral cross sections are often insufficiently known and correction for shielding is much larger (Zijp, 1970). In the case of a single resonance peak, the cross section in the resonance region can be divided into two parts: the resonance contribution $\sigma_r(E)$ and a contribution $\sigma_{1/v}(E)$ due to absence of resonance or

$$\int_{E_{CD}}^{\infty} \sigma(E)dE/E = \int_{E_{CD}}^{\infty} \sigma_{1/v}(E)dE/E + \int_{E_{CD}}^{\infty} \sigma'(E)dE/E \qquad 2.19$$

$$\text{or} \qquad I = I_{1/v} + I' \qquad 2.20$$

I is called the resonance integral cross section. The calculated and measured values for $I_{1/v}$ and I' and the self absorption are usually given in nuclear data tables.

Gamma ray interaction with matter. The most relevant interaction processes of gamma ray with matter are absorption and scattering. If a gamma ray of incidence intensity I_o falls on a target of thickness d, the transmitted intensity I is given by:

$$I = I_o e^{-\mu d} \qquad 2.21$$

where μ is the total attenuation coefficient of the material, equivalent to the sum of the photoelectric absorption, the Compton scattering and pair production processes. (Mukhin, 1987). Gamma ray interacts with matter in several other ways but only these three processes are considered here.

2.1.7 PHOTOELECTRIC ABSORPTION

In the photoelectric absorption process, a gamma ray transfers its total energy to an atomic electron. As a

result the electron is ejected from the atom with kinetic energy T_E given by:

$$T_E = E_\gamma - I_i = h\nu - E_B \qquad 2.22$$

where E_γ = gamma ray energy,

I_i = ionization potential and

E_B = Binding energy of the electron

Subsequent filling of the electron vacancy in the absorber atom is accompanied by the emission of characteristic x-rays and auger electrons as a compensation for the binding energy of the captured electron. The auger electrons have an extremely short range due to their low energy. The x-ray may travel some distance (a millimeter or less) before being absorbed through photoelectric interaction with less tightly bound electrons. (Harsaw-Filtrol, 1984) Photoelectric effect is possible for bound electrons only (Leo, 1985). The weaker the bond between an electron and an atom in comparison with the photon energy, the less probable is the photoeffect. This explains the differences in probabilities of photoeffect for different electron shells, photoelectronic cross section dependence on charge of the medium and the dependence of cross section on energy.

The K-shell photoeffect cross section of a material of nuclear charge Z, for gamma radiation energy E_γ is:

$$\sigma_{phot} \quad \alpha \quad Z^5 / E_\gamma \qquad \text{for } E_\gamma >> I_K \qquad 2.23$$

and $\sigma_{phot} \quad \alpha \quad Z^5 / E^{7/2} \quad$ for $E_\gamma > I_k$ 2.24

where I_k is the ionization potential for the K-shell. This effect is the principal mechanism of absorption of long-wave gamma radiation in heavy materials. The ratio of photoeffect cross section for different shells K, L and M (Mulkin, 1987) are:

$$\sigma l / \sigma k \approx 1/5 \qquad 2.25$$

$$\sigma m / \sigma l \approx 1/4 \qquad 2.26$$

$$\sigma m / \sigma k \approx 1/20 \qquad 2.27$$

2.1.8 Compton scaterring

In this process, the γ-ray interacts with an electron in the absorbing material. The path of the incoming gamma ray is deflected through a scattering angle θ with respect to the original direction. The gamma ray transfers part of its energy to the electron, which is assumed to be initially at rest. The decreased energy $h\nu'$ of the scattered gamma ray photon is given (Bethe and Ashkin, 1952) by:-

$$h\nu' = \frac{h\nu}{1 + (h\nu/m_e c^2)(1-\cos\theta)}$$

$$= \frac{h\nu}{1 + (h\nu/0.511)(1-\cos\theta)} \quad \text{Mev} \qquad 2.28$$

Where 0.511Mev represents the electron rest energy.

The differential compton scattering cross section obtained by Klein and Nishina, and independently by Tamm (Mukhin 1987) is in the form :

$$d\sigma(\theta) = r_e^2 . \frac{1+\cos^2}{2} \frac{d\Omega}{(1+\epsilon(1-\cos\theta))^2} \left[1+ \frac{\epsilon^2(1-\cos\theta)^2}{(1+\cos^2\theta)(1+\epsilon(1-\cos\theta))} \right]$$

where $r_e = e^2/m_e c^2$, $\epsilon = h\nu/m_e c^2$ 2.29

The dependence of the differential compton scattering cross section on scattering angle is shown in figure 2.2 The total compton scattering cross section is obtained by integrating over all angles.

$$\sigma_{com} = 2\pi r_e^2 \left[\frac{1+\epsilon}{\epsilon^2} \left| \frac{2(1+\epsilon)}{1+2\epsilon} - \frac{1}{\epsilon} \ln(1+2\epsilon) \right| + \frac{1}{2\epsilon} \ln(1+2\epsilon) - \frac{1+3\epsilon}{(1+2\epsilon)^2} \right]$$

2.30

If the scattered photons escape the sensitive volume of the detector, then only the recoil energy of the atomic electron is measured. This measurement gives rise to a continuous energy spectrum from zero energy up to the compton edge at an energy given by (Harshaw-Filtrol 1984):-

$$h\nu - h\nu' = h\nu \left[\frac{1}{1+ 2h\nu/0.511} \right] (\text{Mev}) \qquad 2.31$$

2.1.9 Pair production.

For gamma ray having a very high energy, there exist a form of interaction of γ-quanta discovered by Dirac in 1928- the formation of electron-positron pairs (Bethe *et al.*,

1952). The pair production-process occurs in the coulombic field of an atomic nucleus in the absorbing material. The gamma ray energy must exceed 1.022Mev, twice the rest mass energy of an electron. After the pair production, annihilation of the positron and an electron in the absorbing medium follows once the positron is almost at rest. As a result, two annihilation gamma rays of energy 0.511Mev are emitted in the opposite direction. The cross section for pair formation in the field of nucleus is usually given for limited intervals for convenience (Mukhin 1987)

$$\sigma_{pair} = \frac{Z^2}{137} r_e^2 \left[\frac{28}{9} \ln\left|\frac{2E_\gamma}{M_e C^2}\right| - \frac{218}{27} \right] \qquad 2.32$$

for $M_e C^2 << E_\gamma << 137 M_e C^2 Z^{-1/3}$ and

$$\sigma_{pair} = \frac{Z^2}{137} r_e^2 \left[\frac{28}{9} \ln(187.Z^{-1/3}) - \frac{2}{27} \right] \qquad 2.33$$

for $E_\gamma >> 137 M_e C^2 Z^{-1/3}$.

Pair production dominates gamma ray attenuation above 7Mev in NaI(Ti) detectors (Nashaw Filtrol 1984). The relative importance of these processes as a function of incident gamma ray energy is shown in figure 2.3.

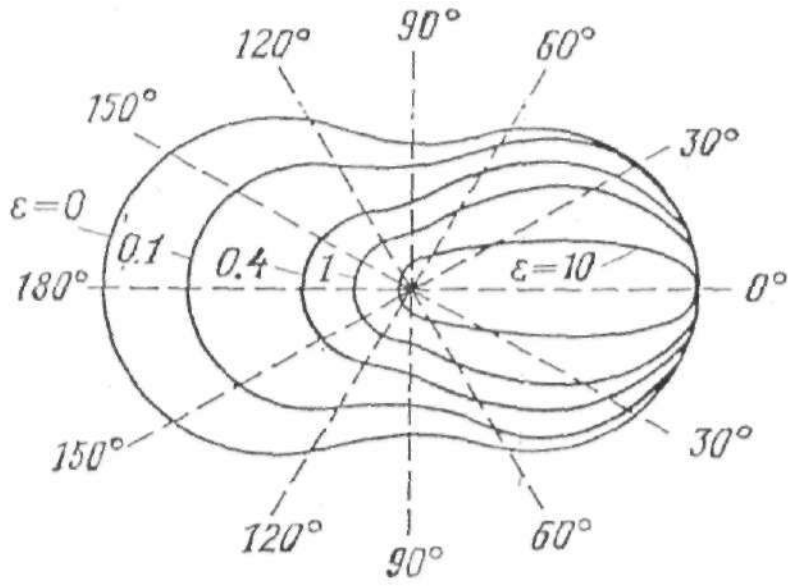


Fig 2.2 Differential Compton Scattering cross section as funtion of scattering angle

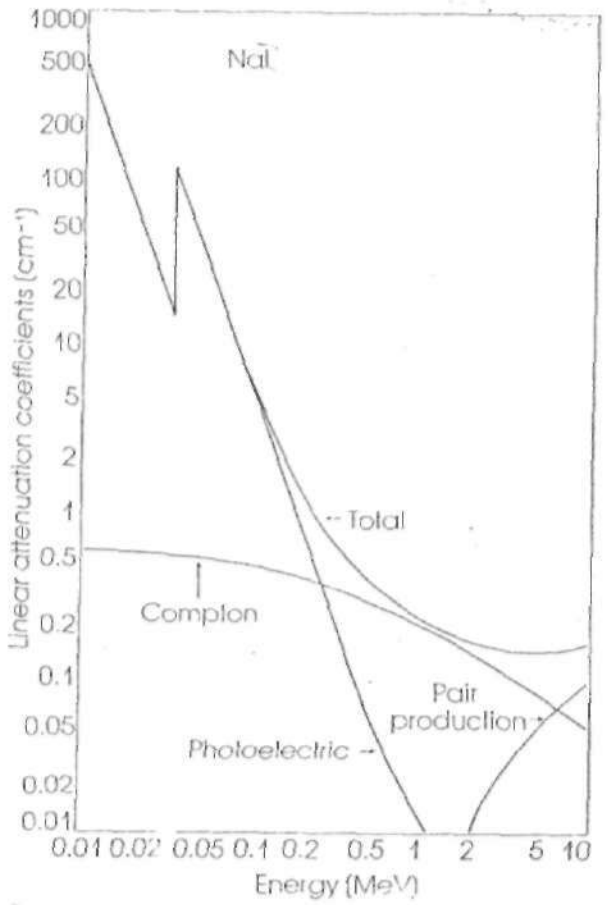


Fig 2.3 Attenuation coefficients in NaI

2.2 X-Ray Fluorescence Analysis (XRF)

2.2.1 Introduction

XRF is a relatively fast, non-destrictive, sensitive and versatile technique widely used for elemental analysis of solids, powders, slurries and liquids. There are two main types of x-ray quantitative analytical spectrometers:- the energy dispersive spectrometer and the wavelength dispersive spectrometer. Energy dispersive spectrometer use radioisotope sources or low power x-ray tubes to excite the characteristic x-ray of the elements in a sample and either absorption filters or detectors of adequate intrinsic energy resolution to isolate and measure the intensity of the x-ray of interest. They have the advantage over wavelength dispersive spectrometers mainly from their cost, and compact sizes.

In general, the energy dispersive analyzers consist of the excitation source (radioisotope or X-ray generator), a detector, and a counting unit which contains a high voltage power supply, amplifier, single or multichannel analyzer. The characteristic peaks are resolved from the spectrum by pulse height analysis. The commonly used sources are ^{55}Fe, ^{238}Pu, ^{241}Am, and ^{109}Cd. The applications of x-ray fluorescence analysis are varied and manifold, such as in geology, archaeology, biology, medicine chemistry, ecology, criminology and mining and metallurgy.

2.2.2 **PRINCIPLE**

An x-ray beam of intensity I_o is attenuated when it passes through an absorbing medium similar to γ-ray. The attenuation depends mainly on photoabsorption and scattering. Two forms of scattering are usually involved- coherent (Rayleigh scattering) with no change in energy and the incoherent (compton scattering) which results in the modification of the energy. The coherent scattering phenomenon, which maintains a definite relationship between the phase of the scattering beam and the incident beam is the basis of diffraction analysis. The important processes responsible for the attenuation of the primary beam and their main application in X-ray analysis is shown (figure 2.4). The Compton scattering which is regarded as scattering

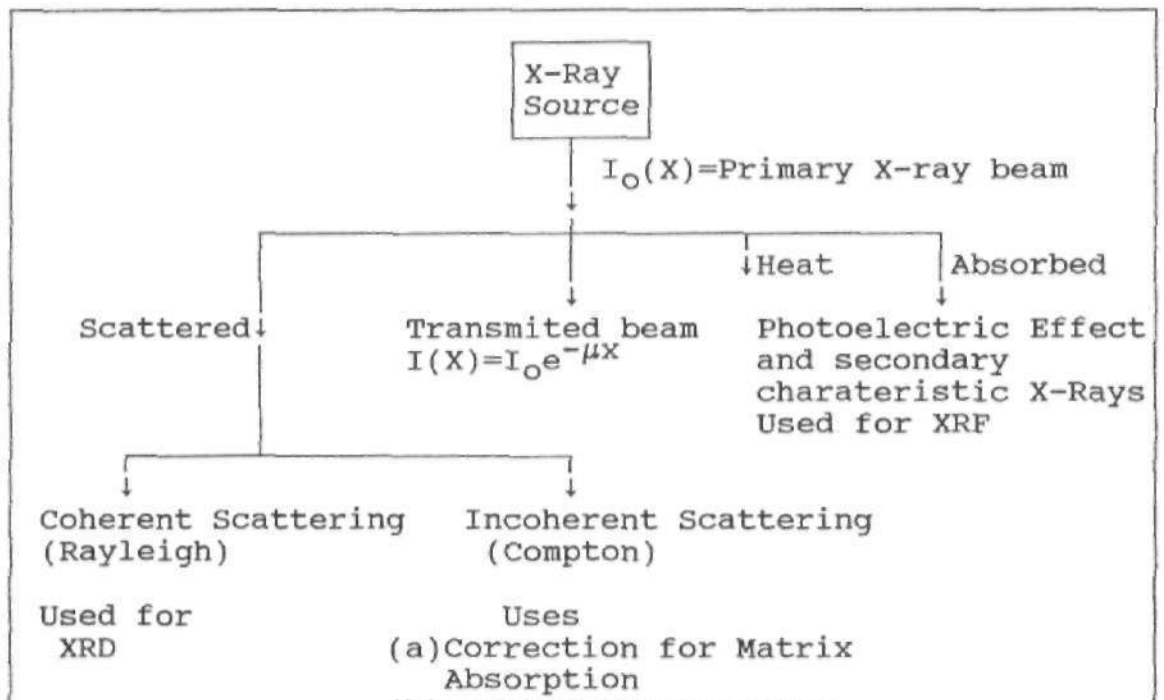


Figure 2.4 Attenuation Processes/Analytical Applications

of photons by free or weakly bound electrons is nearly independent of the Z-number of the material of the scatterer. (Clayton *et al.*,1979).

The photoelectric absorption which results in the ejection of photoelectron, is accompanied by emission of Auger electron and a secondary characteristic (fluorescent) x-ray. The fluorescence competes with the Auger-electron emission as a de-excitation process following the creation of an inner shell hole. This competition is usually expressed as:

$$n_q = n_A + n_R \qquad 2.34$$

where n_q = Number of atoms undergoing transistion

n_A = number of atoms that emit Auger electrons (radiationless transition)

n_R = number of atoms that emit fluorescence (radiative transition)

The radiative transition atoms emit discrete lines so n_R can be considered as the sum of the radiative transition atoms (n_{R1} ,n_{R2} , n_{Ri}) corresponding to these lines.

$$n_R = n_{R1} + n_{R2} + ..+ n_{Ri} = \Sigma n_{Ri} \qquad 2.35$$

The ratio of equation 2.35 and 2.34 is defined as the fluorescent yield (Agarwal, 1979)

$$F_y = \frac{\Sigma n_{Ri}}{n_q} = \frac{n_R}{n_A + n_R} \qquad 2.36$$

or in terms of transition probability:

$$F_y = \frac{P_R}{P_A + P_R} \qquad 2.37$$

The frequency of the characteristics lines from n_R increases systematically as the the atomic number Z and it is expressed by the Moseley law.

$$\left[\frac{v}{R_\infty}\right]^{\frac{1}{2}} = \frac{Z}{n} - \frac{\sigma_s}{n} \qquad 2.38$$

where R_∞ = Rydberg constant

σ_s = Screening constant

These lines consist of K_α, K_β, L_α L_β, etc, but the most intense are the K_α and K_β lines. The emission of the characteristics x-ray by element when bombarded with high enough energy forms the basis for this method of chemical analysis. The analysis is carried out mostly in an energy dispersive x-ray spectrometer.

In the energy dispersive x-ray fluorescence spectrometer, the primary excitation (x-rays, gamma rays, electrons, heavy particles) results in the emission of the characteristic x-ray photons of various energies. These photons enters the depletion volume of the Si(Li) or Ge(Li) detector and loose energies in photoelectric encounters. The resulting photoelectrons ionize the detector material, producing electron-hole pair whose number is proportional to

the energy of the absorbed photon (Langheinrich, *et al.*, 1973) The generated charge, collected by high voltage bias across the detector is converted to voltage pulses and amplified by charge sensitive field effect transistor (FET), a preamplifier and a linear amplifier. The amplitude of each pulse is proportional to the energy of the initial x-ray photon that produced the pulse. The process of generation of the pulse by a photon and collection is accomplished in less than one microsecond (Langheinrich *et. al.*,1973) The Repetition of identical events is a measure of a specific radiation and, hence relates to the concentration of an element in the sample.

2.2.3 SEMICONDUCTOR DETECTORS IN XRF

Lithium drifted semiconductor detectors in elemental x-ray analysis which was first reported in 1966 (Langeinrich, *et. al.* 1973) is today a major detector in x-ray fluorescence analysis, diffraction spectrometers, electron microprobes, and in scanning and transmission electron microprobe. X-ray fluorescence analytical system utilizing solid state detectors usually consists of liquid nitrogen dewar and preamplifier. The high intrinsic resolution (better than 180ev at 6kev) and excellent stability of a semiconductor detector permit a direct measurement of the intensity of the characteristics x-ray of the wanted element, with very little interference from other excited or scattered radiation (Papez and Cameron, 1973). Other

features of the semiconductor detectors are excellent intensity linearity, sensitivity to a wide energy range and ready out put compatibility with computers. The major disadvantages are the associated liquid nitrogen cooling system, high vacuum between semiconductor and x-ray window. An x-ray transparent window (usually beryllium) limits system performance on the low energy side of the spectrum. Detector damage on vacuum loss and temperature rise is possible for the Si(li) detector and certain for the Ge(li).

2.2.4 RADIOISOTOPE SOURCES IN XRF

In energy dispersive x-ray fluorescence spectroscopy, the high excitation efficiency is achieved when the energy of the exciting radiation is restricted to an energy which is just above the absorption edge of the element to be determined (Clayton *et. al.*,1973). The use of monochromatic radiation sources allows selective excitation of the characteristics x-rays of one or more elements in a group of elements of near-adjacent atomic number.

The number of the available radioisotopes provides a high degree of flexibility as this is important in applications where heterogeneity problems maybe serious like the geological samples. Radioisotope also presents reduced safety hazard compared to x-ray tube generator excitation, although the photon output is relatively low (10^6 - $10^8 s^{-1}$) adequate sensitivity is obtained if the energy of the

emitted radiation is just above the absorption edge of the analyte.

2.2.5 MATRIX ABSORPTION IN X-RAY ANALYSIS

In many assays, an adequate correlation can be obtained between characteristic x-ray intensity and the elemental concentration, but in about half of the applications of energy dispersive analysis, the correlation is inadequate *due to the matrix absorption and enhancement effects* (multiple excitation) caused by variation in the concentrations of other elements present in the sample (Papez and Cameron, 1973). The intensity of a fluorescent line from an element is not strictly proportional to the atomic fraction present because of these two major interfering effects:-

(a) Matrix absorption. As the composition of sample changes so does its absorption coefficient, as a result, there are changes both in the absorption of the primary radiation travelling into the sample and in the absorption of the fluorescent radiation travelling out.

(b) Enhancement (multiple excitation). This is the multiple excitation on an element by the fluorescent x-ray of an excited element of higher energy in combination with the primary excitation of incident x-ray from the tube or radioisotope.

These effects complicate the calculation of fluorescent intensities that quantitative analysis is usually performed

on an empirical basis by the use of standard samples of known composition. Matrix effects are generally considered as self absorption, interelement effects, mineralogical differences among samples, and inhomogeneity of the sample particles. Evaluation of these problems has been approached by use of internal standards, comparison with standards approximate in composition to the unknowns, fusion and dilution with transparent materials, fluorescent/scatter intensity ratio (Andermann and Kemp (1958), Shenberg and Amiel (1973) and Burkhalter (1971)), mathematical corrections and reduction of particle size by fine grinding (Wheeler *et al.*, 1976).

The use of a fluorescent/scatter intensity ratio to replace the fluorescent intensity in empirical calibration curves was first reported in 1958 by Anderman and Kemp and since then has been widely used. Fluorescent/scatter ratio methods is important for partial compensation for varying x-ray tube voltage and current and sample position, particle size and matrix absorption. The principle of this method of analysis is discussed below.

The intensity of characteristic x-rays excited in geochemical samples of saturation thickness and optimum particle size (Clayton and Packer, 1979) is given by

$$I_R = k_1 . I_o . F_k . r / \Sigma_i (\mu_e + \mu_R) . r_i \qquad 2.39$$

where k_1 = overall detection efficiency for the characteristic x-ray radiation,

F_k = the excitation frequency

μ_e = mass absorption coefficients of element i for the incident radiation

μ_R = mass absorption coefficients of element i for the fluorescent radiation

r_i = is the concentration of element i and

r = is the concentration of the wanted element.

The corresponding intensity of the scattered radiation is given by

$$I_{scat.} = (I_{coherent} + I_{Compton}) \qquad 2.40$$

$$= k_2 I_o \left[\frac{\Sigma_i (\sigma_{coh})_i r_i}{\Sigma_i (2\mu e)_i r_i} + \frac{\Sigma_i (\sigma_{comp})_i r_i}{\Sigma_i (\mu_e + \mu_{comp})_i r_i} \right]$$

where I_o = incident radiation intensity,

k_2 = overall detection efficiency of the system (including geometrical efficiency),

σ_{comp} = compton scattered coefficient,

σ_{coh} = coherent scatter coefficient and

μ_{comp}= mass attenuation coefficient for scattered radiation for element i.

As mentioned earlier, compton scattering is nearly independent of the atomic number and $k_1 = k_2$ (usually), so that from equations 2.39 and 2.40 it can be shown that

$$\frac{I_R}{I_{comp}} \propto \left[\frac{\Sigma_i(\mu_e + \mu_{comp})_i r_i}{\Sigma_i(\mu_e + \mu_R)_i r_i} \right] .r \qquad 2.41$$

If the energy of the exciting radiation is nearly the same as the energy of the characteristic x-rays, $(\mu_R \approx \mu comp)_i$ except for the element being excited, and the ratio of I_R/I_{comp} is then proportional to r and independent of the matrix.

The use of scattered radiation in XRF analysis provides an alternative to the common problem of matching samples to standards of similar composition. The backscatter peaks are sometimes treated as fluorescent peaks from internal standards (Nielson, 1978) since they suffer the same matrix absorption as fluorescent peaks and behave similarly with instrumental variations. They are better described as total matrix peaks, however, because the scattering originates from all elements in the sample matrix rather than from a single element. They thus provide the only direct spectral measure of the total or average matrix of geological or other materials containing significant quantities of C, O, or other light not observed by fluorescent peaks.

2.3. X-RAY DIFFRACTION ANALYSIS (XRD)

2.3.1 INTRODUCTION.

XRD provides the basis for quick and reliable identification of minerals and structural information about a material under investigation. It is the only satisfactory

method of distinguishing among polymophs (Cullity, 1970) or detecting a compound in the presence of others containing the same elements, so it is an indispensable qualitative analytical method for mineral identification.

This qualitative analysis is based on the principle that every crystalline powder produces characteristic diffraction pattern when exposed to a beam of monochromatic X-ray. The law for the selective reflections was first proposed in 1913 by Bragg. The Bragg law opened the way for construction of crystal spectrometer and provided many avenues for studies ranging from qualitative analysis to the study of internal defects in the arrangement of atoms. The studies involve the interpretation of diffraction pattern with respect to the values of the Bragg angle θ that it represents and intensities of diffraction. The basic principles of the original Bragg spectrometer still prevails in the most modern automatic instruments: a central movable table or goniometer upon which the crystal analyzer can be mounted and rotated to vary the angle of incidence θ; and an ionization chamber, or modern Geiger, proportional or scintillation counter which can be mounted on a rotating arm, the position of which may be read on a scale. This records the angular 2θ value of any spectral emission line or absorption edge and by the Bragg law, the characteristic wavelength. (Cullity, 1970).

The identification of mineral(s) is achieved by a careful comparison of the unknown pattern with catalogue of standard data on XRD such as the X-ray powder data file published by the American Society for Testing and material (ASTM).

2.3.2 PRINCIPLE

The intensity (energy per second) of a reflection (hkl) in a powder diffraction pattern is separated into six parts (1) a constant factor for aparticular diffractometer, (2) structure factor characteristic of the diffracting sample, (3) an angle factor known as the Lorentz- polarization factor, (4) a temperature factor to correct for thermal vibration of atoms, (5) an absorption factor which attenuates the diffracted x-rays, and (6) the volume of powder in the primary x-ray. This intensity equation is given (Chung, 1974) bellow:

$$I(hkl) = \left[\frac{I_o e^4 X^3 d}{32\pi m^2 c^4 r}\right] (N^2 p F^2) \left[\frac{1 + \cos^2 2\theta}{\sin^2\theta \cos\theta}\right] .T.A.V \qquad 2.42$$

Where I = Intensity of X-rays diffracted by (hkl) plane.

I_o = Intensity of primary X-rays.

e,m = Charge and mass of electron.

X = X-ray wavelength.

d = Slit width of detector.

c = Velocity of light.

r = Specimen-to-detector distance.

N = Number of unit cells per unit volume.

p = Multiplicity.

F = Structure factor.

θ = Bragg angle.

T = Temperature factor.

A = Absorption Factor.

V = Volume of powder in the beam.V

The resultant of the reflections from all other planes in a powder diffraction is conveniently expressed by the Bragg equation:

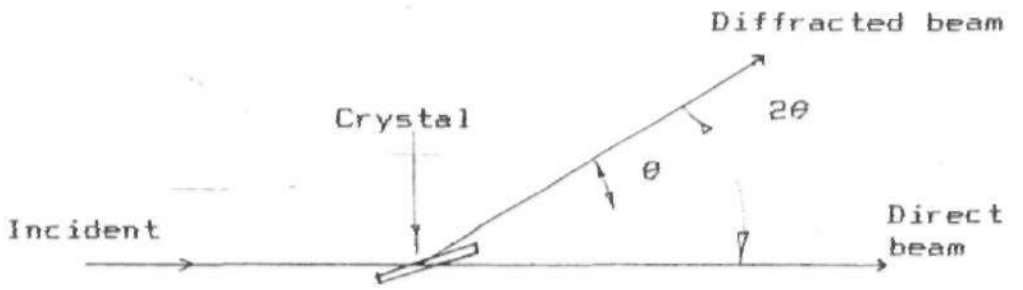
$$n\lambda = 2.d.\sin\theta \qquad 2.43$$

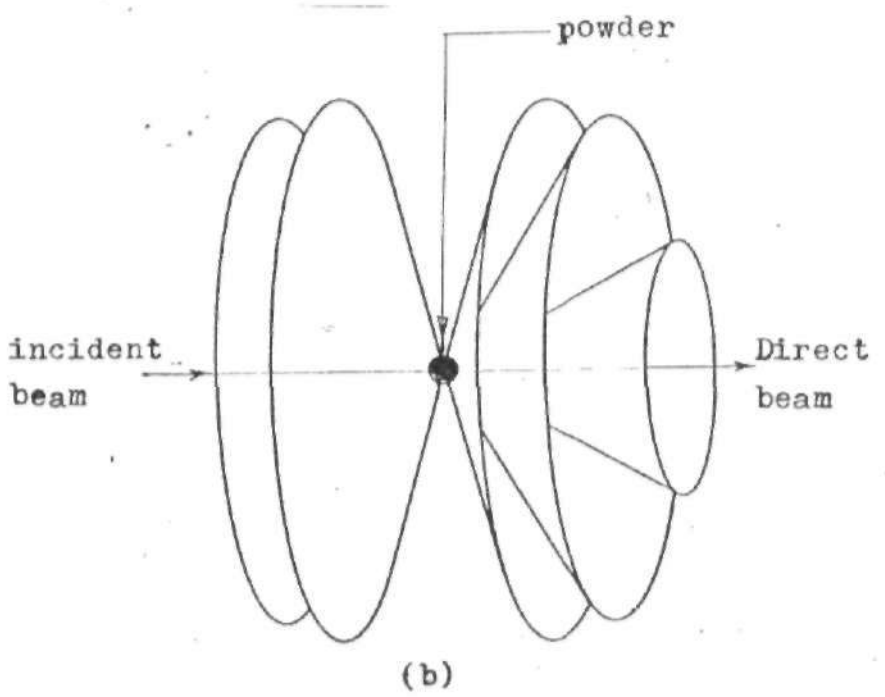
where λ = the wave length of the X-ray

d = interplanar spacing

n = order of reflection

Each particle of the powder is a tiny crystal, or assemblage of smaller crystals oriented at random with respect to incident beam so that every lattice plane will be capable of reflection. The large number of crystallites having all possible orientations, is equivalent to a single crystal rotated about all possible axes, in a beam of monochromatic X-ray. This implies that at all times a certain fraction of these crystallites will have their (hkl) planes at the right Bragg angle with the incident x-ray beam. The reflections from the planes result in conical sheet of diffracted radiation, and each lattice plane is accompanied by its cone (figure 2.5). Thus various diffraction cones are associated with any powder





(b)

Fig.2.5 Diffraction Cone formation in powder method

diffraction spectrum.(Zoltai, 1967). All diffractometers are designed to record these diffraction cones; however many of them differ in geometry and design. The major differences between them are the detector type (Geiger Muller, proportional and scintillation counters) and the geometrical arrangement of the goniometer -vertical or horizontal type.

CHAPTER THREE

MANGANESE OCCURRENCES, CLASSIFICATION AND SAMPLE COLLECTION

3.1 Geology of North Western, Nigeria

Mn occurences in Nigeria are found on the North western half of Nigeria associated with schist belts. The North Western Nigeria is underlain by gneisses, migmatites and metasediments of Precambrian age which have been intruded by a series of granitic rocks of the late Precambrain to lower Palaeozoic age (McCurry, 1973). The Pan-African tectonics imposed the general N-S structural trends on the region; its magmatism led to the widespread emplacement of granites and charnockites (Turner 1983).

The oldest rocks in the region are represented by a series of older metasediments and gneisses believed to be of Birrimian age or older. These rocks have been variably metamorphosed and granitised through at least two tectono-metamorphic cycles so that they have been largely converted to migmatites and granite-gneiss. Younger- metasediments believed to be upper Proterozoic in age, were deposited on this granitised basement and folded along with it during the Pan-African Orogeny. These are of low metamorphic grade and are now represented as synclinal troughs among older rocks in N. W. Nigeria. Intrusive into both the basement rocks and the younger supercrustal cover is a series of basic intermediate and acid plutonic rocks known as the Older Granites. The youngest rocks in the area belong to a suite

of volcanic rocks intruded into the Older Granite bodies during lower palaozoic epeirogenic uplift following the Pan-African Orogeny (McCurry, 1973).

The rocks in N.W. Nigeria can be grouped into basement complex, metasediments and the older granites. The localities that the manganese samples were taken from fall into three major belts: Maska belt : (Tudun Kudu), the Maru schist belt (Ruwan Dorowa and Maraba Hills) and The Zungeru-Birnin Gwari schist belt (Figure 3.1).

In the Maru belt, pelitic rocks are dominant, mainly as phyilites and share interlaminated with siltstones. Banded iron formation, containing magnetite, hematite or garnet and grunerite. Impure micacious quartzites occur near the eastern margin of the belt. Mafic volcanic rocks are present by the amphibolites at several localities. (Turner, 1983). The manganese occurrence here are linked up with banded iron formation and rich in magnetite.(Mucke *et al.*, 1984)

The Maska belt occurs within Precambrain metasediments. These are Late Proterozoic rocks folded into synclinorial belts within the crystalline basement complex and metamorphosed to phyllites, quartzites, and pelitic and psammitic schist of low to medium grade (McCurry, 1973) Folding is generally steep and isoclinal with predominantly north-south trending axial plane (Wright and McCurry, 1970)

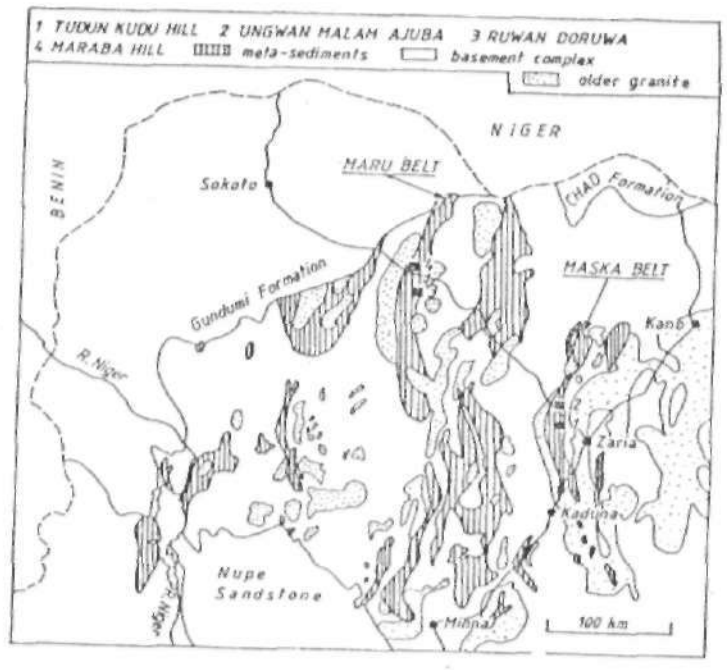


Fig 3.1 Geographical and Geological setting of Mn occurrences in Northern Nigeria (Mucke and Okujeni, 1984)

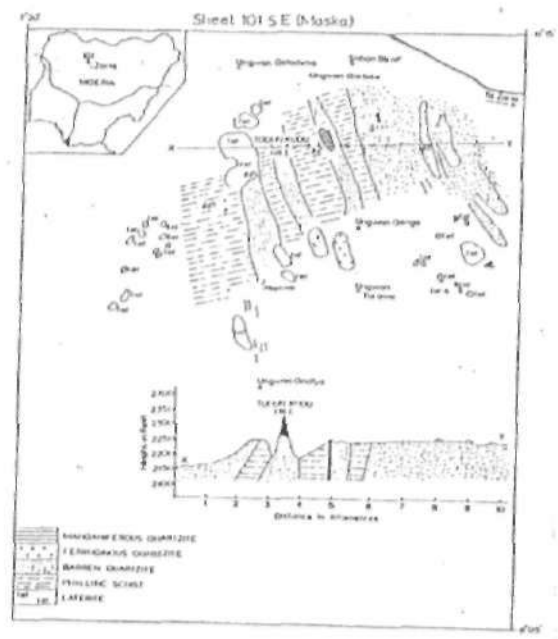


Fig 3.2 Geological Map and section of Mn occurrence at Tudun-Kudu (Moneme et. al., 1982)

The Tudun Kudu manganiferous ores occur in the metasediment associated with quartzites. The geological map for the occurrence is shown figure 3.2 Three kinds of quartzites are recognized in these areas : Barren quartzite, without any iron or manganese mineralization, Quartzite rich in MnO_2 minerals (manganiferous quartzites) and the third variety rich in oxidized iron minerals (ferruginous quartzites). (Moneme *et al.*, 1982). The Birnin Gwari schist formation and the underlying quartzo-feldspathic rocks of the Zungeru formation together, form a single structural unit. The Zungeru formation outcrops on both flanks of the schist belt. It is largely made up of fine-grained quartzo-fieldspathic rocks which are interbedded with amphibolities and some quartzites (Turner, 1983). The quartzo-feldspathic rocks originated as feldspathic sandstones. (Trustwell and Cope, 1963) and (Ajibade, 1982). The Birnin Gwari schist formation occupies the synclinal axis of the schist belt. The lower part consists of finely banded phyllites in the west and higher grade biotite muscovite schists in the east. They are overlain by the Durimi-pebble schist, a metamorphosed mudstone conglomerate containing some beds of impure quartzites or metagreywacke. The pebbles and boulders are varied-quartz, quartzite, quartzo-feldspathic rock, metabasalt schist (Turner, 1983). The manganese mineralisation in this belt are also rich in ferruginous quartzites like the Tudun Kudu occurence (Moneme *et al.*1982)

3.2 Classification of Mn Ores and Minerals

The Mn sources are classified into four types: (a) Mn ore (those ores containing over 35% Mn),(b) ferruginous Mn ore (ores containing 10-35% Mn) (c) manganiferous ores (5-10% Mn) and Iron Ores (ores containing less than 5% Mn with the balance mostly Fe) (Kirk-Othmer, 1966). The average exploitable Mn ore body has a grade close to 45% (Chapman 1985).

The important ore forming Mn minerals are the carbonate rhodochrosite and a large number of oxides in which Mn occurs in both higher (Mn^{4+}) and lower valency states. The typical Mn minerals and their environments (Chapman, 1985) is shown in figure 3.3.

Rhodochrosite ($MnCaO_3$) is a typical mineral of the hydrothermal Mn deposits. Economically it is important as the dominant Mn mineral of the sedimentary Mn carbonate formation which may form both ore and protores. It can be altered by supergene processes to oxide minerals and may also be formed by the reverse processes from the oxide minerals. Kutnachorite ($CaMn(CO_3)_2$) is the Mn member of the dolomite group and is relatively rare. Pyrolusite (β-MnO_2) is virtually pure manganese dioxide and is common in low temperature deposits. Nsutite (γ-MnO_2), structurally distinct and non-stoichometric, is the usual mineral in supergene oxide deposits derived from carbonates.

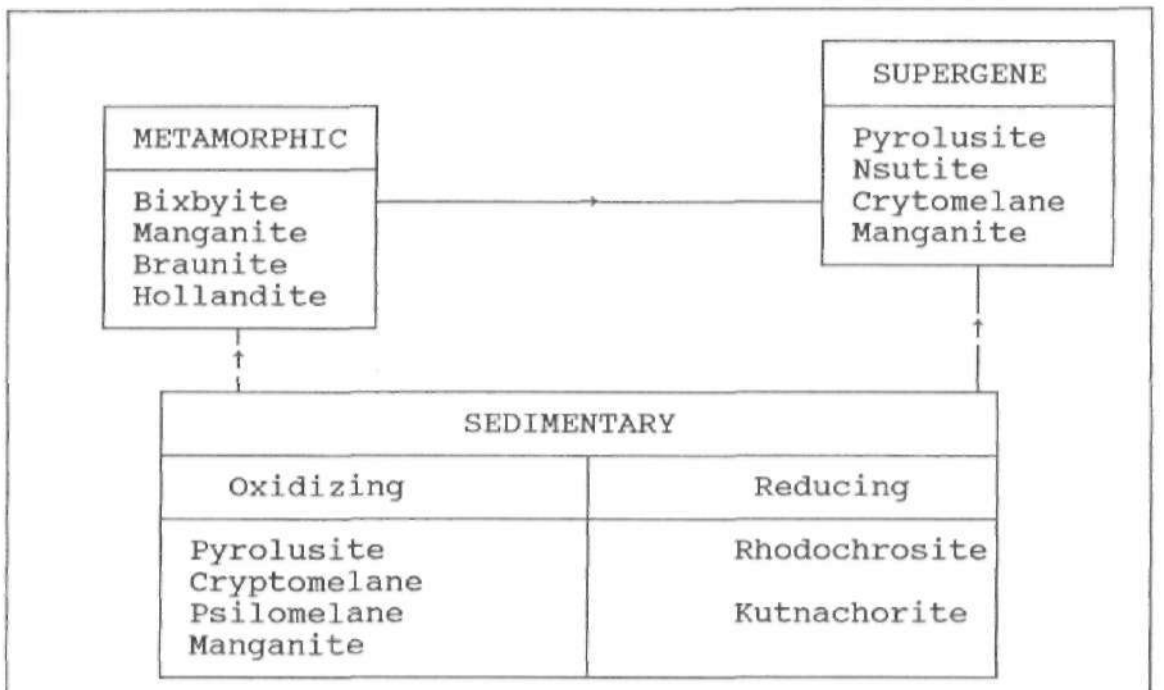


Figure 3.3 Typical Mn Minerals and their Enviroments (Chapman, 1985)

Cryptomelane ($KMn_8O_{16}xH_2O$), hollandite ($(Ba,K)Mn_8O_{16}xH_2O$) and other species form an isostructural series in which large exchangeable cations, such as Ba^{2+} ,Pb^{2+} ,K and Na occur in the structure. Psilomelane ($(Ba,K,Mn,Co)Mn_5O_{10}xH_2O$) is a name that has been loosely applied to any manganese oxide that shows botryoidal form; it is common in sedimentary deposits. Manganite (MnOOH) is one of the three naturally occurring varieties of manganese hydroxide and common in both sedimentary and supergene deposits.(Chapman, 1985)

The lower oxide found in nature are braunite ($3Mn_2O_3.MnSiO_3$) which normally has about $10SiO_2$ in the structure. Bixbyite ($(Mn,Fe)_2O_3$) and hausmanite (Mn_3O_4) which is one of the four phases in the system Fe_2O_4-Mn_3O_4. All three oxides occur commonly in metamorphosed manganese oxide deposits, together with the high temperature tetravalent oxide, hollandite (Chapman, 1985)

3.4 Field Work and Sampling

The field work covered the major Manganese occurrences (figure 3.1). The trip was done in two phases: the first phase which started early November, 1992 covered the localities of Tudun-Kudu, Ruwan-Dorowa Maraba Hills, Bungudu and Dandato. The second phase which started in early January, 1993 and extended to February of the same year, covered the Zungeru, Kontagora, Bonu, Kunji, Maganda, Birni-Guari, Kirazo, Saulawa, and Farin Ruwa localities.

Samples were obtained from the outcrops and pits dug to 1 metre deep. It was the representative ore that was taken from every sampling point. Hand held hammer was used to discard weathered rock and to have access to the fresh ore especially the inner part of the outcrop. For an extensive deposit like the Farin Ruwa, the sampling points were at interval of 100 metres

CHAPTER FOUR

MATERIALS AND METHODS

4.1 Neutron Activation Analysis

4.1.1 The Design of the paraffin moderator.

The paraffin neutron moderator was designed for the 5Ci Am-Be isotopic source with the consideration of the following important factors:-

1. Best condition for maximum thermal flux
2. Reproducible irradiation geometry
3. Availability and ease of handling paraffin
4. Reasonable safety from radiation hazard

The flux level in a moderator depends on the source-sample position for given source strength. Fumio *et al.*, 1958 measured the best position and direction of a sample placed in a paraffin moderated ^{226}Ra-Be neutron source and observed that the largest induced activities occurred at 1.7cm. Riepo (1983) observed by measuring the average neutron activation cross section of $^{115}In(n,\gamma)^{116}In$ reaction as function of thickness of the paraffin layer placed between the 5Ci ^{241}Am-Be neutron source and a thin indium foil target, got a maximum when the paraffin layer was about 2.5cm. Mustapha *et al.*,1994 studied the thermal flux distribution in a perspex using a 5Ci ^{241}Am-Be source and obtained an optimal position of 2.5cm from the source. Based on these observations, we chose 2.5cm as the source-sample position.

The neutron flux from an isotopic source is relatively low, for sufficient activity, a large amount of sample is necessary. This also implies large sample container. Some workers like Beress, (1966) have used up to 38 grams in a single irradiation position to analyze Mn ore. In this design, a sample vial diameter of 30mm was chosen for two reasons:- (1) the 30mm diameter is the same as the source diameter so, as to minimize the problem of treating sample and source holes differently, (2) this vial diameter, with a height of 5cm, can contain up to 63 grams powder of density $1.8g/cm^3$. The choice of 30mm sample hole limited the number of such to six (25mm from 30mm source diameter) for symmetric positioning of samples.

The dimensions of the outer part of the moderator are based on the safety consideration. From the manufacturers specification (CIAE, China, 1989), the dose rate on the surface of the 5Ci ^{241}Am-Be source is 25mrem/h. This exceeds the maximum permissible dose (MPD) of 2.5mrem/h (40hr-week) and has to be reduced to an acceptable level by the moderating system itself. Krumbein (1968) has shown that 25cm thick paraffin reduce fast neutron dose by more than 100 times, this is equivalent to 0.25mrem/h (fast neutron dose), for the isotope source. However, the thermal flux component has a contribution to the dose rate. To estimate this at 25cm from the source, the flux at this point was calculated using the two group method (Beckurts and Wirtz,

1964). Details of the calculation are in appendix 5. The calculated value is 263.4n/cm^2s^{-1}. Using table of flux versus dose rate (Goussev, 1968), this is equivalent to 0.963mrem/h. Therefore the dose rate from both thermal and fast neutrons from the 5Ci ^{241}Am-Be source covered with 25cm thick paraffin is far below the MPD. A cylindrical paraffin of 75cm in diameter and a height of 60cm was chosen. With source in the center, the minimum source to surface diameter is 25cm.

The last major factor of the design is durability. Commercial paraffin is soft, that means persistent use of source and sample will result in rapid wear, it was therefore necessary to put a sleeve in the source/sample positions in form of a harder hydrogenous material. Polyethylene pipes, a readily available material, with higher resistance to wear than paraffin were chosen.

Seven polyethylene pipes, one for the source and the other six for sample holders were first prefixed. The pipes were glued to a rigid phenolic sheet at source/sample distance of 2.5cm with impact adhesive at both bottom and top, then reinforced with araldite adhesive. After setting, it was placed in a large cylindrical mold (75cmϕ by 60cm) made from commercial phenolic ceiling board. About 200kg commercial paraffin was melted at 85°C and poured into the mould containing centralized tubes, then allowed to cool and set overnight.

Six plugs of paraffin (31mmϕ by 200mm height) were forced into sample holes from below to act as stoppers/bases for samples and the seventh paraffin plug (31mmϕ by 250mm height, fitted with a tiny polyethylene tube) was forced fitted into the source tube from above. The tiny polyethylene tube allows the source cord to pass through and acts as wear resistant in place of paraffin. This tube has an inner diameter of 2mm, about the diameter of the cord carrying the neutron source to avoid fast neutron streaming through the void. The entire assembly is shown in plate 4.1 and figure 4.1

4.1.2 Safety considerations.

Ionizing radiation was recognized as a hazard within six months of the discovery of X-rays by Roentgen and again a few years later after the isolation of radium by Curies (Dungster, 1961). These early effects were confined to superficial damage to the skin and it was some years before the link between radiation and cancer was suspected.

Of primary concern in radiation protection is the risk of radiation induced genetic and late somatic effects. To control this risk, the International Committee on Radiation Protection (ICRP) has adopted concepts that are based essentially on two principles (Burger and Schwartz 1988). firstly all exposures of people shall be kept as low as reasonably achievable (ALARA) and, secondly the dose equivalent of individuals shall not exceed recommended

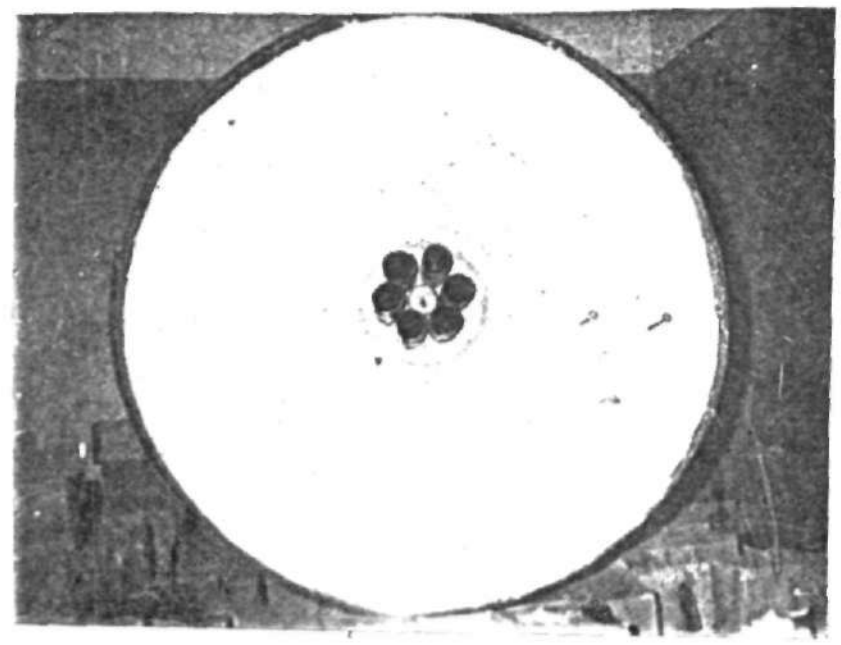
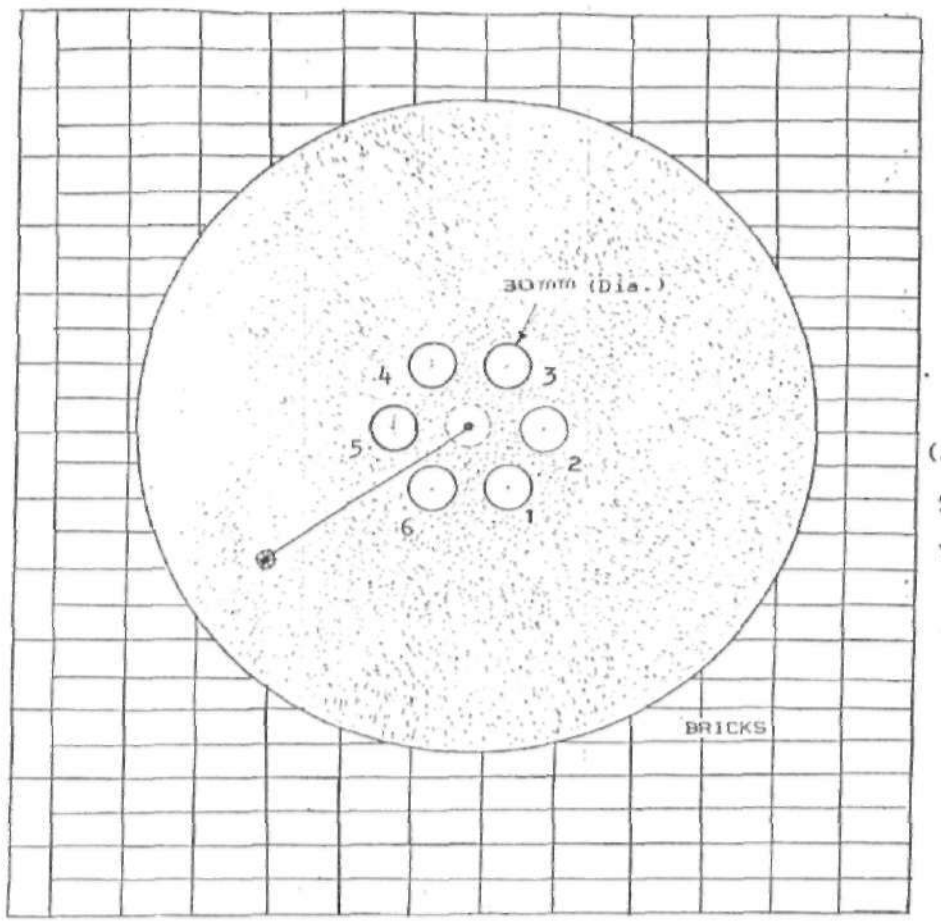
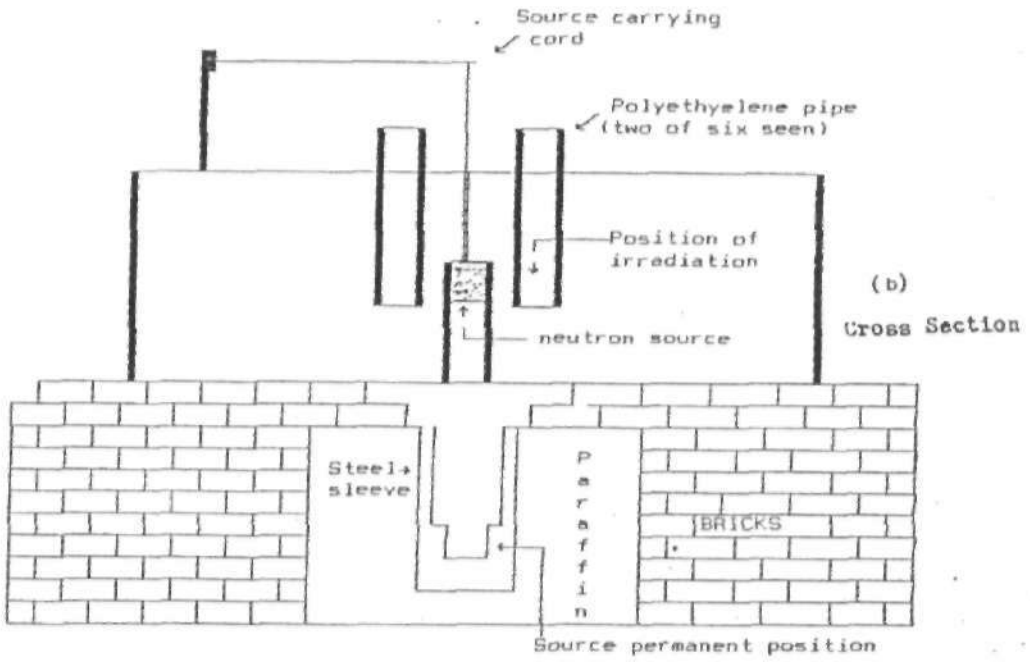


Plate 4.1 Photograph of the Irradiation setup



(a)
Top
view



(b)
Cross Section

Figure 4.1 Illustration of the irradiation setup

limits (2.5mrem/h) of MPD for external radiation dose rate at the shield or barrier round a radiation source, if the point of highest dose rate is occupied for 200 hours per year by a worker from age 18 years onwards.

In compliance with regulations to occupational exposure in radiation protection, exposure rate was estimated during the design of the moderating system and latter measured when the source was put in place by using a BF_3 neutron monitor (model NM2, manufactured by Nuclear Enterprises Ltd, U.K). This device is a calibrated radiation protection monitoring instrument calibrated in mSv/h (1mSv = 100mrem). The maximum measured dose on the surface of the paraffin moderating system was 8mSv/h equivalent to 0.8mrem/h. This is still within the MPD specification.

4.1.3 Preparation of standard for the NAA.

A critical part of NAA is the preparation of adequate standards. It is desirable that the standard be as close as possible in all respect to the form in which the samples are prepared. The properties of the standard that should be close to that of the sample include the thickness, density, form, mass and the volume. Sample holders should be identical , the activity of sample and standard should be close. To achieve this, a series of standards are usually prepared.

Standards for Mn minerals. The common minerals in Tudun -Kudu, Maraba hills, and Ruwan-Dorowa are manganoan-ilmenite ($(Fe,Mn)TiO_3$), Cryptomalene ($(K,Ba,Ca)Mn_8O_{16}xH_2O$), lithiophorite ($(K,Ba)Mn_8O_{16}xH_2O$), limonite FeOOH, geothite α-FeOOH and quartz SiO_2, (Mucke and Okujeni, 1984). Thus, a potassium permanganete,($KMnO_4$) diluted by a composite containing 20% Fe_2O_3 and 80% SiO_2 was found to be a suitable standard based on the fact that these are the common compounds in a typical soil and rocks.

The standards were prepared from potassium permanganete 99% A.C.S.(American Chemical Society) reagent of 50μM particle size, silicon(IV)oxide 99.99%, 50μM particle size and iron(III)oxide 99.9% purity. Each powder compositions was thoroughly mixed using a motor driven mechanical mixer for about 30 minutes until homogeneity was ensured.

The standards for the solution were prepared by dissolving the required quantity of the $KMnO_4$ with distilled water. Here it was easy to attain lower concentration with potassium permanganete within its solubility level. The volume of the liquid used for each sample holder was 15ml.

Preparation of standards for AL, AS, W, Mo, V, Br, I and Na. All the standards prepared were from pure chemicals. The elements and the chemical standards include: Al (Al_2O_3-99.9%, 50μM particle size), Na (NaCl-99+ % A.C.S reagent), As (As_2O_3 -99.9% analytical grade), I (KI-99+% A.C.S

reagent), Mo (MoO_3 -99.5% Analytical Grade), Br (NaBr 99+ % Analytical grade), V (V_2O_5 98+ % A.C.S reagent), W (WO_3 - 99.99 % A.C.S reagent).

Lower concentrations of these chemicals were prepared by mixing individual chemicals with the appriopraite amount of SiO_2 powder. SiO_2 was chosen for the reason of the low thermal neutron cross section of its elemental constitution, which in turn eliminates the problem of interfferences of the chemical used as blank.

4.1.4 Irradiation

Irradiation was carried out in the paraffin moderating system designed for this work. Two types of irradiation were carried out, the first was to characterize the system:- flux estimate for individual irradiation position (thermal and epithermal) using bare and cadmium covered indium foil, detection limits for elements with high thermal capture cross section (Al, Mn, W, Mo, I, Na,Br, As and V) and their calibration curves. The second set of irradiation is for Mn standard and the ores.

For the measurement of the thermal flux at any of the irradiation positions, an indium foil of mass 1.15g, dimension 1cm by 1.5cm was irradiated at the desired position for two half- lives (108 minutes). The position of the foil is such that its plane faces the source. To achieve

this, the foil was attached to polymethylmethacrylate (plexiglass) rectangular sheet, 30mm by 500mm long. The arrangement is shown in figure 4.2. The angle, the plane of the foil makes with the source was well marked on each of the holes. The arrangement ensured easy geometrical reproduction for foils and minimizes the time spent on alignment in the irradiation room. The rectangular sheet (foil attached) is brought out after each irradiation, foil detached and taken for counting. The precise delay time (cooling time) was always noted so that the actual activity of the foil at the end of the irradiation period can be calculated with correction for decay.

The irradiation for epithermal measurement involved placing the indium foil in a closed cadmium box. The dimension, thickness, and the shape of cadmium when used as filter determine its performance (Zijp, 1970). So the shape of the cadmium box used was in accordance with the recommendation of the American Society for Testing and Materials (ASTM). This is shown in figure 4.3 The 1mm thick cadmium box, enclosing an indium foil, was glued to the rectangular polymythylmethacrylate and lowered into an irradiation hole then aligned in the same manner as the bare foil. For each position, irradiation was done for 108 minutes (two half-lives). The irradiation in an open cadmium box was conducted in the same manner but with the

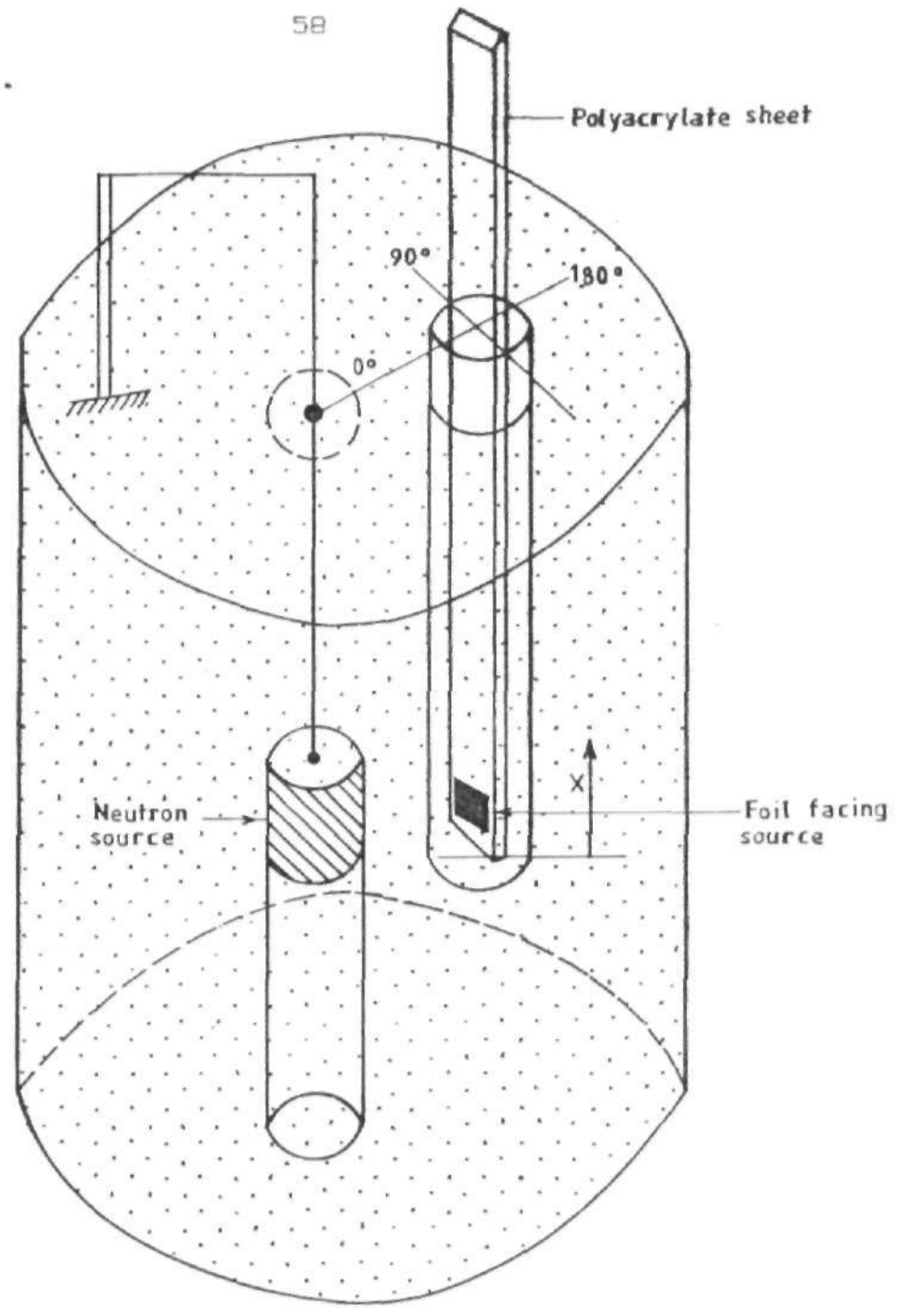


Fig. 4.2. Setup for foil activation.

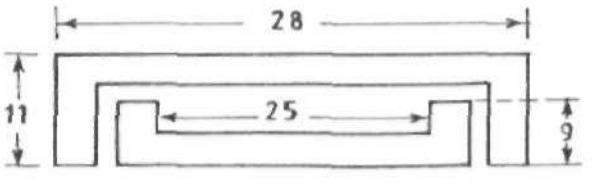


Fig. 4.3. Cadmium Box used for epithermal irradiation.

plane of the foil rotated about the source to check the directional flux distribution within the holes.

The next set of irradiation was for the determination of the detection limit and calibration curves for Al, Mn, As,W, Mo I, Br, Na, V. The irradiation time, cooling time and masses used for each element is shown in table 4.1. The lower concentrations were achieved by mixing to homogeniety analytical grade reagents of the elements with SiO_2 powder. Both Si and O have lower thermal cross section than any of these elements. Here polyethylene aliquot (30mmϕ ,50mm height) with nylon thread attached was used as sample holder.

The last set of irradiation was for the potassium permanganete ($KMnO_4$) (both powder and solution) and the Mn ores, using the polyethylene aliquot. The height of all powder in sample holder were restricted to 30mm from the bottom. The time for Mn irradiation varies from 6 to 50hrs. The cooling time of 2min was maintained for all the measurements

4.1.5 Gamma ray spectroscopy

One of the most efficient methods of counting ionizing radiation such as X-rays, γ-rays, alpha and beta particles and measuring their energies is their detection by scintillation gamma ray spectrometer. The spectrometer, for efficient counting employs a scintillation detector

	ISOTOPE ABUNDANCE	ISOTOPE PRODUCE	CROSS SECTION (BARN)	HALF-LIFE	PHOTO-PEAK (Kev)	IRRADIATION TIME	CHEMICAL USED	RESONANCE ENERGY (eV)	INTEGRAL CROSS SECTION (BARN)
^{27}Al	100	^{28}Al	0.232	2.3m	1779.0	30min	Al_2O_3	-	-
^{23}Na	100	^{24}Na	0.51	15.0h	1368.5	100hr	NaCl	2850	0.3
^{55}Mn	100	^{56}Mn	13.6	2.59h	846.8	6-50hr	$KMnO_4$	337	11.1
^{75}As	100	^{76}As	4.2	26.8h	559.1	100hr	As_2O_3	47	38.5
^{98}Mo	23.78	^{99}Mo	0.15	2.85d	140.5	100hr	MoO_3	-	-
^{79}Br	50.54	^{80}Br	8.4	17.6m	616.2	1hr	NaBr	-	-
^{51}V	99.76	^{52}V	4.9	3.76m	1434.1	30min	V_2O_5	-	-
^{186}W	38.41	^{187}W	37	23.9h	685.0	48hr	WO_3	18.8	276.1
^{127}I	100	^{128}I	5.5	25m	442.9	1hr	KI	-	-
^{115}In	95.77	^{116}In	160	54m	1293.4	108min	In	1.457	2060.2

Table 4.1 Nuclear data of 10 elements of high thermal neutron capture cross section.

which is usually Thallium activated NaI. The NaI(Tl) is a material able to convert energy lost by ionizing radiation into pulses of light. These pulses of light is detected by the sensitive photomultiplier tube. The current pulse is a result of the energy deposited in the NaI(Tl) crystal and may be amplified and used to activate a scaler or ratemeter.

The counting setup for this work (figure 4.4) consists of a Camberra NaI(Tl) detector, Ortec high voltage bias/preamplifier and a computer (Mitac 2060C) containing a multichannel Analyzer card (PCA II) and the corresponding standard soft ware (PCA-NUCLEUS).

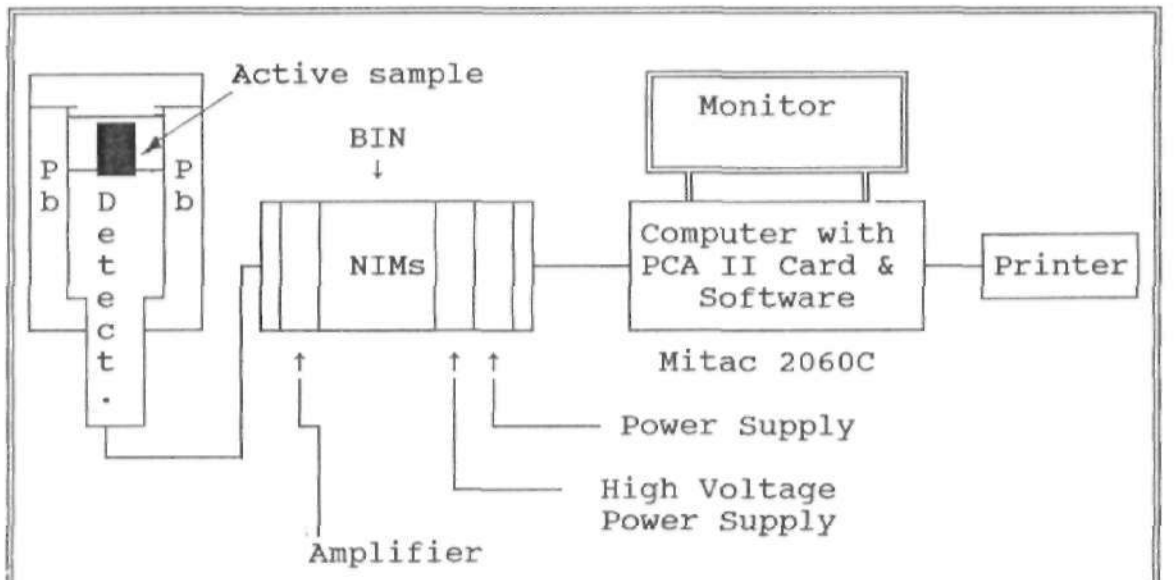


Figure 4.4 NAA Counting Setup at CERT

The Camberra detector (model 802-4) is monoline crystal assembly which includes a 7.6cm diameter by 7.6cm thick NaI(Tl) crystal, a photomultiplier tube, an internal

magnetic/light shield and chrome plated aluminum. The entire system plugs directly into the Camberra tube base (model 2007) which combines the bias network with built in preamplifier. The bias specification for the photomultiplier is 800-1100 volts. 900volts was used throughout the work.

The Ortec high voltage power supply (model 456) and the amplifier (model 485) are in modular form, they fit into the standard Ortec Bin (model 402A). The Bin contains the low voltage power supply and takes any of the standard NIM (Nuclear Instrument Module) for nuclear experiments.

The variable high voltage supply (0-2500volts) supplied the 800-1100volts required by the photomultiplier to function. To attain the 900volts used throughout this work, the variable voltage control nob is turned slowly to allow for gradual increase in voltage, the minimum time required to attain the 900volts is about 30 seconds.

The amplifier takes the pulses from the preamplifier at the base of the photomultiplier, amplifies it to the required level and sends it to the PCA II card installed in the computer. The pulse height is controlled by the gain control nob.

The PCA II card is a second generation multichanel analyzer card. It contains a 100Mz analog to digital converter, single channel analyzer (SCA), multichannel scaler (MCS), and on board memory. The card, along with the

standard software, transforms the personal computer into a full feature multichannel analyzer with 8192 channel acquisition memory (optional 1024, 2048 and 4096 channels). An input of 0-8volts pulses (0.5μsec to 30μsec) from a shaping amplifier is the only external signal necessary for pulse height analysis (PHA) operation. The software utilizes a windowing technique with pull down menus for user friendly operation. All important parameters are displayed on the monitor along with spectral data. The most frequently used operation in the cause of the work were the peak search, energy calibration, peak report, data acquisition and storage.

The program, on request, calculates and displays under the peak report; the peak number (PN), Centroid in the calibrated unit (Kev, for this case), full width at half maximum in kev (FWHM), the net area, background, net counts/sec and percentage error.

4.1.6 Measurements

Before any useful measurement can be done on the NaI(Tl) spectrometer, the first thing is the energy calibration. This involves using various gamma ray standard sources (*eg.* ^{60}Co and ^{137}Cs). When the instrument is set, the standard source with two or three peaks widely separated in energy is placed close to the detector and a reasonably large number of counts is recorded. The peak position is

carefully determined by knowing the peak profile. This analysis is usually performed with the computer. On PCA II data acquisition progam, the peak search command allows the computer to search and mark the prominent peaks, this is followed by the calibration command. On calibration mode, the computer requests for the peak data, which when supplied completes the energy calibration.

The performance of a scintillation detector is usually specified in terms of its energy resolution for the 662 Kev peak of ^{137}Cs. The full width at half maximum was used to determine the resolution (Resolution = FWHM/Peak position) at this energy. The value got was 55 Kev. Also, as part of the evaluation of the spectrometer, the detector efficiency was measured using ^{241}Am,^{137} Cs, ^{54}Mn, ^{22}Na and ^{88}Y. The plot of these measurements is shown appendix 1 and has the value of 4.93% at ^{22}Na (1274.5 Kev) with the source on the detector surface.

Other measurements that were made on the calibrated spectrometer can be grouped into:

(a) Thermal/epithermal flux measurement using indium foil at (^{116}In, 1293 kev). These were done for 30min each after a cooling time of 30 seconds.

(b) Detection limits at background level using 16.6 grams of SiO_2 as blank and different concentrations of AL(1778 Kev), W(479.5 Kev), I(442.9Kev), Br(616.2 kev), As (559.1 Kev), Mn (846.4 Kev), Mo (140.5

Kev), V (1434 Kev), Na (1368.5 Kev).

(c) Counting for Mn standard and the Mn ores were done for 3600 secs. each after cooling time of 2min minutes. All the Mn ores were checked for natural radioactivity before irradiation.

4.1.7 The detection limits

When using isotope source or low neutron flux source, for activation analysis, it is always necessary to measure or calculate the detection limits for elements that are likely to be determined, since neutron flux is an important parameter which places strong limitation on sensitivity or detection limit of the element. The detection limit specifies the minimum amount of the element that can be determined. In general, it is the limit at which a given analytical procedure may be relied upon to lead to detection. It refers to the maximum upper limit of the capabilities of the measurement process (Currie, 1968).

The detection limit for Al, Mo, W, Mn, I, Br, V, As, and Na were calculated using the method given by Currie (1968). The detection limit, L , is given by:

$$L_D = k^2 + 2k \left[\mu_b + \sigma_b^2 + \mu_I + \sigma_I^2\right]^{\frac{1}{2}} \qquad 4.1$$

were k= abscissa of the standardized normal distribution

μ_b= mean number of background counts

σ_b= standard deviation of background

μ_I= mean number of counts from an interfering radiation

σI= standard deviation of of interfering radiation

If the the background rate is b(x) and the time of counting ▲t the mean number of background counts is:-

$$\mu_b = b(x)\ \blacktriangle t \qquad 4.2$$

The detection limit is related to the minimum detectable mass M (Currie, 1968) by:-

$$M_D = L_D/C \qquad 4.3$$

where C is the calibration factor relating the detector response to the mass present. The simplified form of this equation (Khalil (b) 1985) is

$$M_D = \frac{LD/\blacktriangle t}{C/\blacktriangle t} = \frac{L_D(R)}{r} \qquad 4.4$$

Where ▲t is the background counting time and the parameter r is the counts per second per gram and can be got from the slope of the calibration curve for the element concerned. In the evaluation of the detection limit, we used a confidence level of 99.865% corresponding to a value of k = 3 (Khalil (b), 1985)

4.1.8 Mn concentration in the ore.

The concentration of Mn in a sample C_x can be determined from that of standard, C_s by the following equation (Das *et al.* ,1993)

$$C_X = C_S \cdot \frac{M_S A_X (1-e^{-Xt1})_S (e^{Xt2})_X (1-e^{-Xt3})_S \Gamma_S F_{as}}{M_X A_S (1-e^{-Xt1})_X (e^{Xt2})_S (1-e^{-Xt3})_X \Gamma_X F_{ax}} \qquad 4.5$$

Where M = mass (g)

A = counting results in (counts/seconds)

t_1 = irradiation time (seconds)

t_2 = decay time

t_3 = counting time in (seconds)

X = decay constant (sec)

Γ = Geometry Factor =

F = Self absorption Factor

By equalizing irradiation time, counting time for both samples and standards and restricting to the same heights, $H_X = H_S = H$, and using the same mass of standard and sample

$$C_X = C_S \frac{A_X}{A_S} F(\blacktriangle p) \qquad 4.6)$$

Where $F(\blacktriangle p)$ is the correction factor for difference in density between standard and sample it also account for self absorption.

The plot of A_S and C_S gives a calibration curve whose slope depends on irradiation position .Thus the positions were numbered and calibrated separately for standardized fixed height of the aliquots. The concentration of the ore based on the calibration curve is

$$C_X = \frac{A_X}{\text{Slope of the calibration curve}} \qquad 4.7$$

4.1.9 Precision and accuracy of NAA

main sources of variance (errors that may affect the results) are radioactivity counting statistics, reproducibility of positioning of standards and samples, the influence of height and self absorption, weighing, irradiation time and decay, and interferences.

On the counting statistics, the expression for the standard deviation in A_X counts is given (Das *et.al.*,1993) by :-

$$\sigma(A_X) = (A_X + (1 + N/2)B_X)^{\frac{1}{2}} \qquad 4.8$$

where N = number of channels in the peak

B_X = background obtained by linear interpolation between the terminating channels.

The usual techniques to reduce the standard deviation is to maintain a good shielding practice so as to reduce B_X. In the set up, the detector and sample/standard are maintained in a lead shield whenever measurements are taken.

The position of the irradiation container, during irradiation and counting must be controlled with great care for good reproducibility. The positioning of the container during irradiation is not a problem using the aliquot recommended for the work, since the difference in diameter between it and irradiation hole is less than 2mm.

Repeated irradiations of 20% Mn standard at the same sample position gave a standard deviation of 1%. When a foil is used precaution must be taken to control the positioning. The inhomogeneity of the flux distribution with its strong gradients in the near vicinity of the source (Riepo, 1983, Mustapha *et al.*, 1994), where irradiations are preferentially carried out because of the relatively low strength of isotope neutron sources as well as the rapid spatial variation of the thermal to fast ratio (Op de Beeck, 1986), make positioning errors the preponderant source of variance in the case of negligible counting statistical errors. Repeated measurements for indium foil (1mm thick) resulted in standard deviation of 6%.

The systematic error due to height is avoided by maintaining a constant height for both sample and standard throughout the work, however the error due self-absorption is not completely reduced by height restriction as these depends on the density (Das *et al.*, 1993). This error which is less pronounced for powder sample is incorporated in the calibration curve.

If the calibration curve in each case is describe by $Y = aX + b$ were Y and X reprents the counting rate in counts per second and concentration in % respectively, the standard deviation in the concentration (Khalil (a), 1985) is given by:

$$\sigma_x = X \left[\frac{\sigma_y^2 - \sigma_b^2}{(y - b)^2} + \left[\frac{\sigma_a}{a}\right]^2 \right]^{\frac{1}{2}} \qquad 4.9$$

where σ_y^2 = variance in the directly measured value

σ_a^2 = is variance in the slope.

σ_b^2 = is variance of intercept

b = the intercept of the curve and

a = slope of the calibration curve.

4.2 X-Ray Fluorescence Analysis

4.2.1 Instrumentation

The XRF set up used for this work consists of a Silena Si(Li) detector, and its preamplifier (model SLG-13-3- 170), computer controlled high voltage bias/amplifier (model 9300/7), a computer based Emcaplus card acquisition system and interchangeable radioisotope sources (^{55}Fe and ^{109}Cd). The experimental setup is shown in figure 4.5.

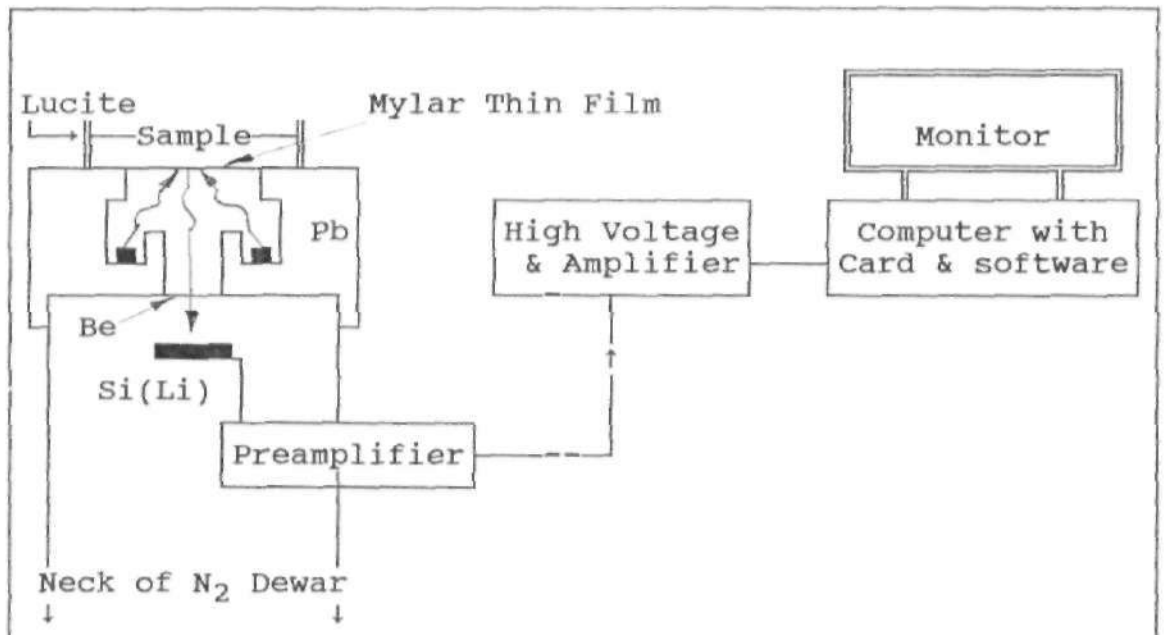


Figure 4.5 XRF Setup at CERT

The energy dispersive x-ray spectrometer in CERT, is combined with a dedicated computer for easy data reduction. With the proper software installed, the computer carries out peak location, energy assignment, element identification, smooothening, background subtraction, normalization, matrix correction, curve fitting, interelement correlation, data print out and other functions.

4.2.2 Measurements

The direct comparison method, with the necessary corrections for absorption using as guide Compton scattered peaks and peak ratio, was used. The analytical usefulness of peaks and peak ratio was studied previously (Shenberg et al, 1971). In a single element system, the ratio of an x-ray fluorescent line to a back scattered line of the target was found to vary linearly with the concentration of the element over a wide range. In a multi-element analysis, involving the use of sample-standard, differences in the Compton peaks could mean variation in matrix or mismatch between standard and sample.

Mathematical corrections can be readily applied in order to resolve the interelemet effects. The equation known as Beers law (Wheeler et al., 1976) was used and it is given by:

$$C\% = A + B.I_C.e^{(M1I1 + M2I2 + .. + MnIn)} \quad 4.10$$

Where C% = Percentage of element C present.

A = the x intercept

B = the slope of calibration curve

I_c = Intensity of element C

M_1, M_2, M_n = Positive or negative constants of interfering elements 1,2,3 derived from the calibration standards

I_1, I_2, I_n= Intensities of interfering elements.

This expression, was found ideal for the Mn-fe component of the Mn ore using ^{109}Cd. Mn has its absorption edge just below the K of Fe and would cause interference in Fe evaluation.

A total of 13 samples were analyzed for Si, Mn, Fe and Ca, The samples chosen here were mainly from the Mn rich zones, as the aim of the XRF method used here is to compliment the NAA so as to be able assess the Mn occurrences. The process involves placing fine powder of sample or standard in a Prolene x-ray spectrochemical sample support with thin film mylar base of thickness 2.5 microns. The thin film support ensures minimum absorption and flat surface for XRF analysis. The counting time after the preliminary energy calibration depends on the radioisotope sources, amount of the wanted element in the sample. One hour was found sufficient counting time to produce well resolved photopeaks of all the elements determined.

4.2.3 Precision and accuracy

Accuracy, precision and the minimum detable concentration depends on the element to be measured, the form of the sample (solid, liquid, powder, slurry, pellet), the concentration of the element, the concentration and variations in concentration of the other elements present, the type of the detector, the energy and intensity of the exciting source and the counting time (Papez and Cameron, 1973). Other systemic factors as sample composition and sample preparation also contribute to sensitivity and accuracy.

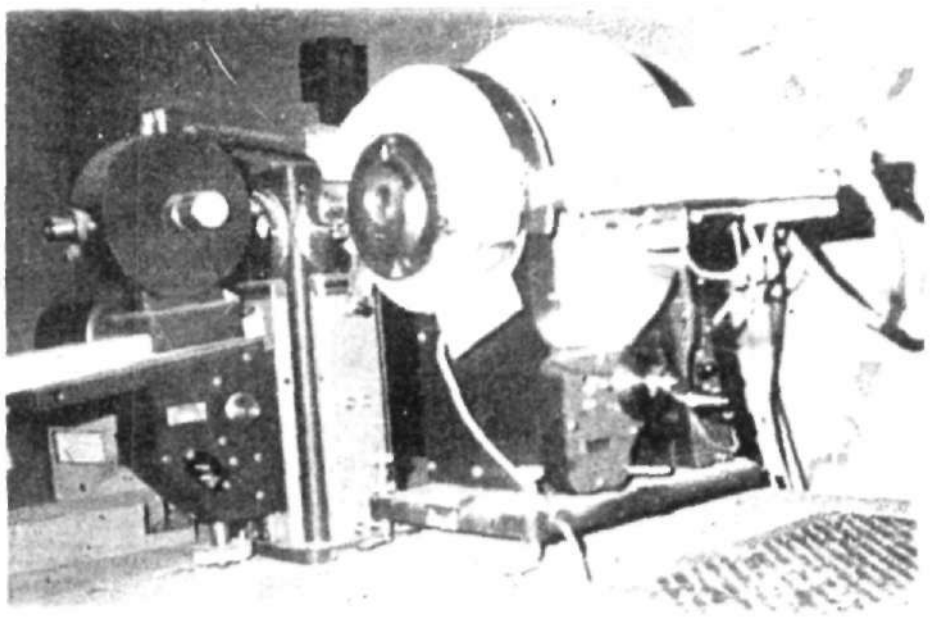
Standards for calibration were made by mixing to homogeneity known quantities of chemically pure powders in a manner that simulates the concentration of the elements in the matrix in which it is to be determined, thus minimizing the error due to matrix absorption. Sufficient number of counts were taken. Precision was determined by replicate analysis of the representative samples.

4.3 X-Ray Diffraction Analysis (XRD)

4.3.1 Instrumentation

The XRD analysis was carried out using a Philips diffraction machine which consists of: goniometer (PW 1050), goniometer power supply (PW 1373), single pen recorder (PM 8203) channel control (PW 1390), 4KW constant potential generator and X-ray tube in its tube shield (PW 1316). Plate 4.2 is the photograph of the X-ray diffractometer.

The set-up can be used for both single crystal and powder techniques. The X-ray tube in the diffractometer system is fully enclosed in a tube shield. This tube shield is mounted on top of the generator cabinet. X-rays can be beamed from four ports. One on each of the four sides of the tube shield. Each port has an electrmagnetically operated shutter which is only opened when power is applied. Unused pots are closed by a blank disc. The shutter can only be opened by operating two push buttons simultaneously on the generator. The goniometer is employed with various accessories for x-ray diffraction. In this instrument, both hollow shaft, in which a specimen holder assembly can be mounted, and a worm wheel to which a counter probe arm can be attached, rotate, around the same axis in the same direction at speeds with ratio 1:2 as required for bragg reflection. A worm gear, a worm wheel and transmission gears are the main parts, the design of which assure high resolution and good reproducibility (Philips, 1985). The goniometer can be operated manually, or be driven by synchronous motor either unidirectional with increasing or decreasing angle, or in oscillatory manner between desired preset limits. The scanning range for the goniometer is approximately -38 to 175°(2θ) at the speeds of 1/8°, 1/4°, 1/2°, 1° and 2° (2θ) per minute. The accuracy of individual measurement of 2θ is ±0.0025°. (Philips 1985)



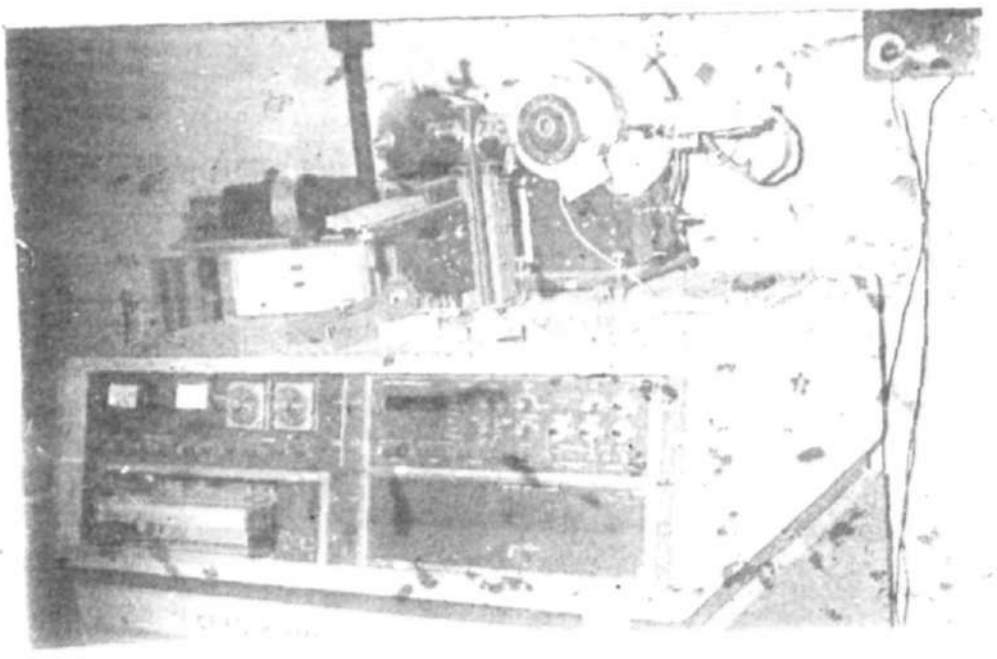


Plate 4.2 Photogragh of the Philips X-Ray Diffractometer

The steps for the operation of the x-ray diffraction machine includes: checking of the cooling water level, putting ON the x-ray radiation monitor, application of power supply, insertion of the suitably prepared sample into the sample position, chart recorder speed setting and the application of the high voltage to X-ray tube.

4.3.2 Sample preparation for XRD.

It is well recognised that the value of classical chemical analysis is critically dependent upon the sampling and sample preparation procedures adopted. This is also true of X-ray diffraction analysis. The influence of particle size upon the results obtained with x-ray analytical methods is well known and has been widely discussed in the literature (Alexander *et al.*, 1948). The character of diffraction ring is affected by the size of the crystallites. A very large size crystallite produces rings which consists of discrete spots. The optimum size results in sharp continous ring while too small a size results in broadening and of less contracting ring. (Vassamillet and King, 1968) Normally crystalline size of less than 50 microns (passing a 325 mesh screen) and larger than 0.5 micron would produce satisfactory results (Starbuck, 1967). To avoid errors due to variation in particle size, special care must be exercised during the grinding proccess.

The grinding for the XRD samples were done in two stages each. After the first stage, it was passed through a 60μM sieve available at the Department of Geology and the larger particles which were unable to pass through the sieve were regrounded and then finally mixed thouroughly. The double grinding ensures most of the particles reaches the uptimum particle size required for x-ray diffraction analysis.

4.3.3 Measurements

The powder diffraction method was used. The philips specimen holder used is a simple circular metal plate with a depression cut into it and a provision for fitting into goniometer. For every run, an excess of powder was sifted into the cavity, the powder tapped gently but firmly and uniformly with the edge of a spatula. Then excess powder was sliced off with a razor blade. Additional loose powder was sifted onto the cavity; then pressed into it with a glass slide. Excess powder was again sliced away and the specimen transferred to the goniometer. With the high voltage and anode current (typically, 40KeV and 30mA) applied to the x-ray tube and the goniometer properly initialized, the machine was allowed to run for 30 minutes, the time required for 60^{o} scanning.

4.3.4 Interpretation.

The mineral types of the powder samples were determined using a reference catalogue containing 2,000 X-ray powder

data files compiled under the auspices of a joint committee representing the ASTM and the American Crystallographic Association (Leonard 1974).

The procedure involves the preparation of the tables of experimental data using d-values in decreasing order along with the relative intensities. The index for the proper Hanawatt group for the strongest line of the unknown pattern is located, followed by search on the second column to find a match for the second strongest line of the pattern. The same procedure is carried out for third strongest line which agrees with the pattern. The unmatched lines, after the first mineral identification are tried in the same manner for the second mineral identification and so on.

CHAPTER FIVE

5.0 RESULTS AND DISCUSSION

The results are presented and discussed in five parts: (a) charaterization of the moderating system, which includes the measurement of thermal/epithermal neutron flux, (b) the determination of the detection limits for 9 elements (Al, Br, Mo, Mn, W, As, I, Na,and V); (c) measurement of Mn concentration in ore samples by NAA (d) measurement of the concentrations of Mn, Fe, Si and Ca in the rich ore samples by XRF and (e) and the determination of the mineralogy of the ores by XRD.

5.1 Thermal/Epithermal Flux Measurement

The results for the flux measurement at each of the six positions are presented in Table 5.1. (The flux calculation based on equation 2.14 was done with indium foil using data in appendix 3). The results for the foil in

Table 5.1 Thermal/Epithermal Flux Values for the Six Irradiation Positions.

	POSITIONS					
	1	2	3	4	5	6
Countrates(cps) (Bare In foil)	341.8	379.6	403.0	453.0	414.7	383.5
Countrates(cps) (In in Cd box)	20.21	22.38	23.96	27.44	25.50	21.93
Cadmium Ratio $R_{CD}=A_{tot}/A_{epi}$	16.9	17.0	16.8	16.5	16.3	17.5
Cadmium Factor $F_{CD}=(R_{CD}-1)/R_{CD}$	0.940	0.941	0.940	0.939	0.938	0.943
Thermal Flux $x10^4 ncm^{-2}s^{-1}$	2.367	2.629	2.791	3.130	2.866	2.650
Epithermal flux $x10^2 ncm^{-2}s^{-1}$	1.151	1.275	1.365	1.563	1.453	1.229

cadmium box subjected to the same irradiation/counting procedure is also shown in Table 5.1.

The variation of the thermal/epithermal flux (Table 5.1) with positions is further illustrated in figure 5.1. The figure shows some anisotropy of the system about the irradiation positions. Position 4 gave the highest flux of 3.130×10^4 n/cm^2/sec followed by position 5 with (2.8659×10^4 n/cm^2 /sec), position 3 (2.791×10^4 n/cm^2/s), Position 2 (2.6287×10^4 n/cm^2/sec), Position 6 (2.649×10^4 n/cm^2/sec) and Position 1 (2.3667×10^4 n/cm^2/sec). This variation in flux is also true for the indium foil in the cadmium box. The measured cadmium ratio ($R_{CD} = A_{to}/A_{epi}$), for individual positions are : Position 1 (16.9), Position 2 (17.0) Position 3 (16.8), Position 4 (16.5), Position 5 (16.3), and Position 6 (17.5) This results in an average value of 16.83 for the cadmium ratio, R_{CD}.

Table 5.2 represents the directional dependence of the thermal flux. Here the foil is covered on one side by an open cadmium box and exposed on the other. The angle the plane of the foil makes with source is 0° if the open end is facing the source. This particular result is vital for foil samples activation as direction or position within any particular irradiation hole produces slightly different flux values. The following countrates/angle values were got 0° (27.138 c/s), 45° (29.825 c/s), 90° (32.070 c/s), 135° (33.937c/s) and 180°(33.954c/s). The plot of the directional dependence of the flux is shown in figure 5.2. This was done

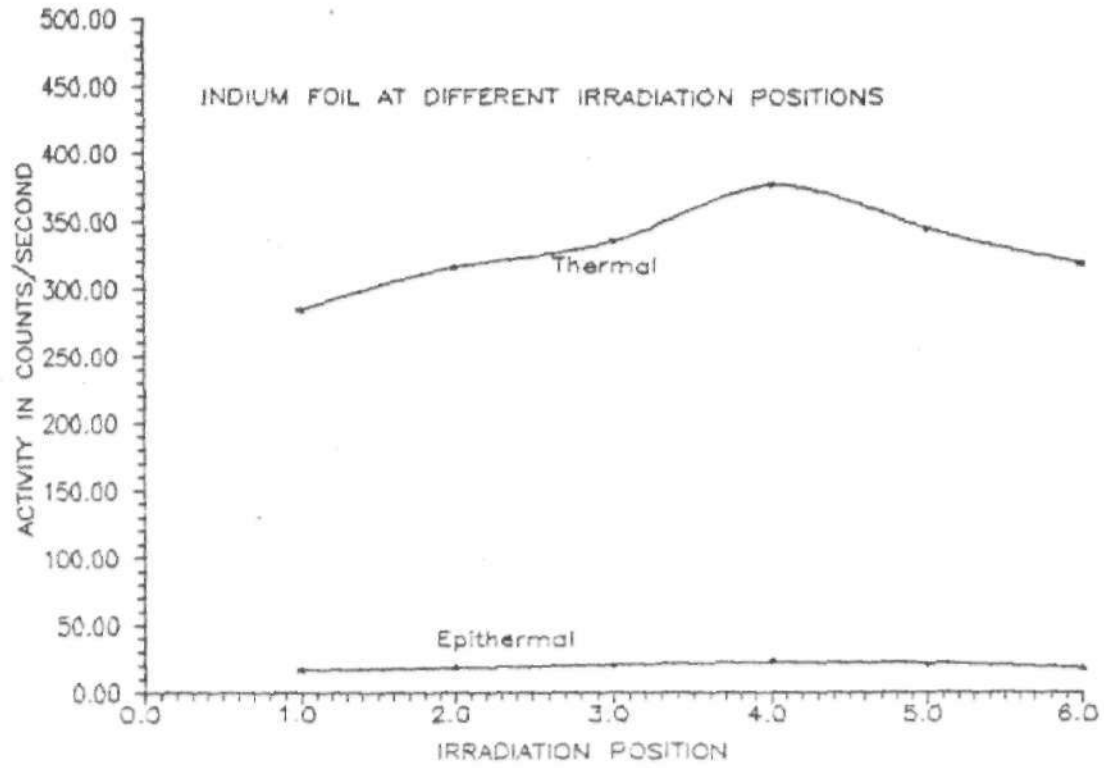


Figure 5.1 Thermal/epithermal activity versus position of irradiation with indium foil

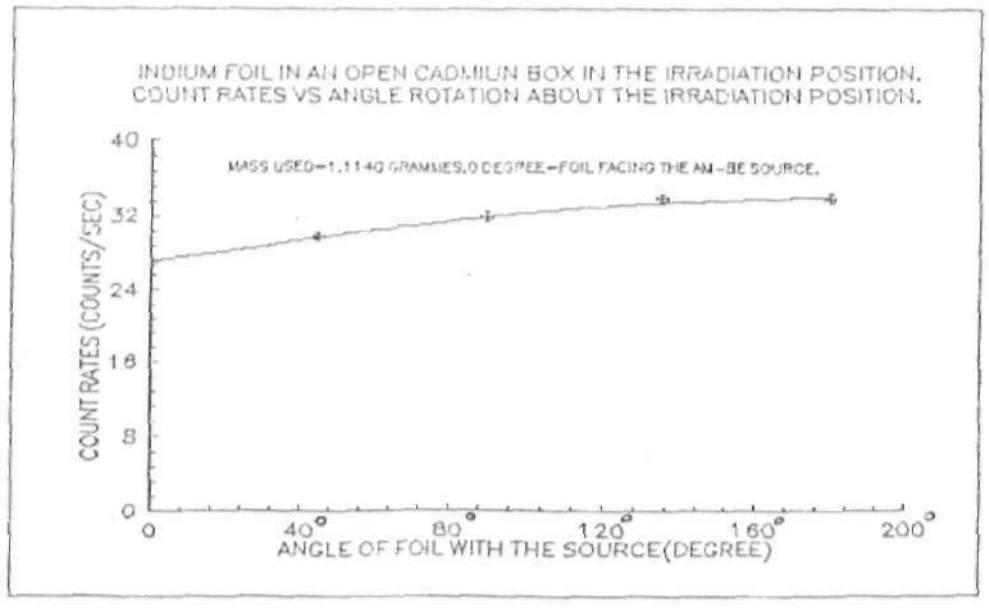


Figure 5.2 Directional dependence of activity at position 3 with an indium foil in open Cd box

Table 5.2 The directional dependence of the Countrates in Position 3

	Angle btw source and position θ°	Countrate (Counts/sec)
1	0	27.138
2	45	29.825
3	90	32.070
4	135	33.937
5	180	33.954

Mass of Indium Foil used = 1.15g

Table 5.3 The Flux Values at Different Heights of Irradiation (Position 3)

	Distance from Base of Irradiation Position (cm)	Countrate (Counts/s)	Flux (n/cm^2 /s)
1	1	94.115	27405.1
2	3	71.027	20682.2
3	5	56.318	16399.1
4	7	43.843	12766.5
5	9	28.580	8322.1
6	11	23.013	6701.1
7	13	17.483	5090.8
8	15	12.628	3677.1

Mass of sample used = 1.15g

for position 3 only, as it represents the flux value closest to the average.

The measurement of the lateral flux variation with height in the irradiation position 3 is shown in table 5.3. and plotted in figure 5.3. A similar measurement was done by Mustapha *et.al*. (1994) for the same ^{241}Am-Be source and a neutron howitzer designed by them. In their work, the measurement was from the surface of the source itself to about 12cm away. In this case, the height is measured from the bottom of irradiation position (2.5cm from the source).

The flux dependence on positions, is an indication of anisotropy of the system, either due to the paraffin moderating system or the Am-Be source itself. The later reason, the anisotropy of the source output depends on the source type, dimensions, encapsulation and support (Burger and Schwartz, 1988). The formal reason may be due to :

(a) shift in the preset source-sample positions due to buckling of the polyethylene pipes as a result of temperature effect during the casting of the paraffin

(b) difference in heights between irradiation positions as result of initial error in the setting of the levels during construction.

An effort to find the reason for the asymmetry in flux between positions was attempted; sample heights were cross checked by measurement, the positions inspected and they were found to be in conformity with the design. Although, a

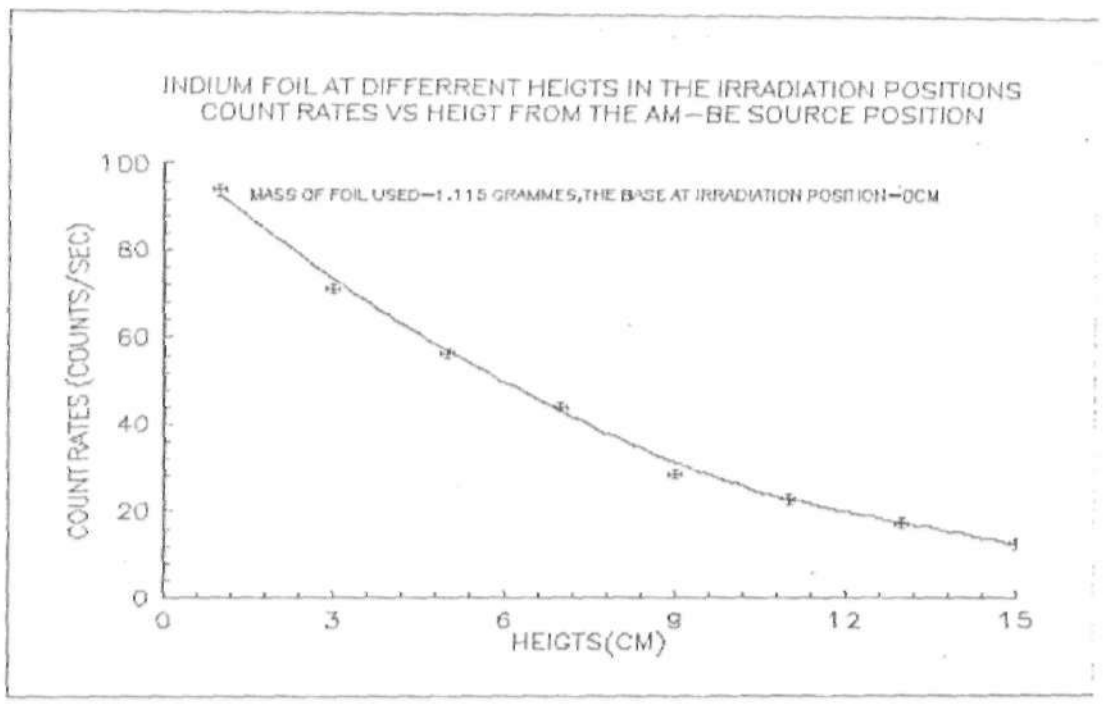


Fig 5.3 Height dependence of activity in an irradiation position3.

small dimensional difference in the neighborhood of source, where spatial variation of flux is significant, can give rise to anisotropy but would not be able to account adequately for the fairly symmetric result about any position, as was observed about position 4. These leaves the the source anisotropy as the probable reason for flux variation with positions. Anisotropy of the bare source is usually determined by a complicated experiment that involves taking special precaution with respect to neutron scattering (Burger and Schurtz 1988), and would be outside the scope of this work.

An interesting result of the evaluation of irradiation system is the lateral variation of the flux within an irradiation hole. Figure 5.3 is the plot of this variation with height. It is seen that the flux values remain significant at a height enough to accomodate one or two extra samples. However, to do this one must remember that such an experimental assembly usually results in shielding and pertubation. A sample under irradiation generally causes a thermal flux depression within its own volume and its immediate vicinity due to the absorption of the neutrons in the sample. A sample may thus be placed where the flux perturbation caused by other experiment become noticable and could give irreproducible results.

5.2 Detection Limits for Na, Al, V, Mn, As, Br, Mo, I and W.

This was based on Currie's method (Currie 1968). The application of the Currie's method for the evaluation

ofdetection limit requires the specific activity. This can be evaluated from the calibration curve for the element. The calibration curves for W, V, Br, I, As, Na, Al, and Mo are shown in figure 5.4. The chemical forms, and weights of the sample used in the experiments, as well as the counting intensities of the most prominent photopeaks in each spectrum are shown in appendix 2. From the calibration curve, the specific activities for the elements are: W (6.450 cps/g), V (6.365 cps/g), Br(0.953 cps/g), I (3.380 cps/g), As (3.66 cps/g), Na (1.47 cps/g), Al (0.447 cps/g), Mo (0.550 cps/g), Mn (38.49 cps/g).

The background using SiO_2 as blank within the channels of the elements and the background corresponding to the lowest concentration of the individual elements are presented in appendix 2. The slope of the calibration curve, the photopeaks used, and the minimum detectable mass for these elements are shown in table 5.4. From the table ,it is observed that Mn has the lowest detectable mass (0.009g)among these elements followed by V (0.110g)

5.3 Mn ORE CONCENTRATION BY NAA.

The calibration for Mn concentration was done for each irradiation position and all the positions together for both powder and solution of potassium permanganate standard. The calibration for every hole and all holes together, is necessary because of the varying degrees of concentration

Table 5.4 Detection Limits for Different Elements

Elements	Photo-peaks (KeV)	Slope of the Calibration Curve (cps/g)	Minimum Detectable Mass (g)
^{23}Na	1368.5	1.470	0.246
^{27}Al	1779.0	0.447	1.031
^{51}V	1434.1	6.365	0.110
^{55}Mn	846.4	38.59	0.009
^{75}As	559.1	3.660	0.191
^{79}Br	616.2	0.953	1.121
^{98}Mo	140.5	0.550	2.898
^{127}I	442.9	3.380	0.327
^{187}W	479.5	6.450	0.105

of the Mn bearing ore-the rich ore could be analyzed with a single irradiation position while for the low grade ore, irradiation using all the position at a time is much more suitable. Tables 5.5 to 5.6 are the concentrations versus activities of manganese in potassium permanganate ($KMnO_4$) for individual position. The results for the six positions irradiated and counted together are in Tables 6.7-8.

Based on the calibration curves of the standard, the concentrations of Mn in the ores from the different localities were evaluated. Table 5.9 shows the localities and the respective ranges of the concentration of Mn. Farin-Ruwa has the highest concentration of Mn with the

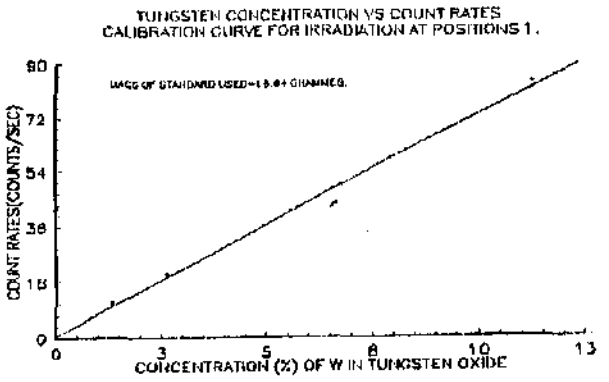


Fig .4 Calibration curve tungsten

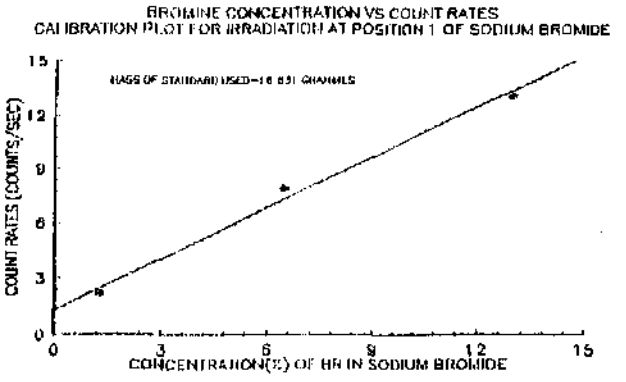


Fig. .6 Calibration curve for Bromine

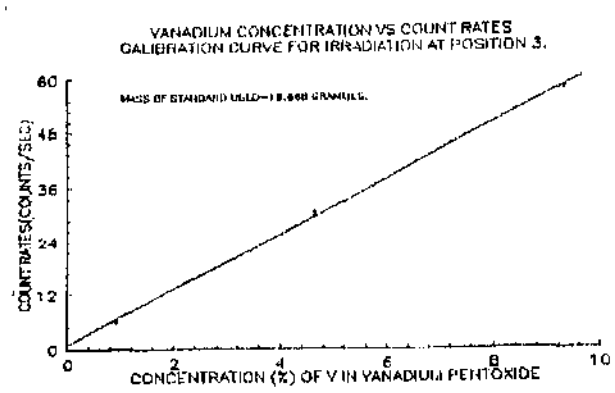


Fig 5 Calibration curve for vanadium

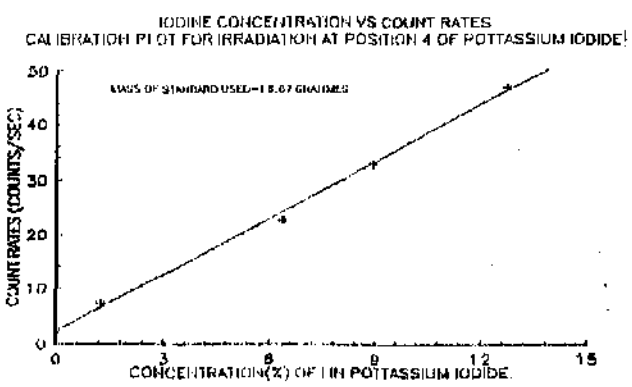


Fig. .7 Calibration curve for Iodine

Fig 5.4a Calibration Curves for W, Br, V, I

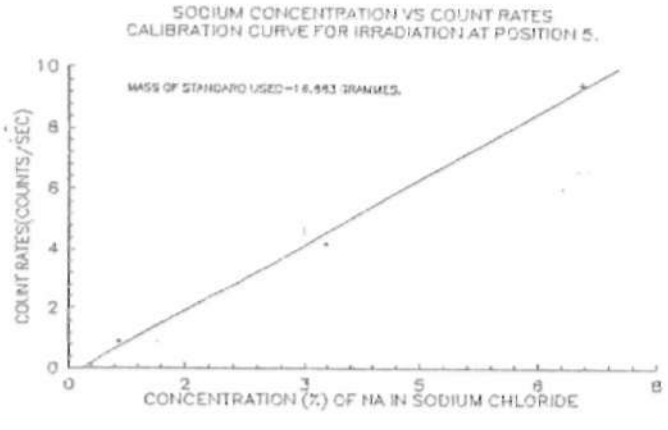


Fig .9 Calibration curve for Sodium

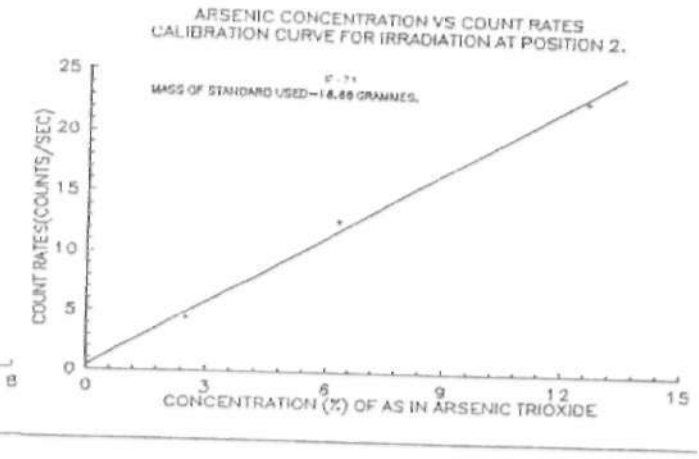


Fig .8 Calibration curve for Arsenic

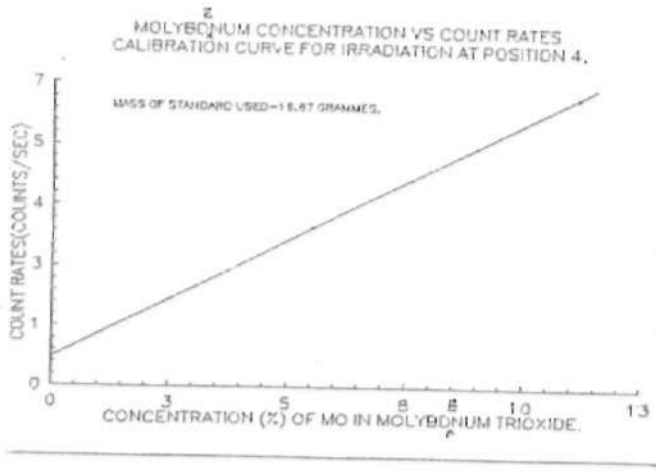


Fig 6.11 Calibration curve for Molybdenum

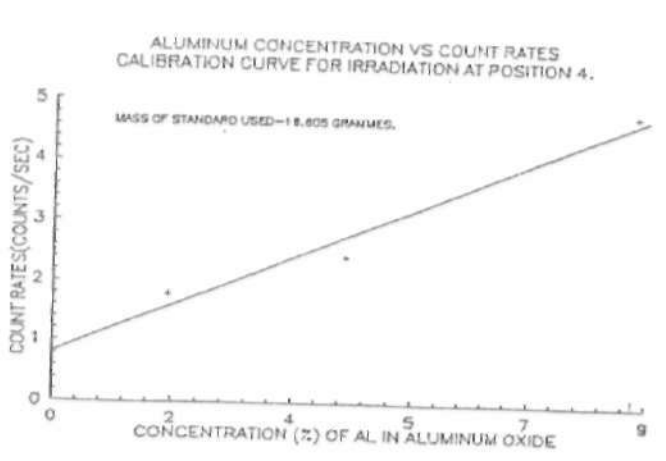


Fig 6.10 Calibration curve for Aluminum

Fig 5.4b Calibration curves for Na, As, Mo, and Al

Table 5.5 Count Rates/Mn Concentration for the Six Irradiation Positions (16.66g $KMno_4$)

$KMnO_4$ (Wt%)	Mn (Wt%)	Count Rate (Counts/sec) at Positions (P) 1	2	3	4	5	6
10	3.48	19.80	21.80	23.38	26.03	23.39	21.27
20	6.96	39.30	44.81	47.76	52.60	45.81	43.71
30	10.44	59.36	65.49	67.73	76.62	68.79	63.59
40	13.92	76.55	87.82	96.78	101.38	90.60	81.57
50	17.41	95.52	106.61	116.37	130.52	115.96	102.68
60	20.89	115.36	129.90	133.19	151.86	138.48	126.30
70	24.37	140.61	155.11	154.38	173.06	155.60	143.84
80	27.85	162.22	169.45	179.47	195.46	173.17	160.26
90	31.33	174.38	184.18	197.33	214.17	186.99	177.96
100	34.81	185.03	191.23	207.13	222.95	198.11	189.62

Table 5.6 Count rate/Mn concentration for the six positions of irradiation (15Ml $KMnO_4$ solution)

$KMnO_4$ Solution (g/l)	Mn (g/l)	Count Rates (Counts/sec) at Positions (P) 1	2	3	4	5	6
10	3.48	1.39	1.94	2.09	2.63	2.36	2.24
20	6.96	2.79	3.41	4.04	4.18	4.06	3.86
30	10.44	4.00	6.00	6.84	8.09	6.73	5.07
40	13.92	6.40	7.34	9.78	9.99	8.90	9.38
50	17.40	7.26	10.21	11.17	12.27	11.26	10.19

Table 5.7 Count Rate / Mn Concentration at All Positions Counted Together (100g $KMnO_4$ Powder)

$KMnO_4$ Powder (Wt%)	Mn Weight (Wt%)	All Positions Counted together. Count Rate (Counts/sec)
10	3.48	138.15 ± 0.580
20	6.96	278.24 ± 0.835
30	10.44	410.51 ± 1.194
40	13.92	527.54 ± 1.161
50	17.41	702.55 ± 1.194
60	20.89	817.28 ± 1.225
70	24.37	929.41 ± 1.673
80	27.85	1032.42 ± 1.651
90	31.33	1120.98 ± 1.569
100	34.81	1218.34 ± 1.816

Table 5.8 Count Rate /Mn Concentration at All Positions Counted together (90ml $KMnO_4$ solution)

$KMnO_4$ Solution (g/l)	Mn in Solution (g/l)	All Positions Counted Together Count Rates (Counts/sec)
0.1	0.04	0.202 ± 134 %
1.0	0.35	0.994 ± 29.9%
10	3.48	12.900 ± 2.38%
20	6.96	24.198 ± 1.49%
30	10.44	37.783 ± 1.03%
40	13.92	54.376 ± 0.82%
50	17.41	64.971 ± 0.68%

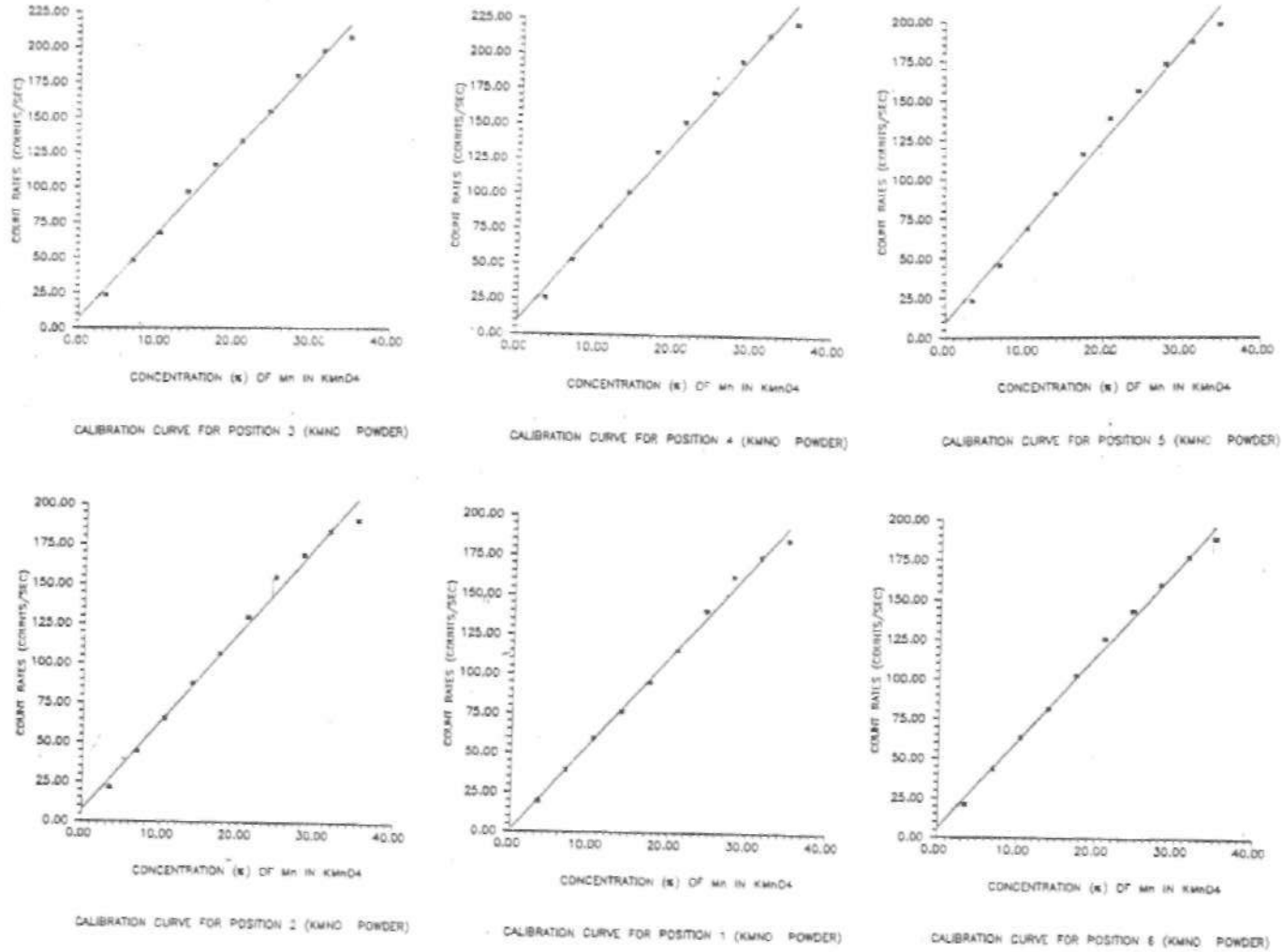
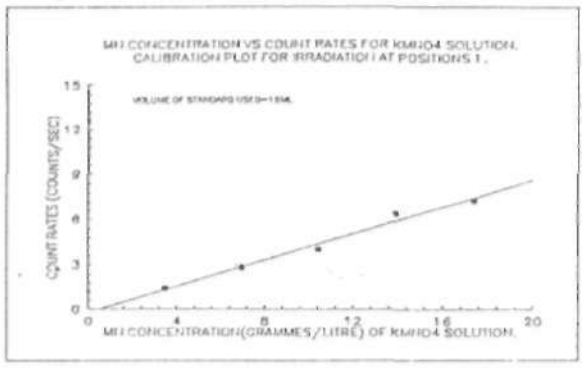
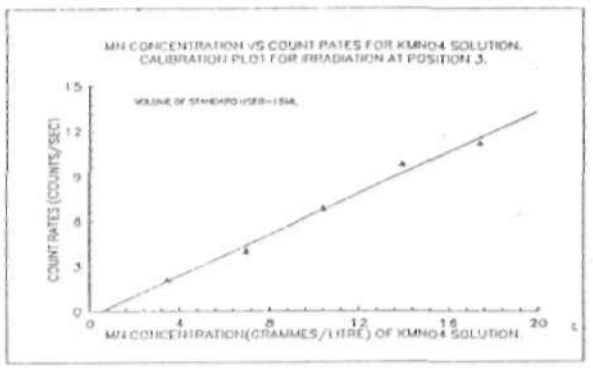


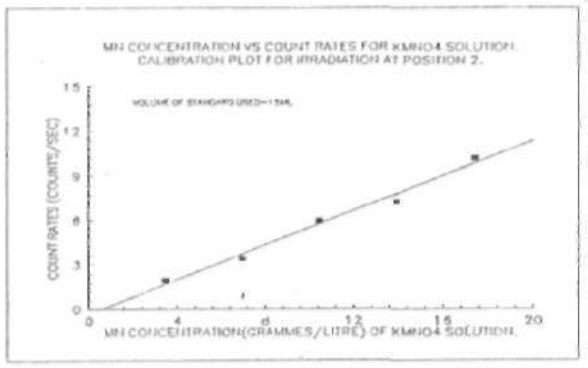
Fig 5.5 Mn calibration Curves for the six irradiation positions (powder 16.66g-$KMnO_4$)



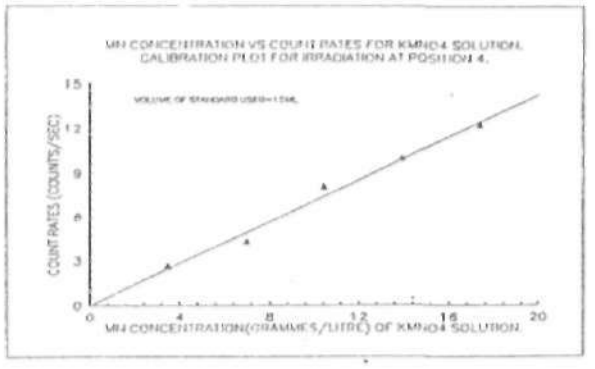
Calibration curve for position 1 (solution)



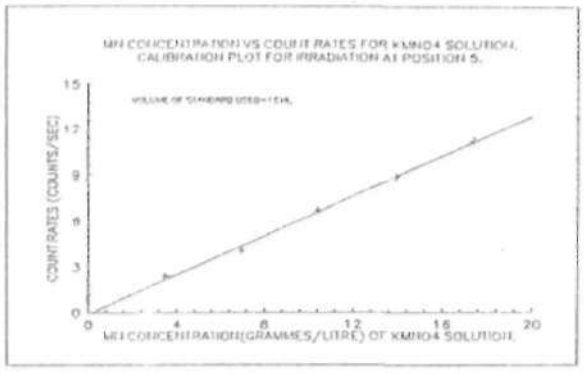
Calibration curve for Mn at position 3 (solution)



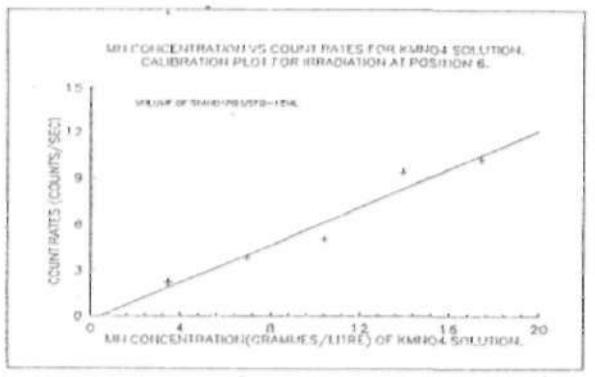
Calibration curve for Mn at position 2 (solution)



Calibration curve for Mn at position 4 (solution)

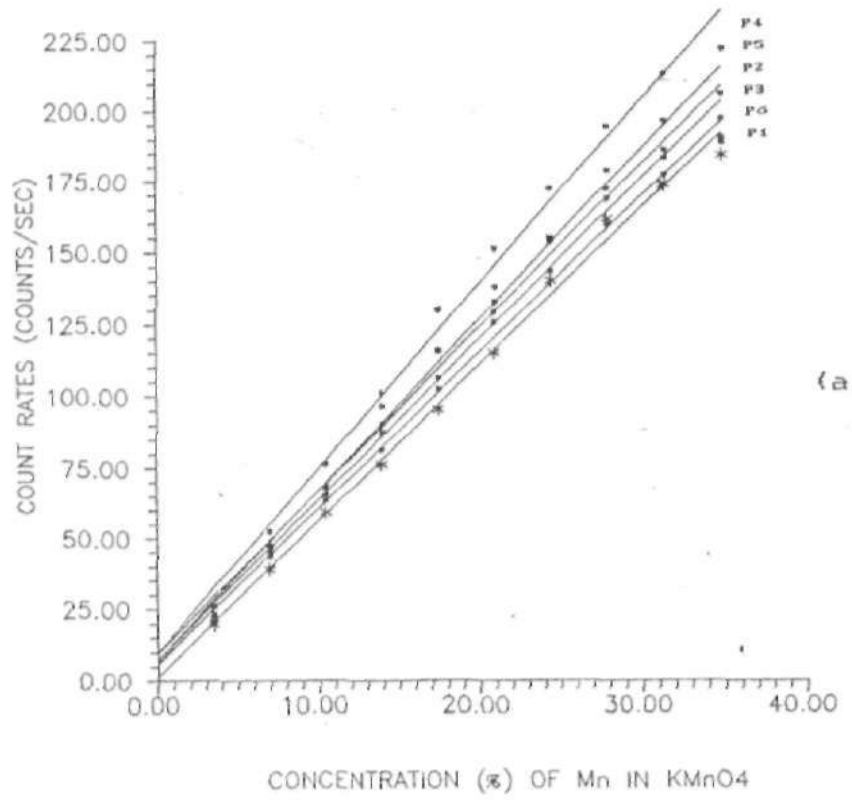


Calibration curve for Mn at position 5 (solution)

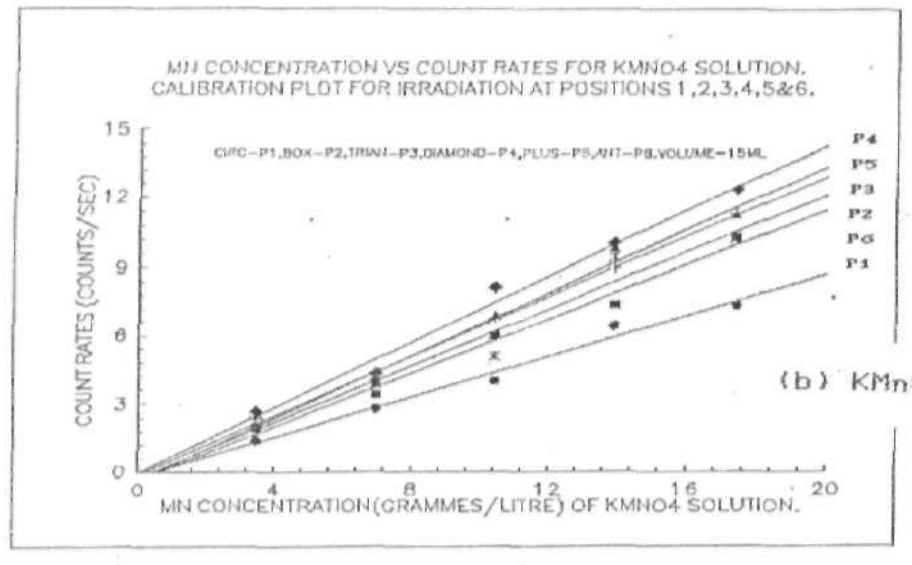


Calibration Curve for Mn at position 6 (solution)

Fig 5.6 Mn calibration Curves for the six irradiation positions (solution 15ml $KMno_4$)



(a) $KMnO_4$ – POWDER



(b) $KMnO_4$-SOLUTION

Fig 5.7 Comparison of calibration curves for Mn at the six irradiation positions

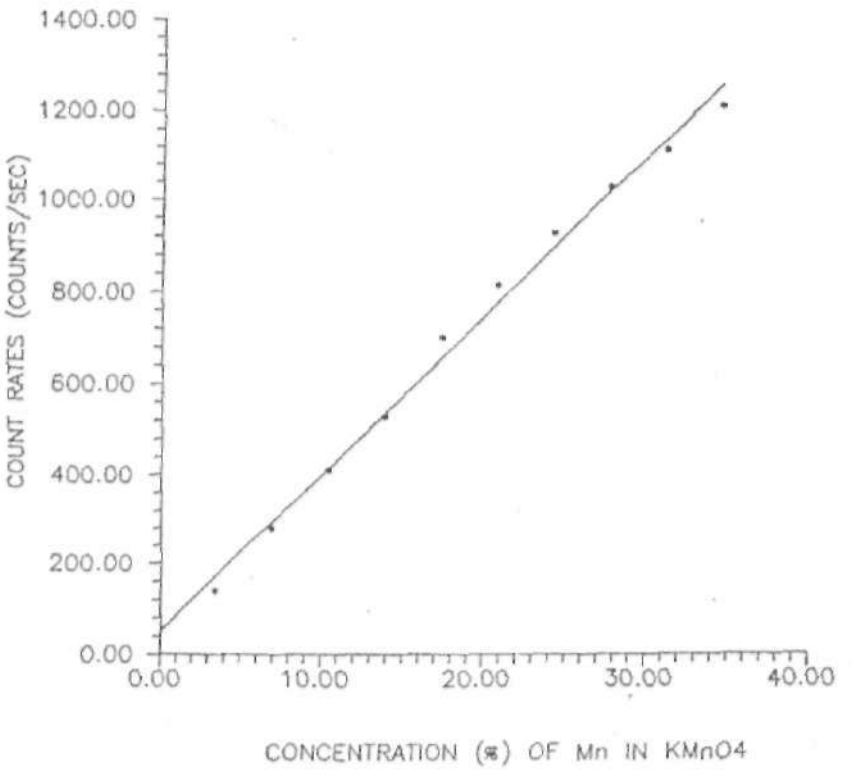


Fig. 5.8 Calibration Curves for Mn at all six positions counted together (100g $KMnO_4$ powder)

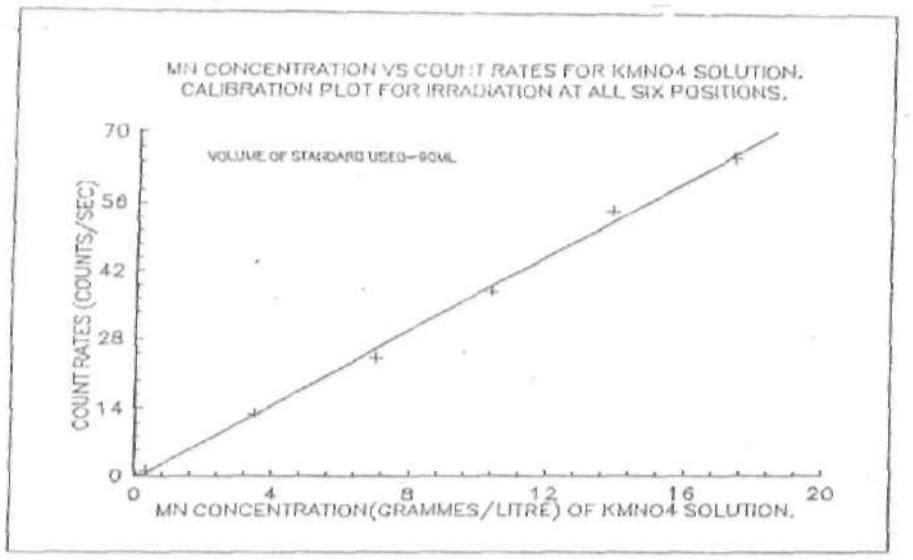


Fig. 5.9 Calibration Curves for Mn at all six positions counted together (90ml $KMnO_4$ solution)

Table 5.9 The concentration Mn in the rock samples

Locality	Sample number	Count Rate (Counts/sec)	Mn Concentration (Wt%)
Tudun-Kudu	TK1	299.21 ± 1.0	8.55 ± 0.12
	TK2	p6 122.63 ± 0.5	22.31 ± 0.14
	TK3	p1 102.81 ± 0.5	18.65 ± 0.11
	TK4	1068.46 ± 1.4	30.53 ± 0.42
	TK5	758.15 ± 1.1	21.66 ± 0.23
	TK6	934.90 ± 1.3	26.71 ± 0.37
Ruwan-Dorowa	RD1	312.71 ± 1.0	12.77 ± 0.18
	RD2	470.44 ± 1.0	13.44 ± 0.18
	RD3	436.12 ± 0.9	12.46 ± 0.18
	RD4	417.67 ± 0.9	11.93 ± 0.17
	RD5	446.47 ± 0.7	8.93 ± 0.12
Maraba Hills	MH1	207.34 ± 0.7	5.92 ± 0.09
	MH2	249.54 ± 0.9	7.13 ± 0.11
	MH3	320.41 ± 0.9	9.16 ± 0.14
	MH4	194.07 ± 0.7	5.55 ± 0.08
	MH5	218.15 ± 0.8	6.23 ± 0.09
Anguwangudu	AG1	153.59 ± 0.7	4.39 ± 0.07
	AG2	p2 47.98 ± 0.5	8.47 ± 0.09
	AG3	p4 36.13 ± 0.4	5.54 ± 0.10
Kansani-Kuyazo	KK1	153.73 ± 0.7	4.39 ± 0.07
	KK2	222.16 ± 0.8	6.35 ± 0.10
	KK3	185.42 ± 0.7	5.30 ± 0.09
	KK4	p3 32.30 ± 0.3	5.37 ± 0.08

Table 5.9 The concentration of Mn in the rock samples

Locality	Sample Number	Count Rate Counts/sec)	Mn Concentration (Wt%)
Farin-Ruwa	FR1	640.878 ± 1.3	18.31 ± 0.25
	FR2	p_2 260.036 ± 1.3	45.91 ± 0.64
	FR3	1543.136 ± 1.7	44.09 ± 0.61
	FR4	1194.161 ± 1.7	34.12 ± 0.47
	FR5	1234.887 ± 2.1	35.28 ± 0.48
	FR6	1190.601 ± 1.7	34.02 ± 0.47
	5KMF	197.440 ± 0.7	5.64 ± 0.09
Old Birnin	OBG1	135.895 ± 0.6	3.88 ± 0.07
	OBG2	174.021 ± 0.7	4.97 ± 0.08
	OBG3	140.131 ± 0.6	4.00 ± 0.07
	5KMD	36.587 ± 0.4	1.05 ± 0.43
Saulawa	SW1	199.049 ± 0.8	5.69 ± 0.09
	SW2	190.915 ± 0.7	5.46 ± 0.09
	SW3	224.045 ± 0.8	6.40 ± 0.10
Kirazo	KZ1	193.869 ± 0.8	5.54 ± 0.09
	KZ2	197.705 ± 0.8	5.65 ± 0.09
	KZ3	241.437 ± 0.9	6.90 ± 0.10
	KZ4	194.057 ± 0.8	5.54 ± 0.09
	KZ5	226.360 ± 0.8	6.47 ± 0.10
Maganda	MG1	299.362 ± 0.8	8.55 ± 0.14
	MG2	329.423 ± 1.0	9.41 ± 0.15
	MG3	208.978 ± 0.6	5.97 ± 0.10
	MG4	270.728 ± 0.9	7.73 ± 0.12

Table 5.9 The concentration of Mn in the rock samples

Locality	Sample Number	Count Rate Counts/sec)	Mn Concentration (Wt%)
Maganda	MG5	267.990 ± 0.8	7.66 ± 0.12
Kunji	KJ1	59.689 ± 0.5	1.71 ± 7%
	KJ2	24.118 ± 0.3	0.69 ± >40%
	KJ3	74.412 ± 0.5	2.13 ± 0.08
	KJ4	84.866 ± 0.6	2.43 ± 0.08
Bungudu	BG1	4.229 ± 0.3	0.12 ± >40%
	BG2	3.162 ± 0.3	0.09 ± ,,
	BG3	6.311 ± 0.3	0.18 ± ,,
Dandato	DT1	0.407 ± 0.3	0.01 ± ,,
Bonu	BN1	4.647 ± 0.3	0.13 ± ,,
	BN2	6.058 ± 0.3	0.17 ± ,,
Zungeru	ZG1	6.449 ± 0.4	0.18 ± ,,
	ZG2	7.174 ± 0.4	0.21 ± ,,
Kontagora	KG1	13.581 ± 0.3	0.40 ± ,,
	KG2	2.157 ± 0.3	0.06 ± ,,
Farin Ruwa Junction	FJ	421.596 ± 1.0	12.05 ± 0.18

concentration, ranging from 18.3-45.9%. Tudun Kudu has the second highest concentration about 8.6 to 30.5(%W) .Some localities, Dogodawa, Bunu, Zungeru, Dandato and Kontagora have recorded very low value of manganese that the ores there can be considered non Mn ore. From this table, the Mn

occurrences can be classified as follows :

(a) Mn ore- Farin Ruwa

(b) Ferruginous Mn ores- Tudun-Kudu and Ruwan Dorowa

(c) Manganiferrous ores- Maraba Hills, Anguwagudu, Kansani-Kuyazo, 5Km from Farin-Ruwa, Kirazo, Saulawa, and Maganda

(d) Fe ores or non ores- Kunji, Bungudu, Dandato, Bonu, Zungeru, and Kontagora

From the NAA results on Table 5.9, it is seen that the concentration values of Mn occurring in the Mn minerization show some variations within the same locality. This maybe as the result of the formation processes and the influence of later geological or geochemical processes. The Mn mineralization under study, is said to be epigenetic (Mucke and Okujeni ,1984), that is, the host rock and ore mineralization are not of the same age. Thus the concentration values of these elements do not show normal distribution from the point of view of frequency distribution, but vary between broad limits depending on the position of sampling.

The Mn ore sampling for this work was done without any definite objective of selecting only very rich ore that would satisfy industrial and chemical purposes but with the aim of analyzing the most representative samples so the great variation in concentration within the same locality is not due to inadequacies in the method of analysis or sampling.

5.4 XRF Measurement

The results of the measurements of K_α , K_β , I(compton) and the peak ratios for Ca, Si, Mn and Fe are on tables 5.10-5.13 respectively. K_α was used for Mn, Ca and Si determination but K_β radiation was used for iron evaluation because of the spectral overlap between the K_β of Mn and K_α of iron using Cd source. Spectral data for Ca, Si were accumulated using Fe source. The compton peak for this source (^{55}Fe) is at 5.9kev, this corresponds to the Mn K_α peak, so the observed compton peak variation was low for the ores and standard containing Mn.

Table 5.14 shows the result for the effect of Mn on 12.1(wt%) of Fe. This measurement is neccessary for the determination of the correction factors in the Beers law. This dependence as measured here is $\exp(-0.006376I_{\alpha,Mn})$ where -0.006376 is the negative constant of the interferring element (Mn) and $I_{\alpha,Mn}$ is the Mn K_α intensity.

The calibration curves for Mn, Fe, Ca and Si are shown in figure 5.10. The corresponding peaks, compton peaks and peak ratios are in figures 5.11. To estimate possible success for compensation in Fe determination, in the ore, the x-ray peaks for Mn K_α , Fe K_β together with the variation in the compton scattered intensity with matrix for all the ores were examined and compared in figure 5.13. It is to be observed that the K_α -compton peak ratio follows the trend of its Mn composition, but MnO_2 standard has peak ratios far from that of the ores. For reason of similarity

456075

MnO_2 in Al(OH) (Wt%)	Mn in (Wt%)	Mn I_α (C/sec)	20Kev Compton I_C (C/sec)	Peak Ratio I_α/I_C
20	12.64	3.099	6.165	0.503
40	25.28	7.812	5.779	1.352
60	37.92	11.232	2.584	4.347
80	50.55	14.860	2.191	6.782
100	63.19	18.232	1.492	12.219

Table 5.10 Mn K_α Intensity and the Compton Peak Ratio

$FeSO_4$ in Al(OH) (Wt%)	Fe in (Wt%)	Fe I_β (C/sec)	20Kev Compton I_C (c/sec)	Peak Ratio I_β/I_C
5	1.01	0.083	9.278	0.009
10	2.01	0.146	10.016	0.015
20	4.02	0.274	9.077	0.030
40	8.04	0.574	7.408	0.077
60	12.05	0.789	7.149	0.110
80	16.07	1.069	5.452	0.196

Table 5.11 1 Fe K_β Intensity Compton Peak Ratio

between ores and standard, the manganese standard with 12.1(wt%) iron was used for the Mn determination. Tables 5.15 and 5.16 are the measured K_α, K_β, I (Compton) and the concentration results for the selected Mn ore samples.

The objective of the XRF was the determination of Fe, Si and Ca in the Mn ores. This is important, since they have influence on most industrial processing methods for

$CaCO_3$ in Al(OH) (Wt%)	Ca in (Wt%)	Ca I_α (C/sec)	5.9Kev Compton I_C C/sec)	Peak Ratio I_α/I_C
1	0.41	2.476	12.236	0.202
3	1.20	6.062	11.929	0.508
5	2.02	7.019	11.633	0.603
10	4.14	19.706	11.461	1.719

Table 5.12
Ca K_α intensity and intensity Ratio

SiO_2 in Al(OH) (Wt%)	Si in (Wt%)	Si I_α (C/sec)	5.9Kev Compton I_C (C/sec)	Peak Ratio I_α/I_Cx10
10.0	4.68	0.883	15.153	0.583
20.0	9.35	1.456	12.853	1.132
40.0	18.69	2.041	12.018	1.698

Table 5.13
Si K_α intensity and Compton Peak Ratio

MnO_2 in 12% Fe +AL(OH) (Wt%)	Mn in (Wt%)	Mn I_α (C/sec)	Fe I_β (C/sec)	Compton I_C (C/sec)	Peak Ratio I_α/I_C	Peak Ratio I_β/I_Cx10
0.0	0.00	0.00	7.191	7.525	0.00	0.096
10.0	6.32	1.840	6.197	6.084	0.302	1.019
20.0	12.64	3.511	6.001	5.419	0.648	1.107
30.0	18.96	5.861	5.998	4.063	1.442	1.476
40.0	25.28	7.964	5.981	3.171	2.146	1.886

Table 5.14 The Evaluation of the Effect of Mn on 12.1% Fe

the Mn ore. In this investigation, the distribution of SiO_2 and CaO do not vary charateristically in samples of Mn ore but a fairly regular relation between MnO_2 and Fe_2O_3 in the ore is observed as in Table 5.17 and Figures 5.14-5.16. The result of correlation calculation is as follows:

			correlation coefficient
MnO_2 (W)%	-	Fe_2O_3	-0.77

Hence an increase in MnO_2 is accompanied by a fairly regular decrease in Fe_2O_3 in the Mn ore sample.

Anohter important observation of the XRF analysis is that MnO_2 +Fe_2O_3 +SiO_2 equivalent exceeds 70% by weight (Table 5.18) of most ore samples analysed by XRF except three samples: MH3 (60.48%) from Maraba Hills and FR5 (68.45%), FR6(52.94%) from Farin Ruwa. This could be interpreted as good coverage by the analytical techniques even thought only four elements were sought.

An important mineral that usually associates with Mn is Al_2O_3, however it was not investigated, though its value is indispensable for geological evaluation of an Mn ore sample but do not play any significant role in the quantification of the ore (Berress, 1966) for industrial use

Table 5.18 is the comparison of the results of NAA and XRF for some localites. It is seen that the results agree fairly well except for Farin-Ruwa, where the variation of

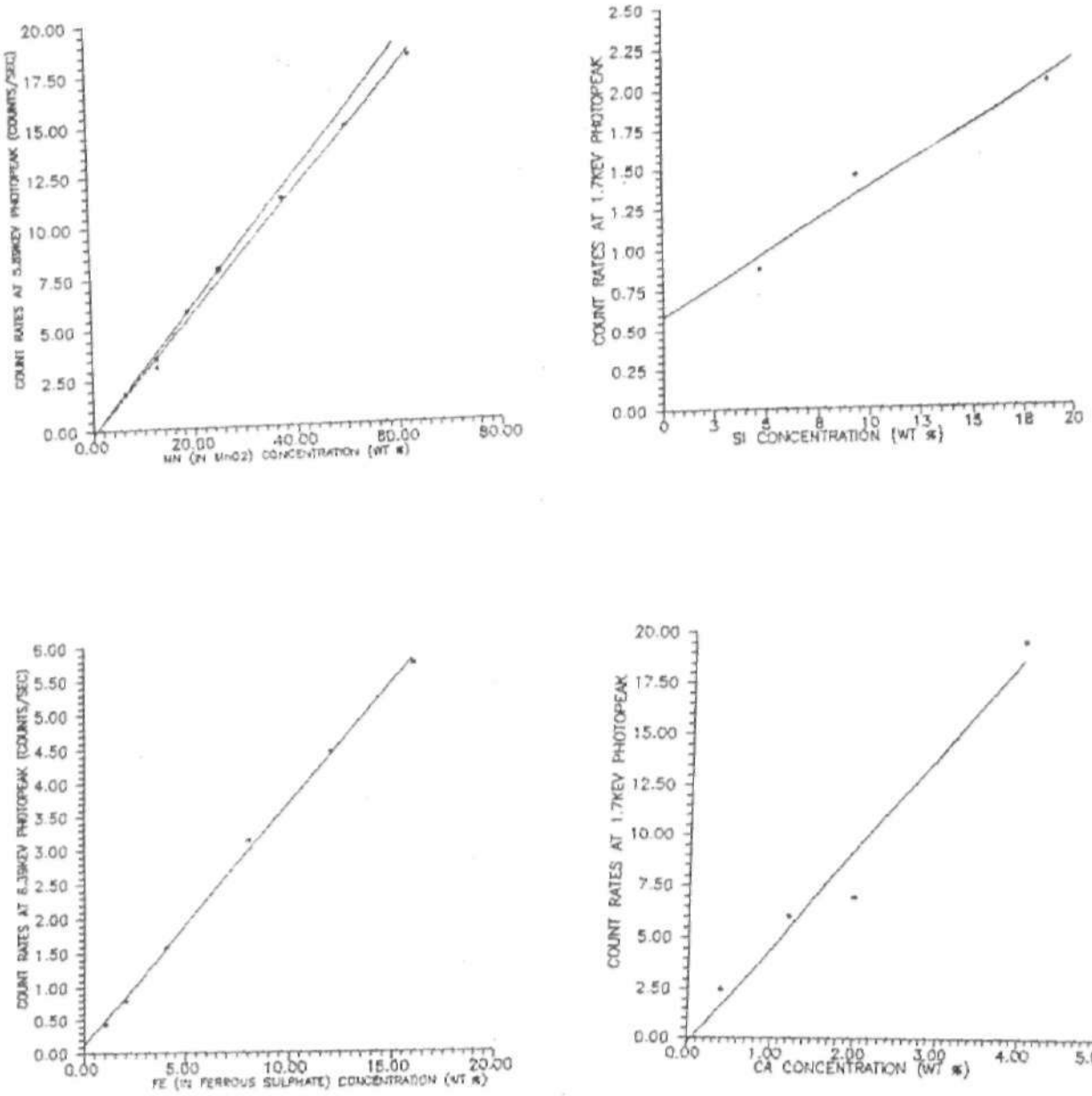
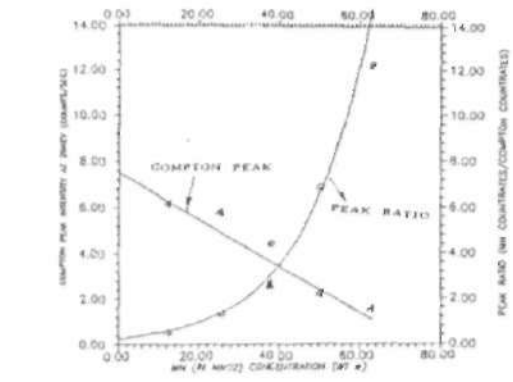
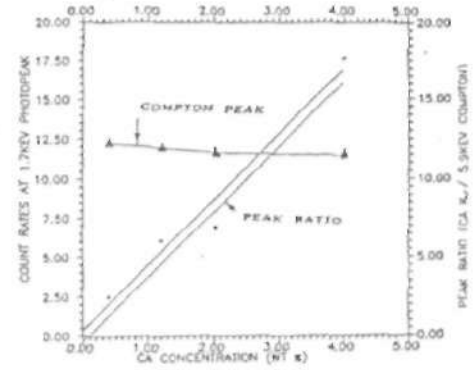


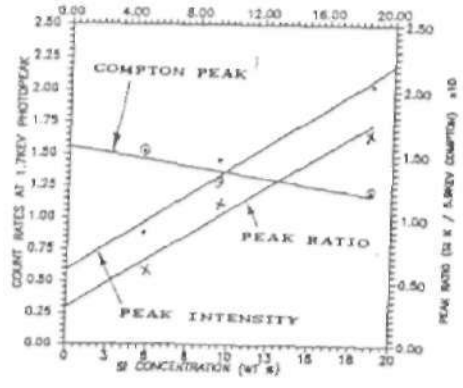
Figure 10 XRF Calibration Curves for Mn, Fe, Si, and Ca.



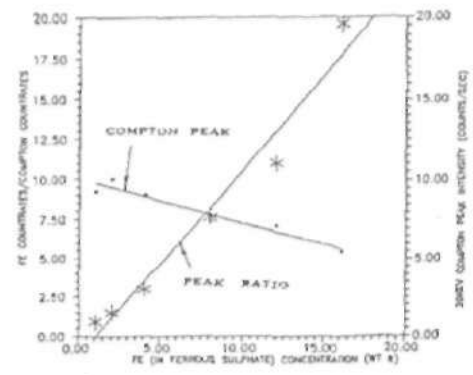
VARIATION OF COMPTON PEAK INTENSITIES AND PEAK INTENSITY RATIO WITH Mn



VARIATION OF PEAK INTENSITY AND PEAK INTENSITY RATIO WITH Ca



VARIATION OF PEAKS AND PEAKS INTENSITY RATIO WITH Si



VARIATION OF FE PEAK INTENSITIES AND PEAK INTENSITY RATIO WITH FE CONCENTRATION

Fig 5.11 Variation of peak intensity and peak intensity ratio with concentrations of Mn, Ca, and Fe

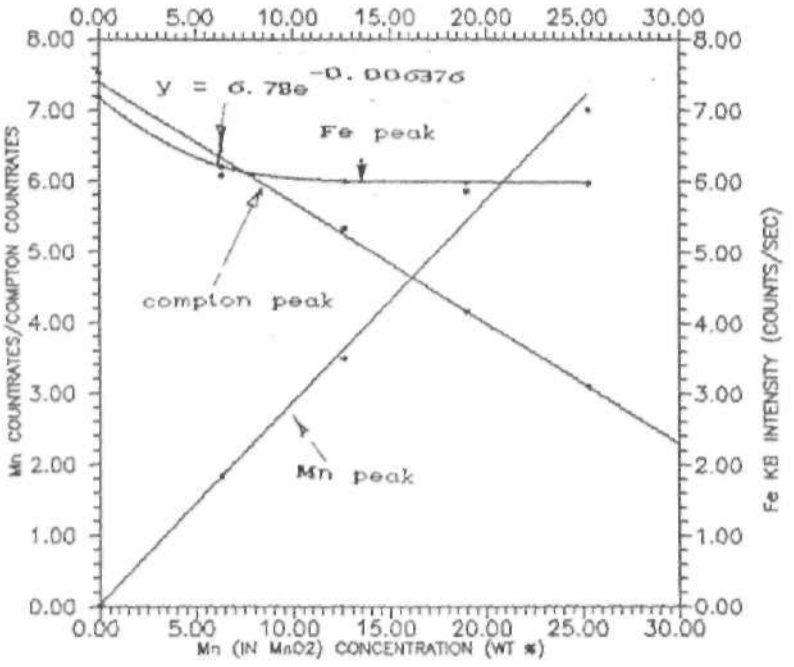


Fig 5.12 Effect of Mn on 12.1 (wt %) Fe

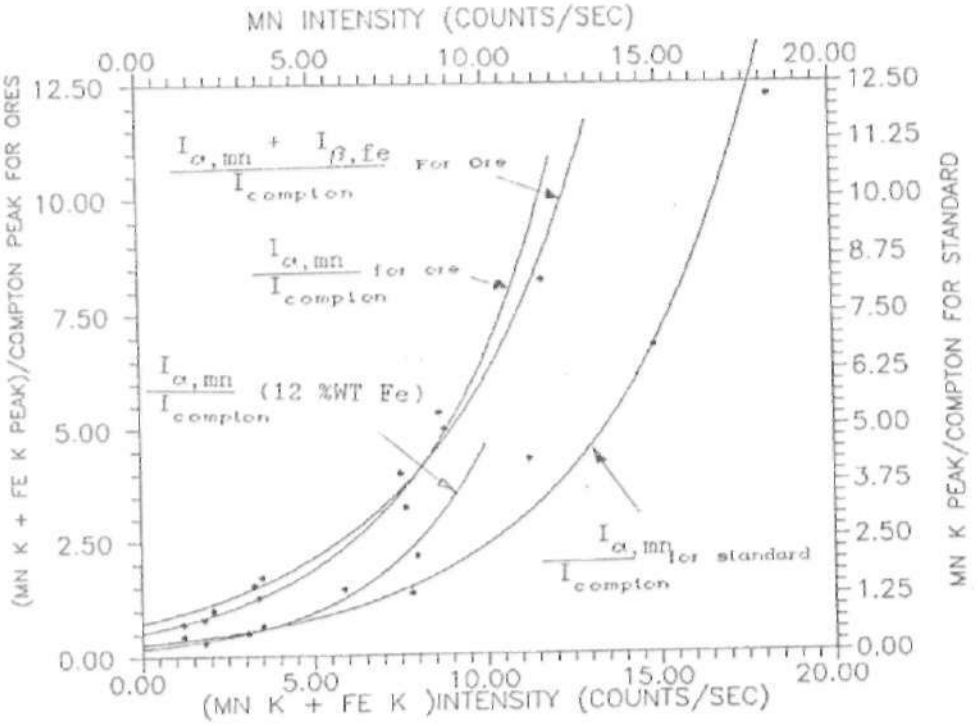


Fig 5.13 Comparison of peak ratios for Mn standard and ores

XRF over NAA exceeds 30% for one sample. This variation can easily be attributed to overcompensation for Fe in the standard used for Mn determination (12.1% Fe) using the XRF technique.

Table 5.15 Evaluation of peak intensities and peak intensity ratio for the ores

Locality	Sample No	Mn I_α (C/sec)	Fe I_β (C/sec)	Compton I_C (C/sec)	Peak Ratio I_α/I_C	Peak Ratio I_β/I_C
Ruwan Dorowa	RD3	3.48±.25	1.36+.07	2.03+.13	1.71	0.67
	RD4	3.27±.29	1.06+.09	2.13+.17	1.53	0.50
	RD5	1.82±.34	1.42+.19	2.31+.39	0.78	0.61
Tudun Kudu	TK4	8.80±.61	0.31+.02	1.76+.12	4.98	0.17
	TK5	6.66±.40	1.41+.07	2.77+.21	1.79	0.51
	TK6	8.64±.44	0.25+.02	1.62+.08	5.32	0.16
Maraba Hills	MH3	3.39±.27	0.71+.06	2.66+.23	1.27	0.27
	MH4	1.22±.20	1.33+.18	1.72+.20	0.71	0.77
Anguwangudu	AN3	1.23±.23	1.38+.21	2.76+.46	0.45	0.50
Farin-Ruwa	FR3	11.65±	0.17+.09	1.42+.10	8.22	0.12
	FR5	7.65±.49	0.04+.01	2.36+.15	3.24	0.02
	FR6	7.52±.50	0.42+.09	1.88+.12	3.99	0.24
Kirazo	KR2	2.08±.30	1.78+.21	2.06+.18	1.01	0.86

Table 5.16 Mn, Fe, Si, and Ca concentrations in the Mn ores from XRF.

Locality	Sample No	Mn Concentr. (Wt %)	Fe Concentr. (Wt %)	Si Concentr. (Wt %)	Ca Concentr (Wt %)
Ruwan Dorowa	RD3	11.3±1.91	20.3±3.06	6.5±0.61	0.36±.04
	RD4	10.7±1.36	15.9±2.31	6.0±0.46	0.33±.03
	RD5	6.3±0.84	21.0±1.07	9.2±0.75	0.22±.02
Tudun Kudu	TK4	28.0±1.15	5.0±0.84	8.1±0.73	0.20±.02
	TK5	21.8±1.65	8.0±1.20	6.0±0.32	0.19±.02
	TK6	27.3±1.50	4.4±0.87	8.4±0.65	0.22±.03
Maraba Hills	MH3	11.4±1.01	10.5±0.95	5.9±0.40	0.35±.02
	MH4	4.4±0.68	19.2±2.73	7.9±0.69	0.21±.03
Anguwangudu	AN3	4.3±0.78	20.1±3.21	8.3±0.74	0.24±.02
Farin-Ruwa	FR3	38.1±1.99	2.7±0.34	1.0±0.08	<0.01±
	FR5	24.4±1.34	0.3±0.15	13.7±.08	0.04±.02
	FR6	24.0±1.63	0.7±0.31	5.9±0.44	0.17±.02
Kirazo	KR2	7.0±1.00	26.3±3.33	0.01±0.03	<0.01±

Table 5.17 Equivalent Oxides in the Ore

Locality	Sample No	MnO_2 (Wt%)	Fe_2O_3 (Wt%)	SiO_2 (Wt%)	SiO_2 + Fe_2O_3 (Wt%)	MnO_2 + SiO_2 + Fe_2O_3 (Wt%)
Ruwan Dorowa	RD3	17.9	58.1	13.50	71.6	90.3
	RD4	17.0	45.5	12.80	58.3	74.5
	RD5	10.0	60.0	19.18	79.7	90.0p
Tudun Kudu	TK4	44.4	14.3	17.10	37.4	76.11
	TK5	33.3	23.9	12.80	36.7	70.31
	TK6	43.3	12.6	18.00	30.6	74.21
Maraba Hills	MH3	18.0	30.0	12.62	42.6	60.51
	MH4	6.9	54.9	16.90	71.8	79.01
Anguwangudu	AN3	6.8	57.5	17.80	75.3	82.41
Farin-Ruwa	FR3	60.5	7.7	2.10	9.8	70.31
	FR5	38.7	0.9	28.80	29.7	68.51
	FR6	38.1	2.0	12.62	14.6	52.91
Kirazo	KR2	11.1	75.2	0.02	75.2	86.31

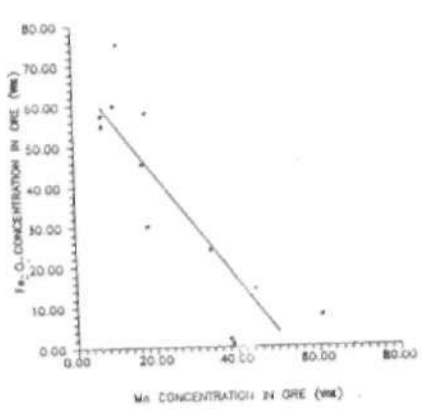


Fig. 5.14 THE PLOT OF MnO VERSUS Fe_2O_3 IN THE ORE SAMPLES

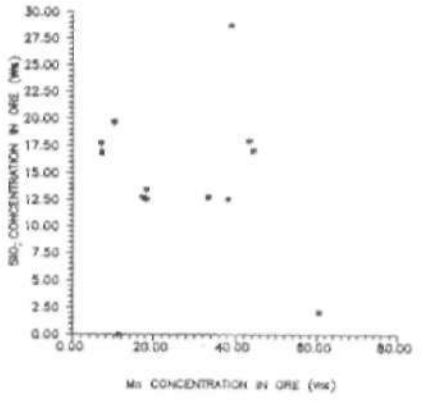


Fig. 5.15 THE PLOT OF MnO_2 VERSUS SiO IN ORE SAMPLES

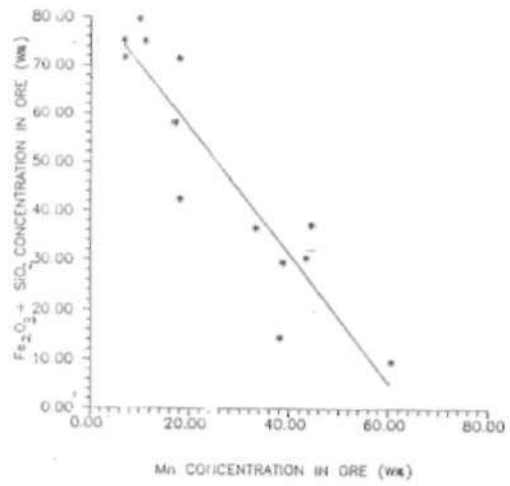


Fig 5.16 Plot MnO_2 versus Fe_2O_3 + SiO_2 in the sample

Table 5.18 Comparison of NAA and XRF results of Mn (Wt%) concentration for some ores.

Locality	Sample No	NAA Mn(Wt%)	XRF Mn(Wt%)	%Difference of XRF over NAA (%)
Ruwan Dorowa	RD3	12.46	11.3	9.3
	RD4	11.98	10.7	10.7
	RD5	8.93	6.3	29.5
Tudun Kudu	TK4	30.53	28.0	8.3
	TK5	21.66	21.8	0.6
	TK6	26.71	27.3	2.2
Maraba Hills	MH3	9.16	11.4	24.5
	MH4	5.53	4.4	20.4
Anguwangudu	AN3	4.39	4.3	2.1
Farin-Ruwa	FR3	44.09	38.1	13.6
	FR5	35.28	24.4	30.8
	FR6	34.02	24.0	29.5
Kirazo	KR2	5.65	7.0	23.8

5.5 Results for X-Ray Diffraction.

The diffractograms of the analysed samples are shown in the Appendix 6. A summary of the interpretations is shown in table 5.18. The table has shown quartz and geothite as a common phase in all the localities. Pyrolusite is identified in one of the localities, Farin-Ruwa. Earlier works by Moneme *et al*. (1982) and Mucke and Okujeni (1984) using

petrographic investigation indicated most of the minerals identified here but pyrolusite is now indentified in this work.

Table 5.19 The distribution of the minerals with localities.

Locality → / Minerals	Tudun Kudu	Ruwan Dorowa	Marraba Hills	Farin Ruwa	Kunji	Old Birnin Gwari	Magandа	Kansani Kuyazo	Kontagora
Quartz	✓	✓	✓	✓	✓	✓	✓	✓	✓
Lithiphorite	✓		✓		✓	✓			
Cryptomelane	✓			✓					
Geothite	✓	✓	✓	✓	✓	✓	✓	✓	✓
Pyrolusite				✓					
Nsutite			✓						
Ilmenite		✓	✓		✓		✓	✓	✓
Manganoan			✓						
Manganoan Cumingtonite		✓				✓	✓	✓	
Manganoan Diosposide						✓		✓	
Manganite		✓							
Almandine							✓		

CHAPTER SIX

6 CONCLUSION AND RECOMENDATION

An important contribution of this work is the establishment of an accurate, easy to use neutron irradiation station for thermal neutron activation of elements of high neutron capture cross section with the ^{241}Am-Be source. Although the neutron flux was low, as it is with most isotopic sources, the prominent photopeaks available for As, Al, W, Mo, I, Br, V, and Mn were analyzed with reasonable sensitivity. The Neutron moderator produced 'clean' neutron flux as no transmutation reaction showed on any of the analyzed spectra, as would have occurred for bare isotope neutron source. Thus by using the cylindrical paraffin moderator, with six large irradiation holes that could hold up to 100g total, Mn ore concentration was determined from +0.5% to +40% by weight

Other contributions include the evaluation of richer ores from Farin-Ruwa, outside the previously emphasized deposits of Tudun Kudu, Ruwan Dorowa, and Maraba Hills. The Fe_2O_3 and SiO_2 contents of the ore in this locality is below the maximum amount for metallurgical needs (24% Fe_2O_3 and 13% SiO_2) and also some samples compete favorably well with the majority of the ores currently mined world wide (5-10% Fe_2O_3 and 2-4% SiO_2) (Moneme, 1982)

The determination of mineralogy of these ores by XRD has not only confirmed some of the earlier works on the

mineral type associated with these deposits, using petromineragraphic techniques but. has also revealed the presence of pyrolusite in the Mn ore for the Farin-Ruwa occurrence.

The complementary role of NAA, XRD and XRF has proven to be effective in the complete determination of the elements and mineral types associated with Mn. The use of XRF here has served two purposes; the determination of Fe, Ca, and Si which are not usually determined by thermal neutron activation analysis and the second role ,the determination of Mn, has provided an avenue for assessing the accuracy of NAA which in turn leads to an evaluation of the irradiation setup.

On comparative basis, the NAA has provided better precision, lesser matrix sensitivity, easier data reduction procedure, but the irradiation time of 6-24hr (typical for Mn in this work) is its major draw back compared to the XRF. However the fairly close agreement between the two results for Mn evaluation is an indication of their reliablity for this and future analyses.

6.2 Recomendations

Although the measurement of these elements at ore levels have been adequately demonstrated here, further improvement can be brought about by providing a better lead radiation shield on the NaI(TI) detector, thereby lowering

further the minimum detectable mass, hence bringing more elements within the favorable detectable limits for the NAA. This was demonstrated by Das et al., (1993), when the performance of the locally fabricated Pb shield (the Pb shield used for this work) was compared with the Canberra Pb shield (Model 727), better results were obtained with the Canberra shield in terms of background reduction (The background reduction at 1461Kev by Canberra Pb shield was six times lower than that of local Pb shield). This background reduction is also desirable in a work like this and we recommend that such a high quality Pb shield be provided.

The Farin-Ruwa locality, which has scarcely been dealt with in the literature, and appears to exhibit large Mn concentration with the presence of Pyrolusite (virtually pure MnO_2), should be given some attention in the future especially with the aim of a complete geological investigation. Such an investigation, could provide a detailed information on the extent of the occurrence. This may result in a vast Mn field for Nigeria, and definitely, a happy end to the search which started in 1979. This will therefore be another major justification for the huge human and material resources already invested at CERT, especially at this time when a Ministry of Solid Minerals is being contemplated by the Federal Government of Nigeria.

REFERENCES

Aalto, E. (1968) Attenuation of Neutrons. In: Engineering Compendum on Radiation Shielding. Jaeger R. G. (Ed.) Springer-Verlag, Berlin. pp497-524

Agarwal B. K. (1979). X-Ray Spectroscopy. Springer series in optical sciences, vol 15. pp 53-119. Springer-Verlag Berlin.

Ajibade A. C. (1982) The Cataclastic Rocks of the Zungeru Region and their Tectonic signicance. J. Min. Geol 18 (2) pp 29-31.

Alexander L. E.; Klug H. P.; Kumer E. (1948) Statistical Factors Affecting the Intensity of X-rays Diffracted by Crystalline Powders. J. Appl. Phys V.19, pp 742-754

Allen P. N.; Hopkins E. B; Tipler R. H. (1953) Mn effect on grain boundary carbides. Journal of Iron and steel Inst. (London) V 174 p 108.

Anderman G. and Kemp J. W. (1958). Scattered X-rays as Internal Standard in X-ray Emmision Spectroscopy. Analytical Chemistry, V.30, No. 8, pp. 1306-1309.

Amaldi, E. (1959). Production and Slowing Down of Neutrons In: Ency. of physics, Vol xxviii/2, Flugge S. (Ed.) Berlin, pp 18-22

Barford, N. C (1967) Experimental Measurements: Precision, Error and Truth. Addison-Wesley Publishing Company. pp. 56-71.

Beckurts, K. H. and Wirtz K. (1964). Neutron Physics, (Springer -Verlag) Berlin. pp 190-195

Beress M. (1966) Application of Neutron Activation Analysis to the Investigation of Manganesian Rocks. IAEA. Radioisotope Instruments in Industry and Geophysics. Vol 1, pp 18-22 .

Bethe, H. A. and Ashkin, J. (1952). Passage of Radiation through Matter. In: Experimental Nuclear Physics. Segre E. (Ed.) John willey and Sons, New York. Vol 1, pp 166-304

Breen R. J. and Hertz M. R. (1955) Phys Rev.98, 599

Burger G. and Schwartz R (1988) Guidelines on Calibration of Neutron Measuring Devices, IAEA Technical Reports Series No 285.

Burkhalter P. G. (1971) Radioisotopic X-ray analysis of silver ores using compton scattered for matrix compensation. Anal. Chem., Vol.43, No.1. PP 10-17.

Campbell W. J. and Thatcher J. W. (1958) Determination of calcium in Wolframite concentrates by fluorescent X-ray spectroscopy. Advances in X-ray analysis. Vol.2, PP.313-332.

Cardoso A,; Lima, F. W.(1976). Determination of Manganese in Ores by activation analysis using Californium-252 neutron source IAEA . 434, 13pp (ENG)

Chapman G. R. (1985)_ Manganese Resources and Production. Transaction of the Institute of Mining and Metallurgy. Section A, V 94, pp 155-159.

Chung F. H. (1974) A New X-Ray Diffraction method for Quantitative Multicomponent Analysis. Advances in X-Ray Analysis. Vol 17 pp 106-115

Clayton C. G. and Packer T. W. (1979) Some Applications of Energy Dispersive X-ray Fluorescencce Analysis in Mineral Exploration, Mining and Process control. Advances in X-ray analysis. V. 23, PP 1-15

Cox A. J. Francois P .E. and Gatrell R .P(1968) Design of Neutron Howitzers. International Journ. Applied Rad. and Isotopes, Vol 19, pp 541-544.

Cullity B. D. (1970) Elements of X-ray Diffraction, Second Edition Addison Wesley ,p 83-189.

Currie A. L. (1968) Limits for Qualitative Detection and Quantitative Determination. Journ. of Anal. Chem. Vol 40. pp 586-592 .

Das H. A., Umar I. M., Elegba S. B. (1993) Reports On Background Mapping Project and on a 5Ci Am-Be at CERT. IAEA Expert Mission to CERT.(unpublished)

De Young J. H. Jr. Sutphin D. M and Cannon W. F (1984) International Strategic Minerals Inventory-Summary Report,: Manganese. U.S. geol. Survey 930-A, p. 22

Droulers, Y.(1970). ThermaL Neutrons. IAEA Technical Reports on Neutron fluence measurements. Series No. 107. pp 45-75.

Dungster, H.J. (1961). Basis of the ICRP-MPD and Application of Basic Safty Standards. Radiation Protection Monitoring IAEA. pp 3-11.

Feld, B. T. (1952) The Neutron. In: Experimental Nuclear Physics. Segre E. (Ed.) John Willey and Sons. Vol 2, pp 209-58.

Frank L. Chan, (1963) .Determination, Confirmation and detection limit of trace amounts of selenium by X -ray methods. Advances in X-ray analysis. Vol. 7, pp 542-554).

Fumio, A. and Minoru, O. (1958). Best conditions for use of the paraffin moderator to the radium-beryllium neutron source: Position and direction of the sample . Dai II-Kai Genshiryoku Symposium, Hobunshi. 3, pp 32-35.

Garg A. N. and Batra R. J.(1986). Isotope Sources in Neutron Activation Analysis. Jour. of Radioanal and Nucl. Chem. 98, 167.

Goussev, N. G. (1968). Relationship Between Dose Equivalent (Absorbed Dose) and Fluence (Flux density). In: Engineering Compendium on radiation Shielding. Jaeger R. G. (Ed.) Springer-Verlag Berlin, pp 12-19.

Harshaw- Filtrol.(1984). Radiation Detectors Harshaw-Filtrol partnership. Publications pp 5-14.

Harshaw-Filtrol (1984). Low level Counting Compton Suppression. Harshaw/Filtrol Publication. pp 1-9

Huang J. (1987) New Wear- and Corrosion -resistant Cast alloy-Medium silicon-Manganese cast iron. Zhuzao, v 3, pp 12-14.

Jordan E. D and Schieling H. E. (1964). Americium Beryllium, Plutonium Neutron sources - Relative effectiveness in prompt gamma-neutron activation analysis. Int. Journ. of Applied rad. and isotopes V. 15, pp 427 -436.

Kaelble, E. F. Qualitative Analysis by Powder Diffraction Hand book of X-Rays. McGraw-Hill, New York pp 11.1- 11.14,

Kaye G. W. C. and Laby T. H. (1983), Tables of Physical and Chemical Constants. Longman London, 14th Edition pp 330-345

Khalil G. I (a) (1985). Determination of Mn and Na in Geological Samples. J. of Radioanalytical Nucl Chem, Letters 96 (5) 539-546 .

Khalil G.I (b)(1985). Detection Limits of Au using Fast and Thermal Neutrons Activation analysis. Journ. Radioanal. Nucl. Chem. Lett. 96 (5) 547-556

Kirk-Othmer, (1966) Encyclopedia of Chemical Technology. Herman F. M. (Ed.) Second Edition Vol.12 pp 887 - 905.

Kisutsyn,V. F. Sidelkovskii, E. Y.; Khisin S.G.; Novoselov, E. A.,and Efimova, L. B. (1987) High manganese Steel. Otkrytiya Izobet (USSR). v 37, p 103 .

Krumbein, A. D. and O Reilly, B. D. (1968). Neutron Attenuation in Hydrogenous Media by the Method of Moments. In: Engineering Compendium on Radiation Shielding. Vol-1. Jaeger. R. G. (Ed.) Springer-Verlag, Berlin. pp 127-152.

Lamarsh, J. (1975) Introduction to Nuclear Engineering. Addison-Wesley Publishing. pp 23-45

Langheirich A. P.; Forster J. W. and Linn, Jr T. A (1973) Current Status and Potential of Solid State Detectors in Industrial and Field Applications In: Neuclear Techniques in the basic metal industries, Proceedings of a symposium, Helsinki 31-7-1972, IAEA, Vienna.

Leo W. R (1985) Techniques for Nuclear and Particle Physics Experiments. Spriger-Verlag, Berlin pp8-15

Leonard G. B. (1974) Selected Powder Diffraction Data for Minerals Search Manual. American Joint Commitee on Powder Diffraction Standards .First Edition

Lorch E. A. (1973). Neutron Spectra of ^{241}Am/B, ^{241}Am/Be, ^{241}Am/F ^{242}Cm/Be, ^{238}Pu/C, ^{252}Cf isotopic neutron sources. Int. Journ. of Applied Rad. and Isotopes. Vol 24, pp. 585-591

Lyon, N. S. (1967) Physical Techniques of Activation Analysis-Survey Paper. In: Nuclear Analytical Techniques in the life Sciences. Proceeding of a Symposium, Amsterdam pp 13.30 (IAEA)

McCurry P. (1973) The Geology of the Precambrain to Lower Palaeozoic Rocks of Northern Nigeria- A Review. In: Geology of Nigeria. Kogbe C. A. (Ed.) pp 1-39

Moneme, P. C.; Scott P. W.; and Dunham A. C. (1982) Manganese Mineralization at Tudun Kudu, Zaria District, North-Central Nigeria. Nigerian Geosciences. pp 30-41

Moteff, J. (1970) Introduction to Neutron Fluence Measurement. IAEA-Technical Report series No 107, pp 1-5,

Myhre F. (1985) Changing Role of Manganese and its Effect on consumption. In: Transactions of the institute of Mining and Metallurgy. Section A Vol.94, PP 172-175.

Mucke A and Okujeni C, (1984) Geological and Ore Microscopic Evidence on the Epigenetic Origin of the Manganese Occurrences in Northern Nigerian. Journal of African Earth Sciences. Vol 2, No 3 pp 209 to 225

Mukhin K. N. (1987) Experimental Nuclear Physics. Volume 1 (Physics of Atoms and Nucleus) Mir Publishers Moscow pp 376-452.

Mustapha A. O; Oladipo M. O. A ; Elegba S. B. (1994) Mean Square Slowing Down Distance of Americium - Beryllium Neutrons in Perspex. J. of Rad. Anal Chem. Vol 181, No 2, pp 343-350

Naskidashvili, I.A.; Mosulishvili, L. M.; Gvakhariya, V V.; Abashidze, K. A.; Baggdavadze, N.V.and Chantladze, T. L. (1963). Neutron Activation Analysis of Manganese Ores. Radioisotopnye Metody Avtomat. Kontrolya, Akad.Nauk Kirg. USSR, 1, pp77-85.

Nielson K. K. (1978) Progress in X-ray fluorescence Correction methods using Scattered radiation. Advances in X-Ray Analysis. Vol. 22, pp 303-315.

Op de Beeck, J. (1986) INAA with Neutron Sources. Of print from Treatise on analytical chemistry. Second edition Part 1, v.14, pp739-757. (John Willey and Sons Inc, USA)

Papez K. and Cameron J. F, (1973). Applications of Energy Dispersive X-ray Fluorescence Analysis in the Basic Metal Industries. In: Nuclear techniques in the basic metal industries. Proceedings of a symposium, Helsinki ,IAEA, Vienna

Philips (1985), PW1729/00 X-Ray Generator. Philips PP 4-14

Rieppo, R. (1983). The Thermalization of Am-Be Neutrons in Paraffin. The Absolute Intensities of Am-Be Neutrons as a Function of Neutron Energy. Int. J. Appl. Rad & Isot.V.35, P 41

Robert-Tissot T. (1985) Manganese-Commercial Aspect. In: Transactions of the Institute of Mining and Metallurgy. Section A, Vol 94, pp 172-175.

Shenberg C.; Haim B. A. and Amiel S. (1973). Accurate Determination of Copper in Mixtures and Ores by Radioisotope Excited X- ray Fluorescence Spectrometric Analysis using Peak Ratios. Anal. Chem. V.45, PP. 1804-1808

Smith P.K. and Barrett C.S.(1978). Special Handling Problems in X-Ray Diffractometry. Advances in X -ray analysis, Vol.22 PP 1-11.

Starbuck J. W. (1968) Introduction to Powder Diffraction. Handbook of X-Rays Kaelble E. F. (Ed.) McGraw -Hill. pp 7.4-7.9.

Suschny, O.(1968) Radionuclides. In: Engineering Compendium on Radiation Shielding. Jaeger R. G. (Ed.) Springer Verlag Berlin Vol.1, pp 20-30.

Svidunovich, N. A.; Parfenov, L. I.; Garost A. I.; Sorokin, G. A;Verbitskili, A.N.; Vashkevich ,V.V. and Gorin A. B. (1987). Complex Ferromanganese for Allowing Steel. Otkrytya Izobret, v 29. p 121.

Tikhonovic, V. I.; Novitskii, V. G.; Kisselev, V. G.; Kondratyuk, S. E; Vinor, B. B. Lutsenko, G. G.; Edemskii V. K. (1987) (USSR). Cast High-manganese steel. Otkrytiya Izobret 1987

Thompson, M. N., Taylor J. M. (1965) Nucl. Instrum. Meth. V.37, p.305

Tittle, C. W. (1950) The Thermal Neutron Diffusion length of Paraffin. Phys.Rev. vol 80, pp 756.

Truswell, J.F. and Cope R.N. (1963) The Geology of parts of Niger and Zaria provinces. Northern Nigeria. Bulletin.of Geological Survey.vol 29 .pp 53

Turner D. C. (1983) Upper preterozoic Schist Belts in the Nigerian Sector of the Pan-African province of West Africa. Precambrain Research, 21 pp55-79.

Van DerZwan L. (1968) $^{9}Be(a,n)^{12}C$ Cross section Between 1.5 and 7.8 Mev. Can. J. Phys v.46, p 1527

Vassamillet, L. F. and King, H. W. (1968) Diffractometer Techniques. In: Handbook of X-Rays. Kaelble E. F. (Ed.) McGraw-Hill. New York. pp 9.1 -40.

Vijaya A. D. and Kumar A. (1973) The Neutron Spectrum of Am-Be Sources. Nuclear Instruments and Methods.V.111 PP 435-440.

Vose P. B. (1980) .Introduction to Nuclear Technology in Agronomy and Plant Biology. Pergamon International Library. pp. 177-197

Wheeler B. D.; Martell D.M. and Cooper J.A. (1976). Chemical Analysis of Nickel ores by Energy Dispersive X-ray Fluorescence. Advances in X-ray Analysis V.20, pp.423-429.

Wright J. B. and McCurry P. (1970) First Occurrence of Manganese ores in Northern Nigeria. Economic Geology. Vol 65, pp 103-106.

Wyckoff, H.O and Rossi, H. H. (1968) Radiation Quantities and Units.In: Engineering Compedium on Radiation Shielding. Jaeger R. G. (Ed.) Springer -Verlag. vol-1 pp 1-5.

Zijp, W. L. (1970) Intermediate Neutrons. In: IAEA technical reports on Neutron fluence Measurement. Series no 107 pp 77- 136.

Zoltai, T. (1968) Camera Techniques. In: Handbook of X-rays. Kaelble E. F. (Ed.) McGraw-Hill, New York. pp8.1 - 8.24.

APPENDIX-1

THE EFFECIENCY CALCULATION FOR THE 7.6 x 7.6cm NaI(Tl) DETECTOR

The effeciency of the detector was calculated from the following expresion

$$\text{Absolute Effeciency} = \frac{\text{Measured Activity}}{\text{Activity of the source}}$$

$$= \frac{\text{Count Rates}}{E_\gamma A_o e^{-xt_2}}$$

where E_γ = branching ratio.

A_o = activity of source at $t_2 = 0$.

t_2 = Life time of source.

Isotope Standard Source	Energy (Kev)	$t_{\frac{1}{2}}$	Source Stren. (μCi)*	Di/sec *** ($x10^4$)	E_γ	Cnts/sec on 5/12/93	Detec Effic
^{241}Am	60	432.2y	1.612	5.964	100	6536.19	10.99
^{137}Cs	661.6	30.1y	1.024	3.789	85	4333.01	14.09
^{54}Mn	834.5	312.5d	1.115	4.126	100	1003.42	12.32
^{22}Na	1274.5	2.6y	1.310	4.847	99.9	1402.37	4.93
^{60}Co	1773.3	5.3y	0.946**	3.501	99.9	1106.89	4.00

*(Source strenght on 10:12:1991) **(Source strenght on 4:1:1988)
***($1Ci=3.7x10^{10}Di/sec$)

Table Ap.1 Efficiency calculation for a 7.6 x 7.6cm NaI(Tl) detector at CERT

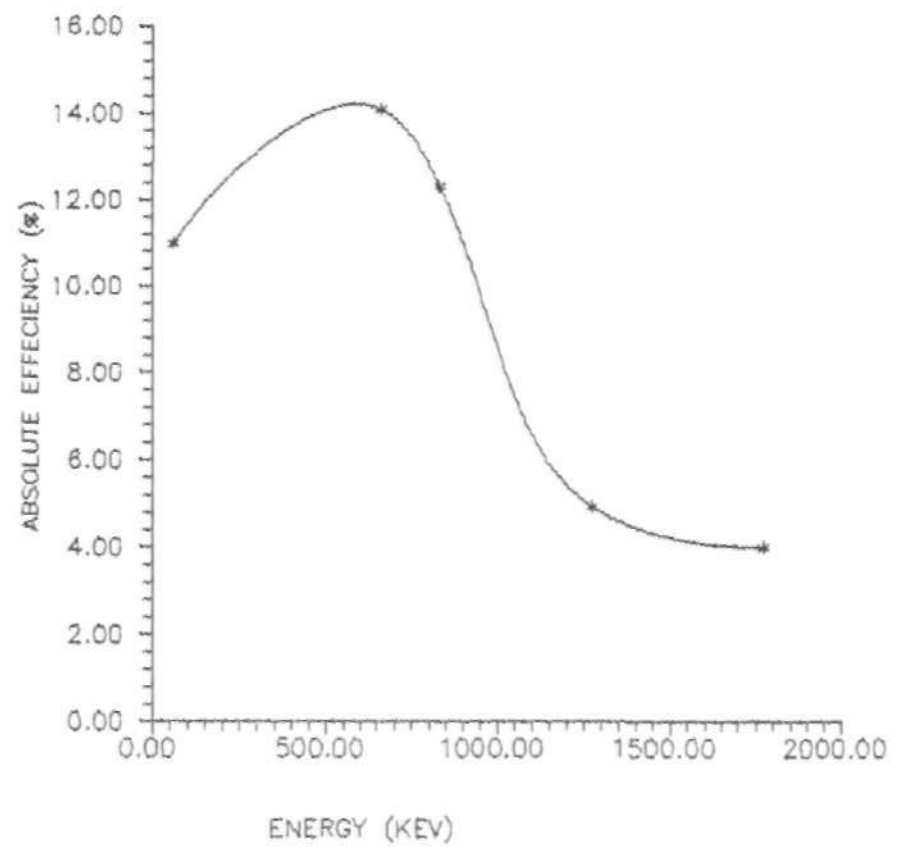


FIG AP1 EFFECIENCY CALIBRATION CURVE FOR NaI(Tl) DETECTOR

APPENDIX 2

DETECTION LIMIT

The detection limit as given in chapter three is

$$L_D(R) = k^2/Dt + 2k(2R_B/Dt)^{\frac{1}{2}}$$

A confidence limit of 99.865% corresponds to k=3 (Khalil (b) 1985) or

$$L_D = 9/Dt + 8.485(R_B/Dt)^{\frac{1}{2}}$$

Where Dt is counting time, R_B is the background rate. The The minimum detactable mass M_D is

$$M_D = L_D(R)/\tau$$

τ = slope of the curve

The computed values for the background rate, slope of the calibration curve, detection limit and the minimum detectable mass are in the table

	Isotope Produce	Half Life	Count time (sec)	Backgrd Rate (cps)	Slope Calib. (cps/g)	$L_D(R)$	Detectab Mass (grams)
^{55}Mn	^{56}Mn	2.59hr	3600	6.34	38.49	0.358	0.009
^{51}V	^{52}V	2.75m	300	1.88	6.37	0.702	0.110
^{186}W	^{187}W	23.9hr	1200	7.53	6.45	0.680	0.105
^{127}I	^{128}I	25.0m	500	8.26	3.38	1.109	0.327
^{75}As	^{76}As	26.3hr	1200	7.91	3.66	0.696	0.191
^{79}Br	^{80}Br	17.4m	500	7.66	0.95	1.068	0.121
^{23}Na	^{24}Na	15.2hr	1200	2.10	1.47	0.362	0.246
^{27}Al	^{28}Al	2.24m	300	0.77	0.45	0.461	1.031
^{98}Mo	^{99}Mo	2.75d	1200	41.97	0.55	1.594	2.898

Table AP.2 Detection limits for element of high thermal neutron cross section

APPENDIX 3
FLUX CALCULATION

(a) Thermal Flux

The flux is calculated from equation 3.12 :

$$\phi = \frac{A.F_{CD}M}{Im\sigma\tau E(6.0210^{23})(1-e^{-xt_i})e^{-xt_d}(e^{-xt_c})}$$

where F_{CD} = Cadmium Factor = $\frac{R_{CD}-1}{R_{CD}}$ and R_{CD} ,the cadmium ratio is given by $R_{CD} = \frac{\text{Total count rate}}{\text{Epicadmium count rate}} = \frac{A_{tot}}{A_{epi}}$

M = molecular weight of indium =144.9,

I = Isotopic abaundance = 0.958

E = detector efficiency at 1293kev = 4.93%

τ = gamma abundance at 1293kev = 84.4%

σ =Thermal neutron cross section = 161barn = 161 x 10^{24} cm^{-2}

X =decay const. =0.693/$T_{\frac{1}{2}}$ =0.693/(54.15x60s) = 0.0002139s

m = mass of indium used = 4.63grams

t_i =irradiation time=106min and t_d = delay time = 30secs.

t_c = counting time = 10min.

(b) Epithermal Flux

The epithermal flux is given by:

$$\phi_{epi} = \frac{A.M}{I.m.\sigma_{res}.\tau.E(6.02x10^{23})(1-e^{-xt_i})e^{-xt_d}(1-e^{-xt_c})}$$

Where σ_{res} = resonance intergral cross section = 2630 barn

APPENDIX 4

CALCULATION OF THE ERROR IN THE MEASURED MN CONCENTRATION

The standard deviation in the concentration of manganese is given by (Khalil,1985):

$$\sigma_x = x\left[\frac{\sigma_y^2 + \sigma_b^2}{(y - b)^2} + [\sigma a/a]^2\right]^{\frac{1}{2}}$$

Where y and x represent the countrates in counts per second and the concentration in wt% respectively. σ_y^2 is the variance of the directly measured values, a is the slope of the calibration curve, σ_a^2 its variance ,and b is the intercept, σ_b^2 is the corresponding variance.

The values of a , b ,σ_a σ_b are found using the method of least sqaures. (Barford,1967)

$$\text{The slope, } a = \frac{(XY)_n - X_n Y_n}{(X^2)_n - (X_n)^2}$$

$$\text{the intercept, } b = \frac{(X^2)_n Y_n - X_n (XY)_n}{(X^2)_n - (X_n)^2}$$

The standard deviation in the slope σ_a is

$$\sigma_a = \frac{[(x_1-X_n)^2\sigma^2(y_1)+(x_2-X_n)^2\sigma^2(y_2)+..+(x_n-X_n)^2\sigma^2(y_n)]^{\frac{1}{2}}}{n((X^2)_n - (X_n)^2)}$$

and the standard deviation of of the intercept σ_b is

$$\sigma_b = \frac{[x_1^2-Xx_1)^2\sigma^2(y_1)+(x_2^2-Xx_2)^2\sigma^2(y_2)+..(x_n^2-X_n x_n)^2\sigma^2(y_n)]^{\frac{1}{2}}}{n((X^2)_n - (X_n)^2)}$$

$$\text{where } X_n = (x_1 + x_2 + ... + x_n)/n$$

$$Y_n = (y_1 + y_2 + \ldots\ldots + y_n)/n$$

$$(X^2)_n = (x_1^2 + x_2^2 + \ldots\ldots x_n^2)/n$$

$$(XY)_n = (x_1y_1 + x_2y_2 + \ldots\ldots + x_ny_n)/n$$

The values as calculated for various irradiation positions are below:

	All positio counted	Positions of Irradiation					
		1	2	3	4	5	6
Y_n	717.65	106.81	115.64	122.34	134.46	119.68	111.08
$(XY)_n$	17231.5	2594.9	2778.9	2942.8	3224.3	2865.6	2674.8
X_n	19.14	19.141	19.141	19.141	19.141	19.141	19.141
$(X^2)_n$	466.203	466.20	466.20	466.20	466.20	466.20	466.20
Slope a	35.001	5.513	5.665	6.021	6.517	5.758	5.496
Interc b	47.454	1.276	7.207	7.079	9.726	9.446	5.880
STD σ_a	0.471	0.016	0.017	0.017	0.018	0.017	0.017
STD σ_b	0.712	0.286	0.292	0.298	0.312	0.299	0.306

Table Ap.4 Error in the Measured Concentration of Mn

APPENDIX 5

CALCULATED FLUX AT 25 CM FROM THE SOURCE IN PARAFFIN

The thermal flux due to fast neutron source in a medium is given by (Beckurts and Wirtz, 1964):-

$$\phi(r) = \frac{Q.L^2}{4\pi Dr}\left[\frac{e^{-r/L}}{L^2-\bar{\tau}th} - \frac{e^{-r/\sqrt{\bar{\tau}th}}}{L^2-\bar{\tau}th}\right] = 263.4 n/cm^2/s$$

Where Q = Source strenght = 1.29×10^7 n/s (IAE,CHINA,1988)

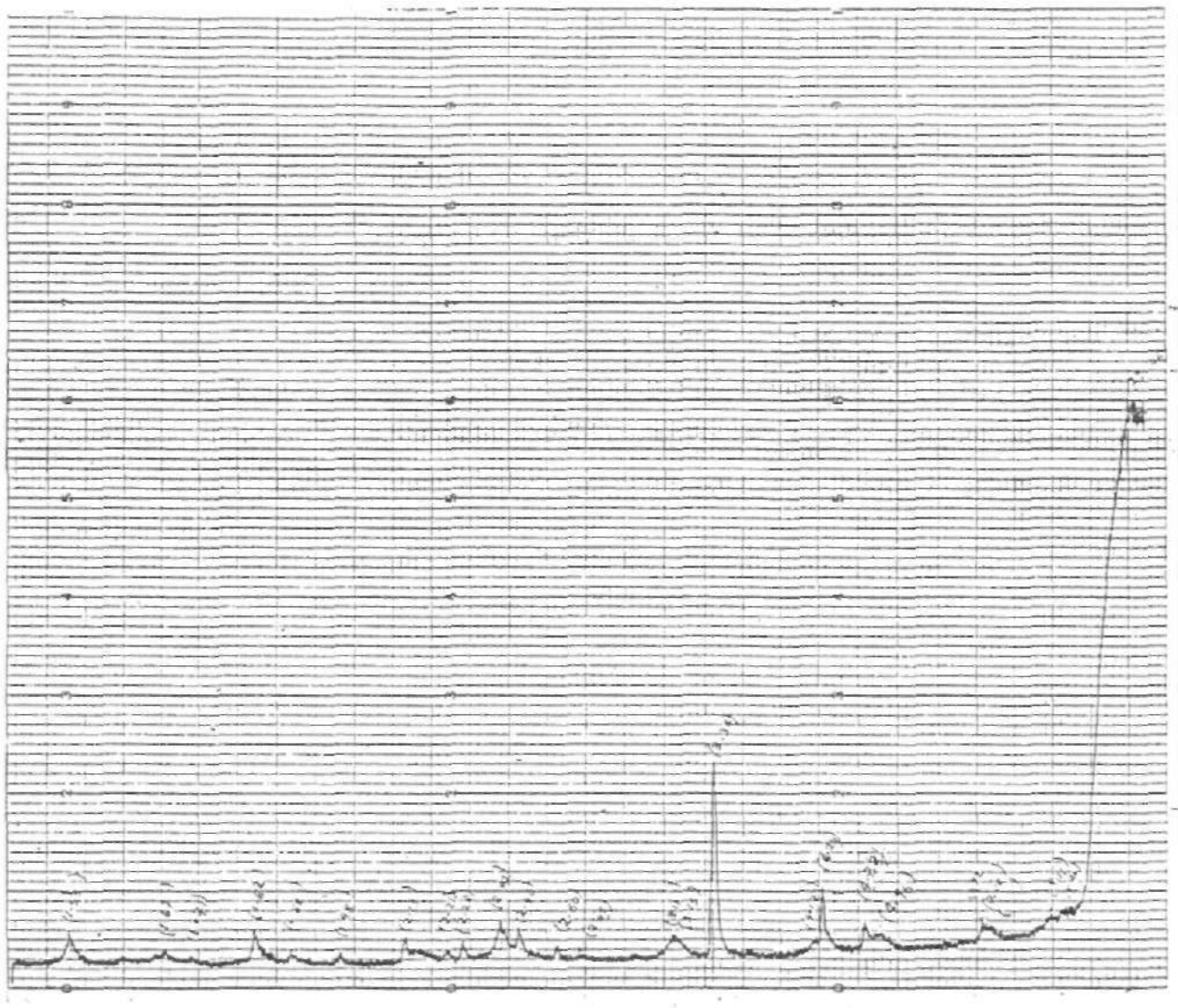
D = Diffusion coefficient = 0.136 (Beckurts *et al* 1964)

L = Diffusion length = 2.4±0.04cm (Tittle, 1950)

$\bar{\tau}th$ = Fermi age = $18.1 cm^2$ (Kaye *et al* 1983)

r = source distance = 25cm.

APPENDIX 6A X-Ray Diffractogram for Tudun Kudu



TUDU KUDU							
2θ	d (A°)						
9.2	9.46		✓				
9.7	9.11						
12.5	7.08						
12.8	6.92			✓			
18.0	4.96			✓			
18.8	4.72		✓				
20.9	4.25	✓					
21.3	4.17				✓		
26.7	3.34	✓					
28.3	3.15			✓			
28.7	3.11			✓			
33.3	2.69				✓		
34.5	2.60						
36.5	2.46	✓					
36.8	2.44				✓		
37.4	2.40			✓			
37.8	2.38		✓				
39.5	2.28	✓					
42.0	2.15			✓			
42.4	2.13	✓					
48.4	1.88		✓				
49.8	1.83			✓			
50.1	1.82	✓					
54.4	1.63				✓		
54.9	1.67	✓					
58.8	1.57		✓				
60.0	1.53	✓					

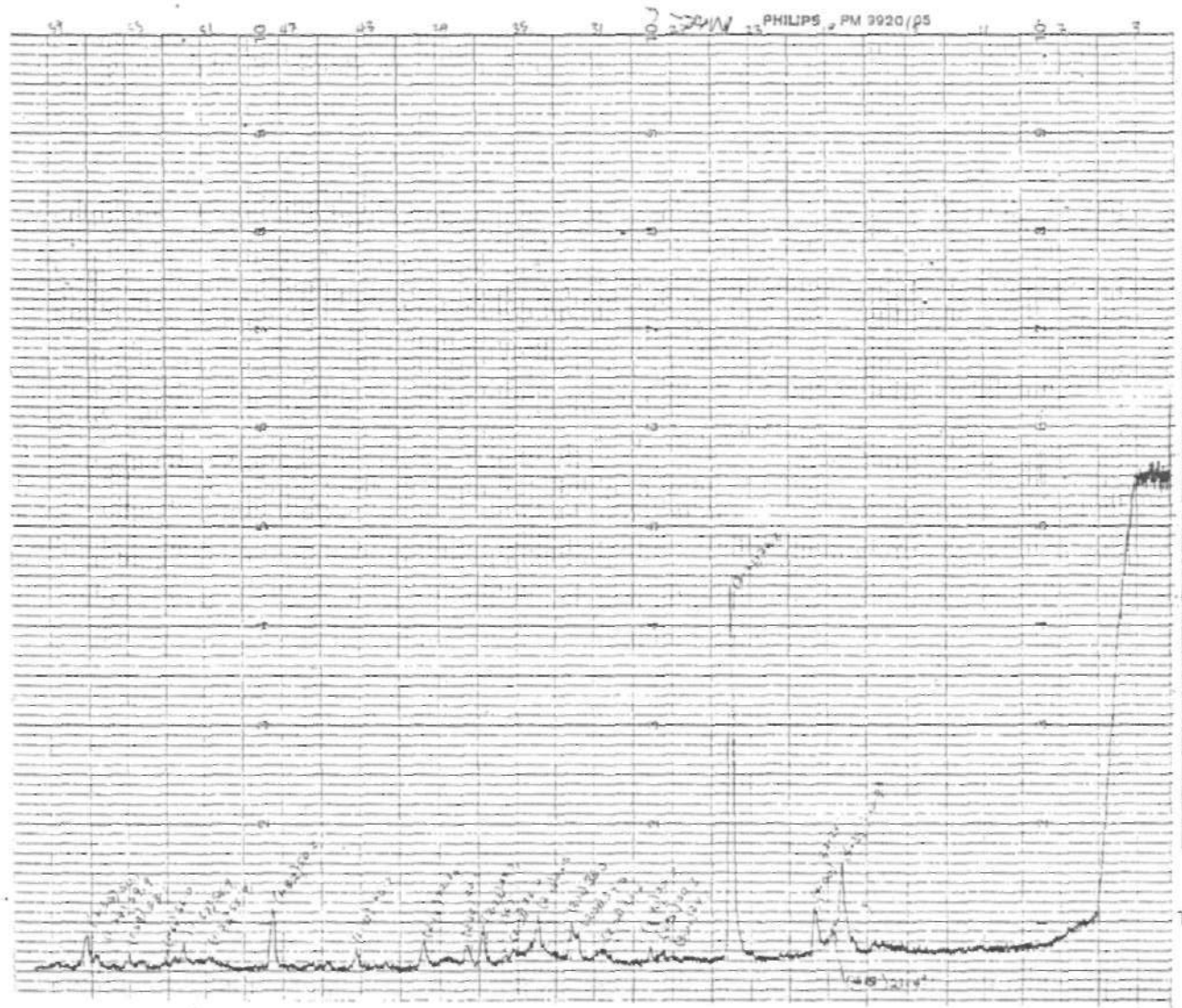
X-ray diffraction

(Tudu Gudu Ore)



RUWAN -DORDWA						
2θ	d (A°)					
10.8	8.35		✓			
20.9	4.25	✓				
21.2	4.19			✓		
26.3	3.39					✓
26.7	3.34	✓				
27.4	3.25		✓			
29.0	3.08		✓			
32.6	2.75				✓	
33.3	2.69		✓	✓		
34.5	2.60					✓
35.6	2.52				✓	
36.6	2.46	✓		✓		
39.6	2.28	✓				✓
41.2	2.19	✓		✓		
42.5	2.13	✓				
45.8	1.98					
50.2	1.82	✓				
54.0	1.70	✓			✓	
56.4	1.63					
57.0	1.62					
59.0	1.57					
60.0	1.52	✓				

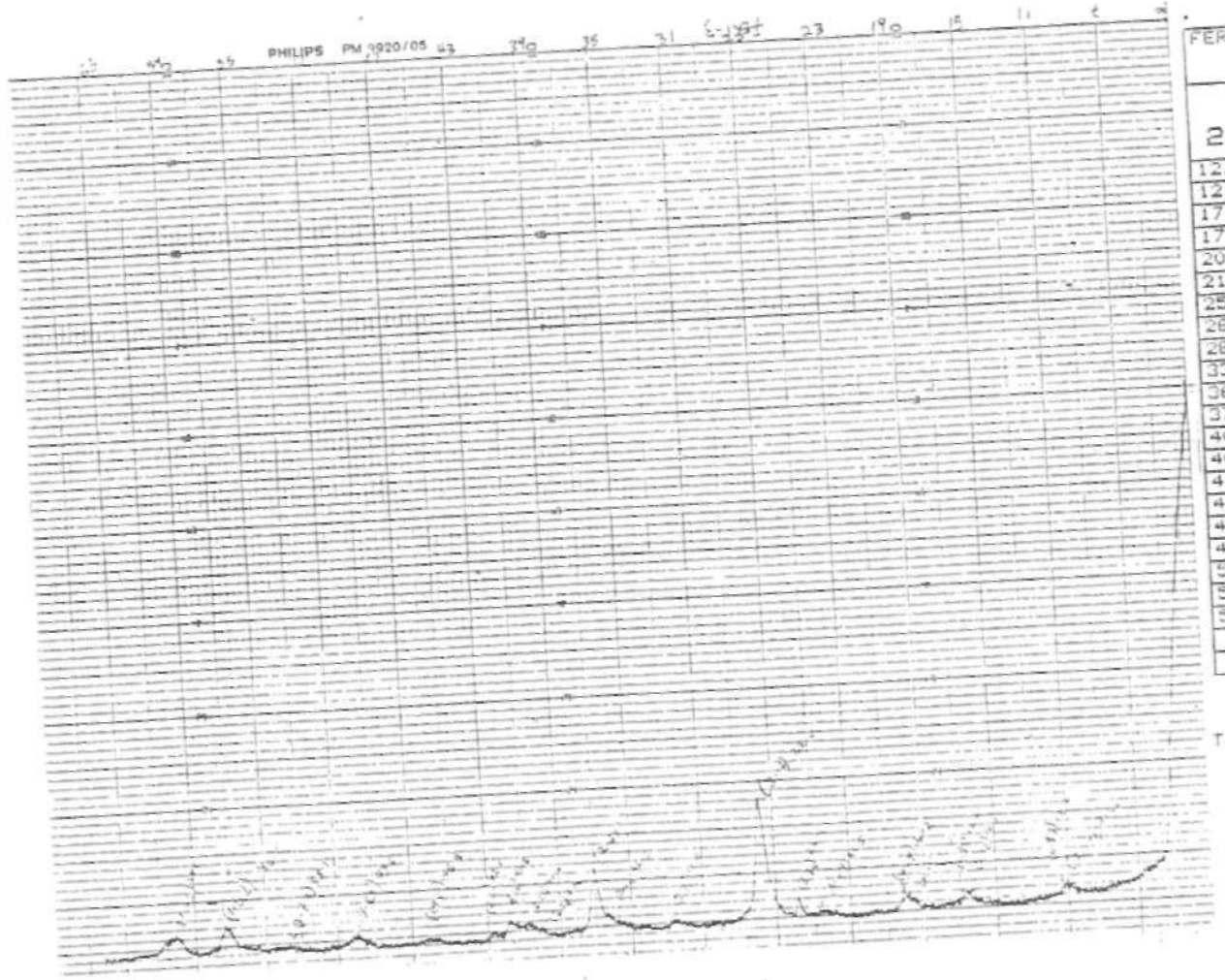
Table X-ray diffraction for Ruwan-Dorowa



MARABA-HILLS							
2θ	d (A°)						
20.9	4.25	✓					
21.4	4.15			✓			
22.2	4.00		✓				
26.7	3.34	✓					
29.7	3.01					✓	
30.3	2.95						✓
30.8	2.90						✓
33.4	2.68			✓	✓		
34.6	2.59		✓				
35.0	2.56					✓	✓
36.3	2.46	✓		✓		✓	
38.0	2.37						
38.3	2.35		✓				
39.5	2.28	✓					
40.3	2.24	✓					
42.5	2.13	✓					
46.2	1.97						✓
50.2	1.82	✓				✓	
53.9	1.70			✓			
55.9	1.67	✓					
56.0	1.64		✓				
58.1	1.59					✓	
59.9	1.54	✓					
60.1	1.50				✓		

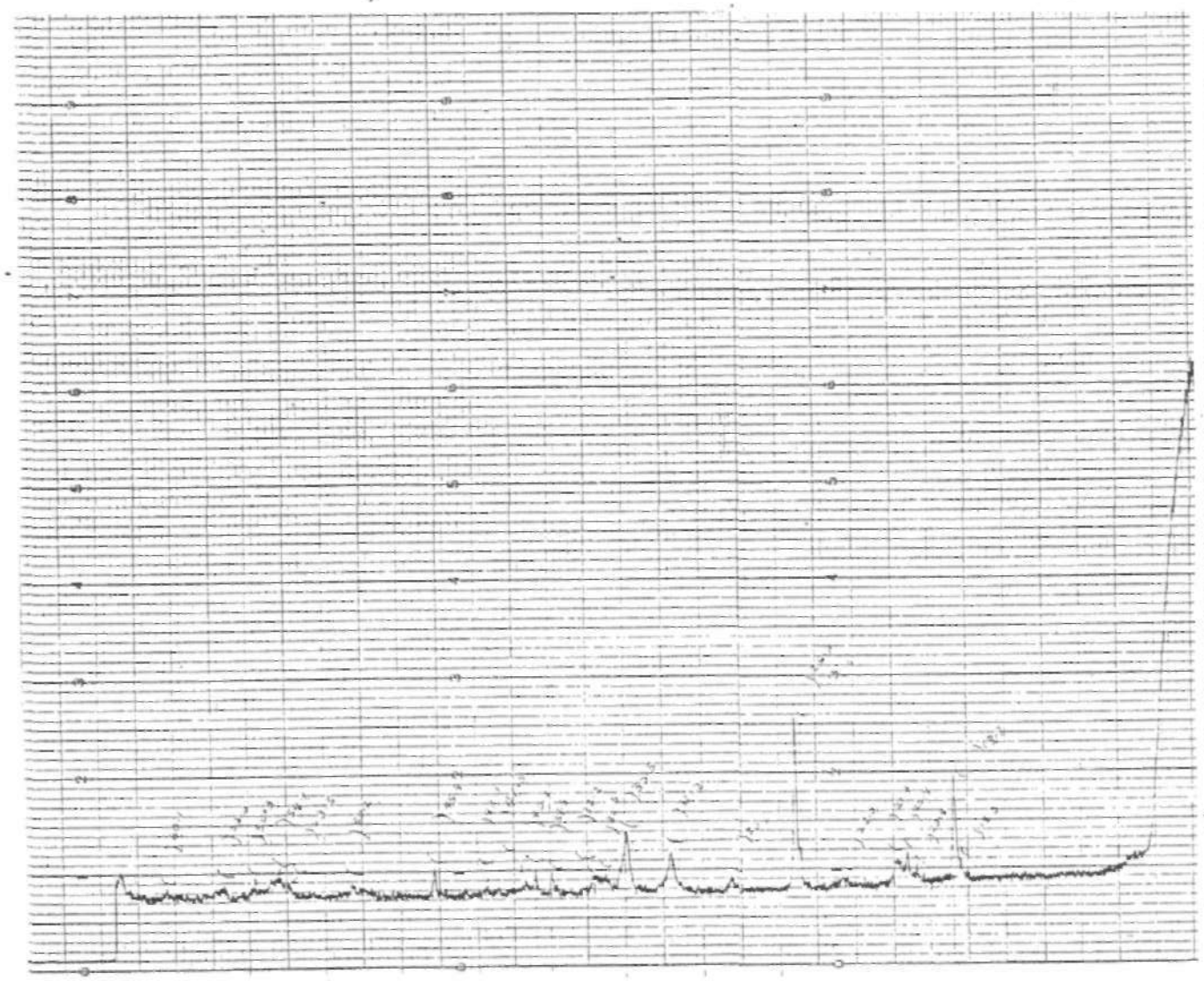
Table X-ray diffraction

Maraba-Hill ore



FERRIRUWA								
2θ	d (A°)							
12.4	7.19							
12.7	6.97			✓				
17.7	5.02							
17.9	4.96			✓				
20.7	4.29	✓						
21.2	4.19				✓			
25.3	3.49		✓					
26.5	3.36	✓						
28.4	3.14		✓	✓				
33.0	2.70				✓			
36.5	2.46				✓			
37.3	2.41		✓	✓				
40.1	2.24							
40.8	2.22			✓	✓			
41.8	2.16				✓			
42.8	2.11		✓					
45.9	1.98		✓					
49.8	1.83	✓			✓			
53.1	1.71					✓		
56.7	1.62		✓					
59.5	1.55	✓	✓					

Table X-ray diffraction for Ferriruwa ore



KUNJI							
2θ	d (A°)						
18.0	4.93		✓				
18.7	4.75			✓			
20.4	4.35						
20.9	4.25	✓					
21.4	4.15		✓				
24.0	3.71				✓		
26.7	3.34	✓					
30.1	2.96						
33.2	2.70		✓		✓		
35.5	2.53				✓		
36.5	2.46	✓					
37.2	2.42		✓	✓			
39.5	2.28	✓					
40.4	2.23	✓	✓				
41.0	2.20		✓				
43.1	2.10	✓					
45.9	1.98						
50.2	1.82	✓					
53.5	1.72		✓				
54.1	1.70	✓		✓			
55.3	1.66						
57.0	1.62				✓		
60.1	1.52	✓					

Table X-ray diffraction for Kunji ore



OLD BIRNIN - GWARI							
2θ	d (A°)						
10.7	8.27						
12.4	7.14						
20.9	4.25	✓					
21.4	4.15		✓				✓
26.7	3.34	✓					
27.4	3.25						✓
29.3	3.05						✓
29.7	2.99				✓		
31.0	2.89				✓		
32.5	2.76						✓
33.5	2.68		✓				
34.7	2.59				✓		✓
36.7	2.45	✓	✓				
38.1	2.36						✓
39.7	2.27	✓					
40.4	2.23	✓					
42.6	2.12	✓					
45.9	1.98				✓		
50.2	1.82	✓					
53.6	1.71		✓				
54.6	1.68	✓					
57.5	1.60						✓
60.0	1.52	✓					

Table X-ray diffraction

(Old Birnin Gwari)

Table X-ray diffractior

For Maganda ore

MAGANDA 2θ	d (A°)	Quartz	Calcite	Feldspar	Kaolinite	Gypsum
10.6	8.35	✓				
20.4	4.35					
20.9	4.25	✓		✓		
21.4	4.15			✓	✓	
24.0	3.71				✓	
24.8	3.59					
26.2	3.40					
26.7	3.34	✓				
27.4	3.21			✓		
29.1	3.07			✓		
30.8	2.90				✓	
32.5	2.76			✓		
33.3	2.69				✓	
34.6	2.59					✓
35.5	2.52				✓	
36.5	2.46	✓				
37.2	2.42				✓	
39.4	2.29	✓				
41.0	2.20	✓				
41.6	2.17					✓
42.5	2.13	✓				
50.2	1.82	✓				
53.7	1.71			✓		
54.0	1.70				✓	
54.8	1.68	✓				
57.2	1.61			✓		
59.9	1.52	✓				

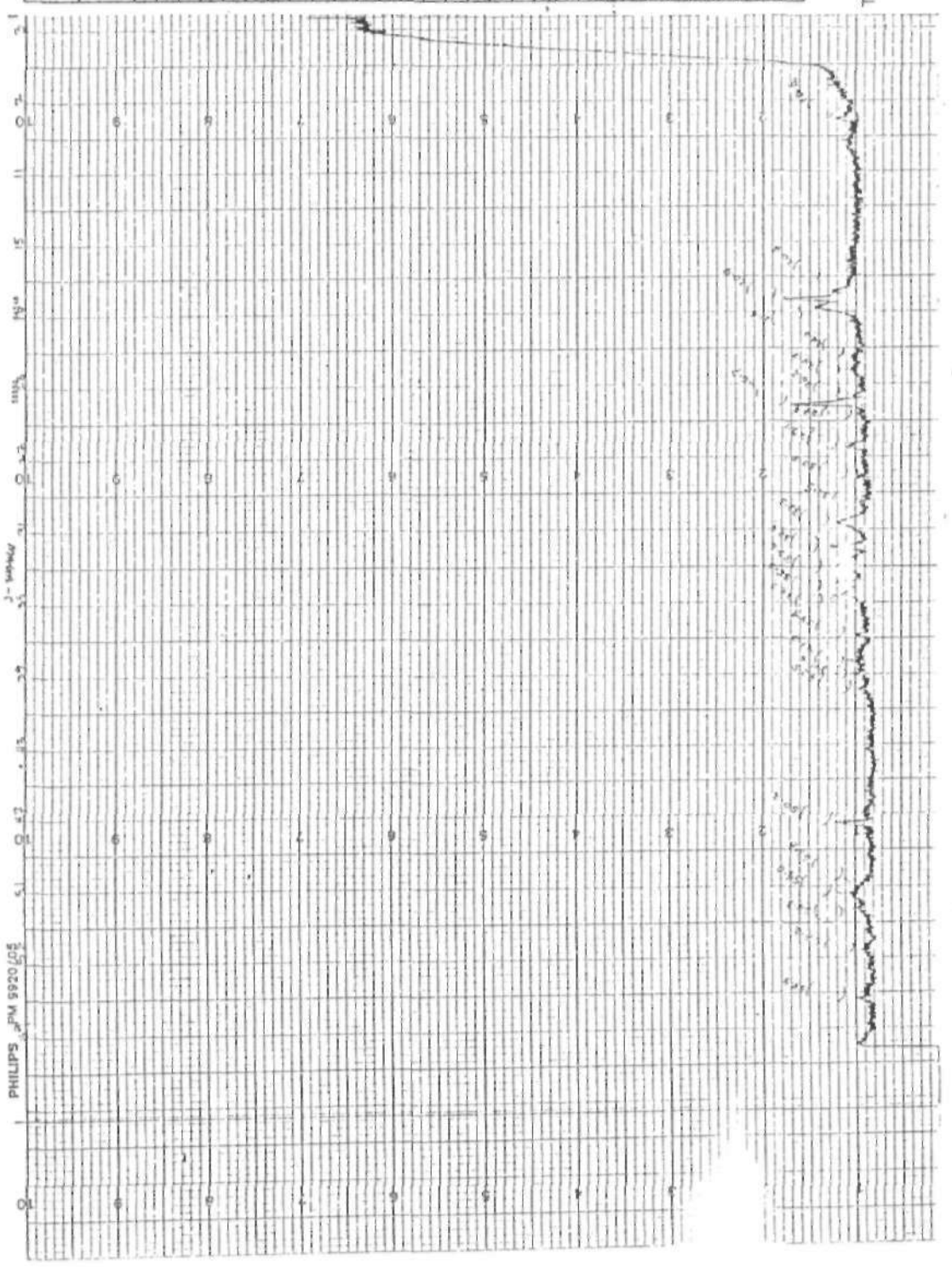
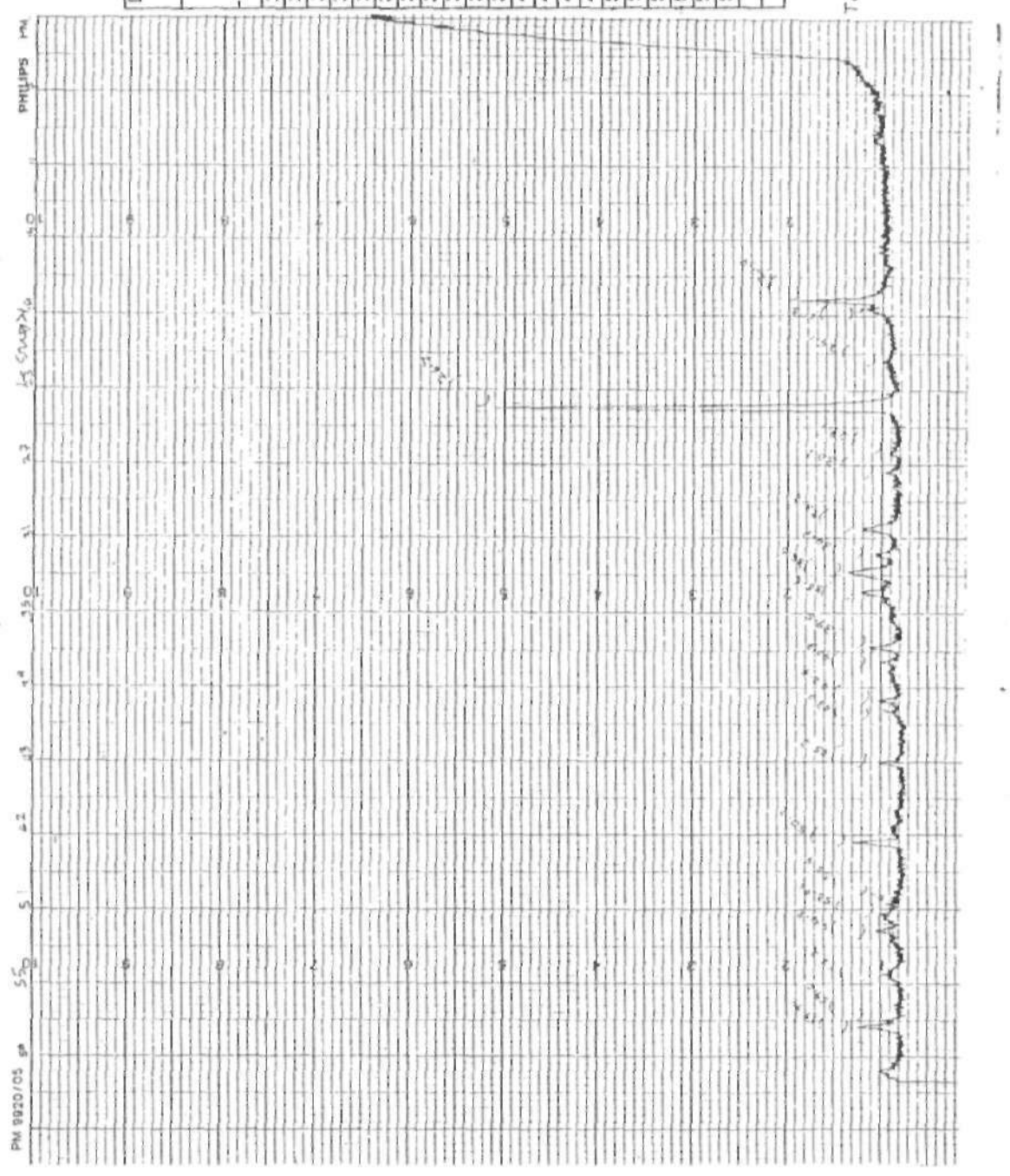
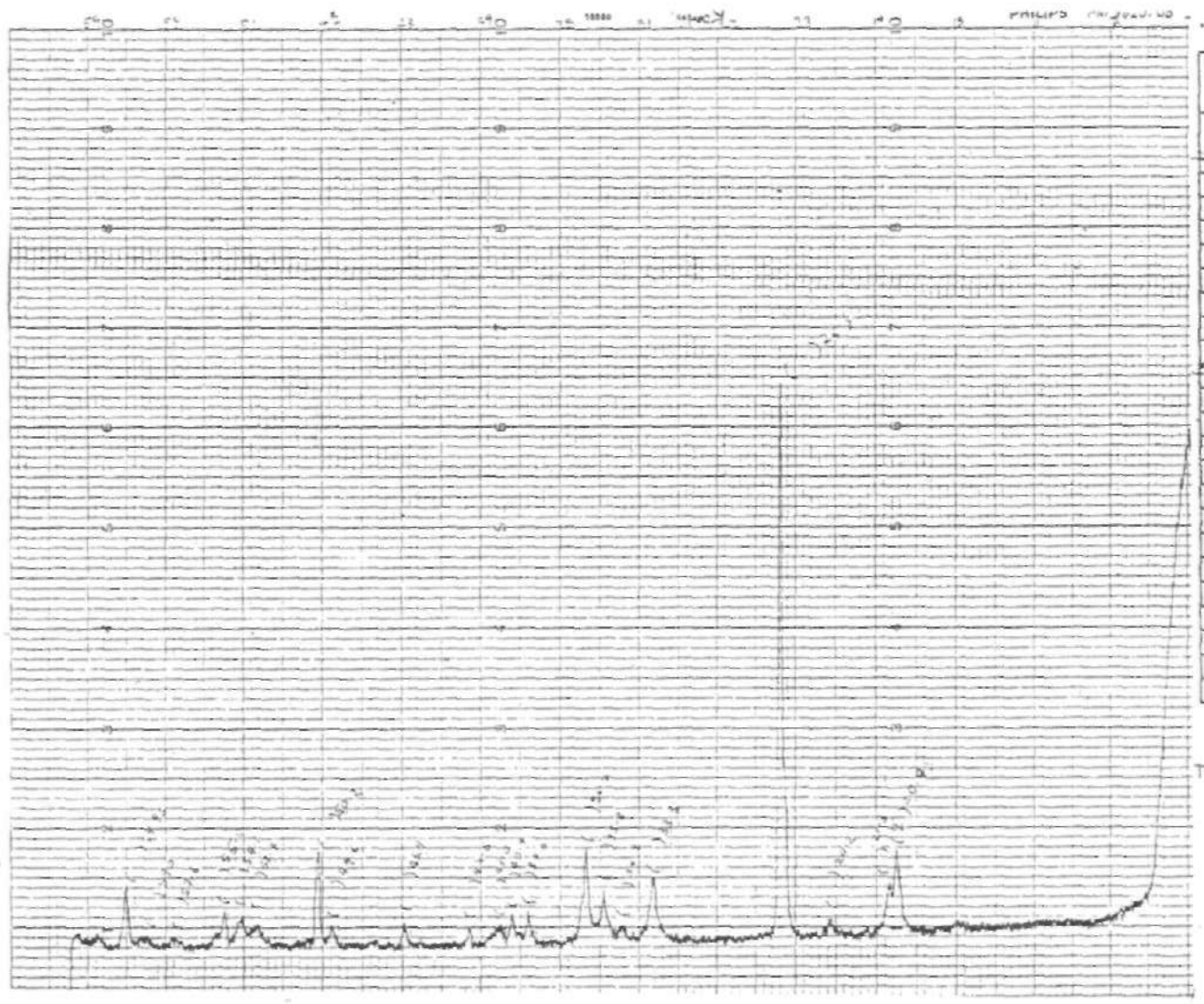


Table X-ray diffraction for Kansani Ore

KANSANI	2θ	d (A°)						
	20.9	4.25	✓					
	21.3	4.17		✓				
	24.1	3.69			✓			
	26.7	3.34	✓					
	29.1	3.07				✓		
	30.1	2.97					✓	
	33.2	2.70		✓				
	34.7	2.59			✓			
	35.5	2.53				✓		
	36.6	2.46	✓					
	39.5	2.28	✓					
	40.3	2.24	✓					
	42.4	2.13	✓					
	43.0	2.10						
	45.7	1.99				✓		
	50.2	1.82	✓					
	53.4	1.72		✓				
	54.8	1.68	✓					
	57.2	1.61				✓		
	59.6	1.55						
	59.9	1.51	✓					



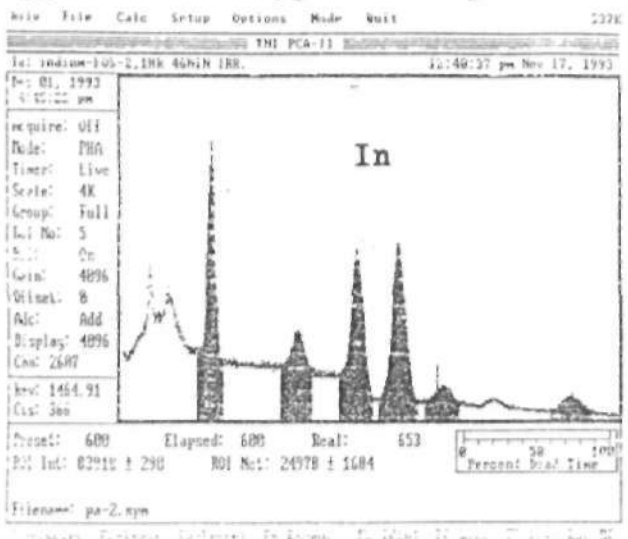


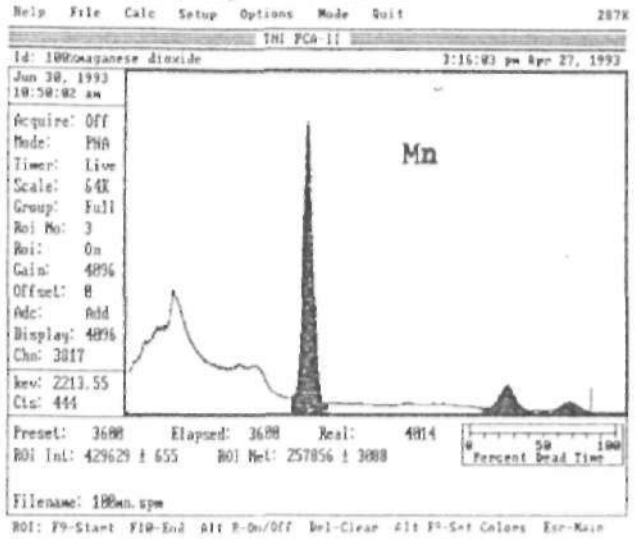
Kontagora		Quartz	Gibbsite	Kaolinite			
2θ	d (A°)						
20.9	4.25	✓					
21.3	4.17		✓				
24.2	3.68			✓			
26.7	3.34	✓					
33.3	2.69		✓	✓			
34.9	2.57						
35.8	2.51			✓			
36.7	2.45	✓	✓				
39.6	2.28	✓					
40.4	2.23	✓					
41.0	2.20		✓				
42.6	2.12	✓					
45.9	1.98						
49.6	1.84			✓			
50.2	1.82	✓					
53.4	1.72		✓				
54.1	1.70						
55.0	1.67	✓					
57.6	1.60			✓			
59.0	1.56						
60.0	1.52	✓					

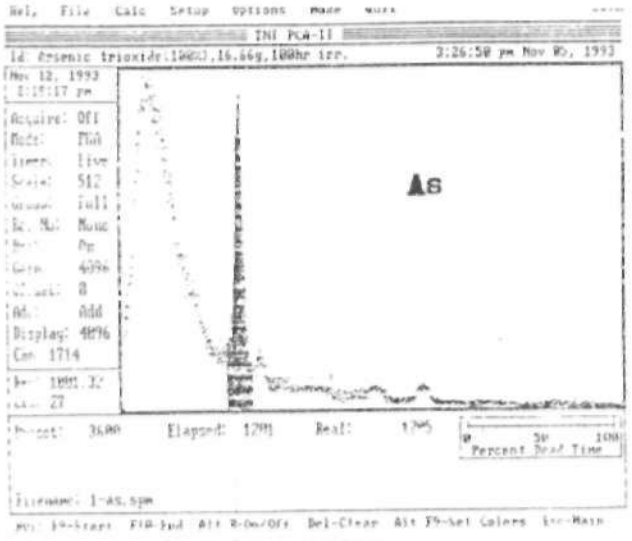
Table X-ray diffraction

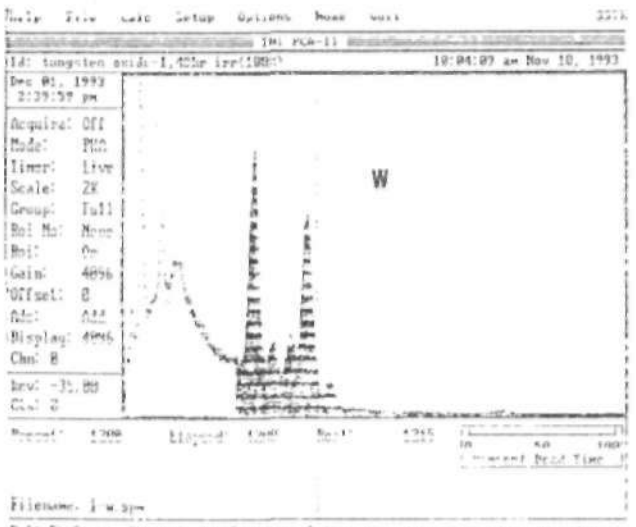
For Kontagora

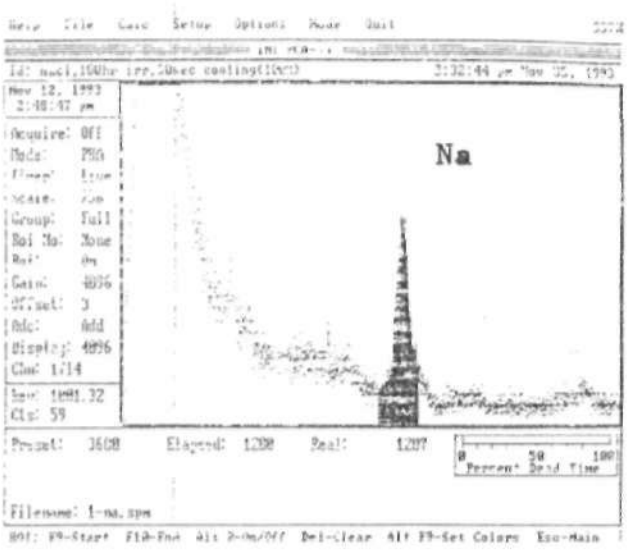
Appendix 7 Typical Outputs from the NaI(Ti) Detector

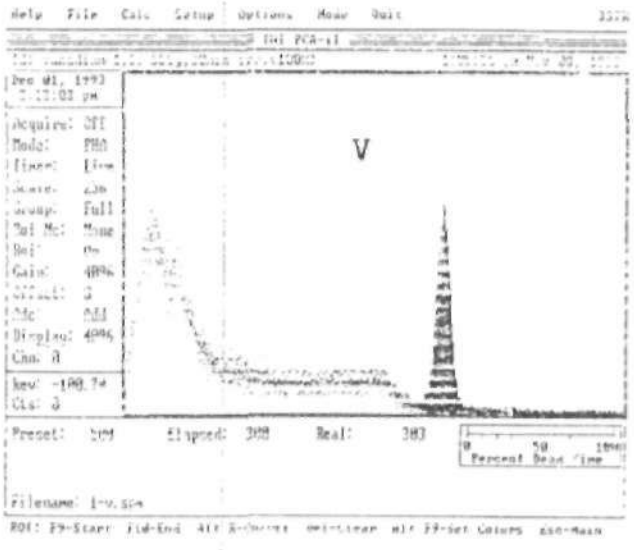




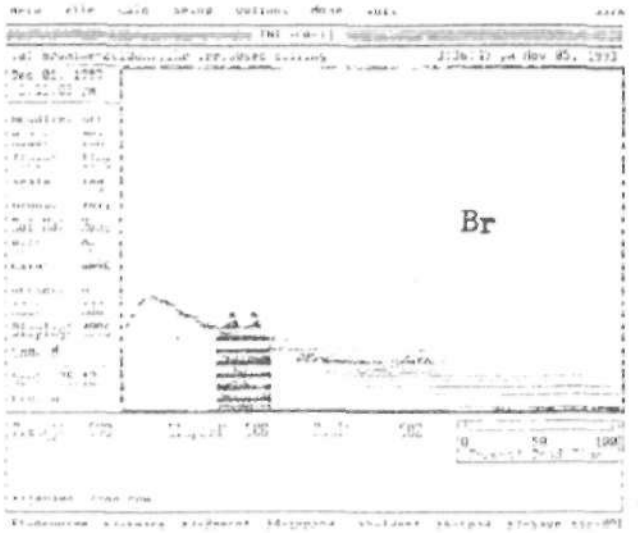


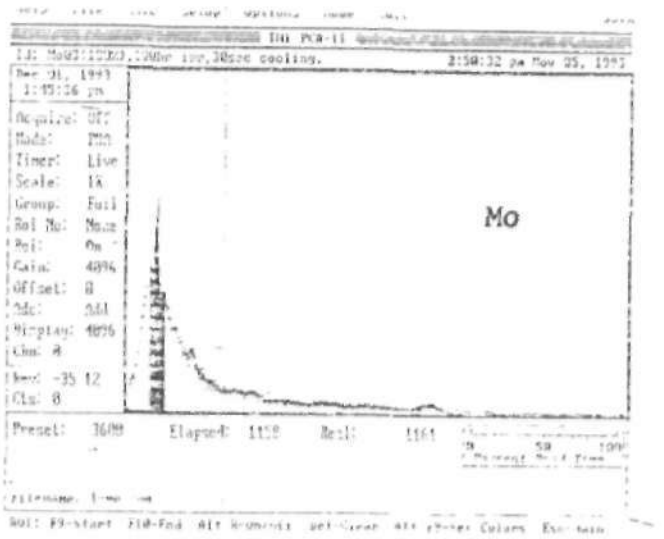


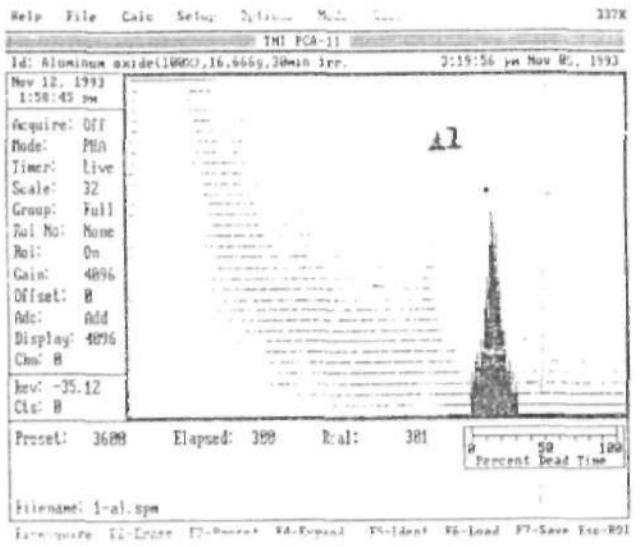


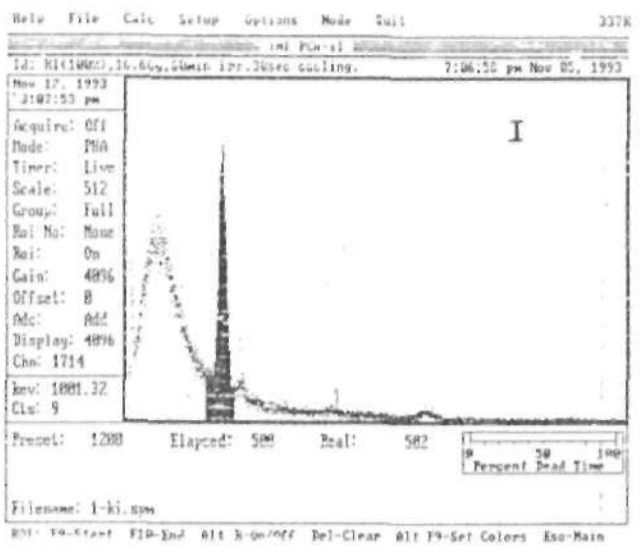


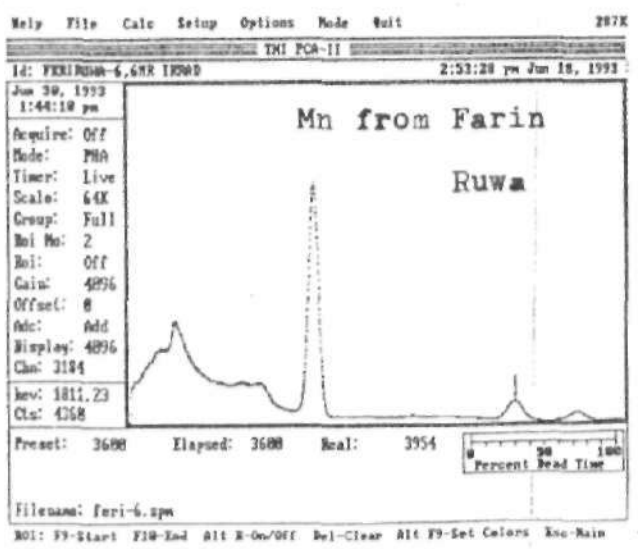
Appendix 7 Typical Outputs from the NaI(Tl

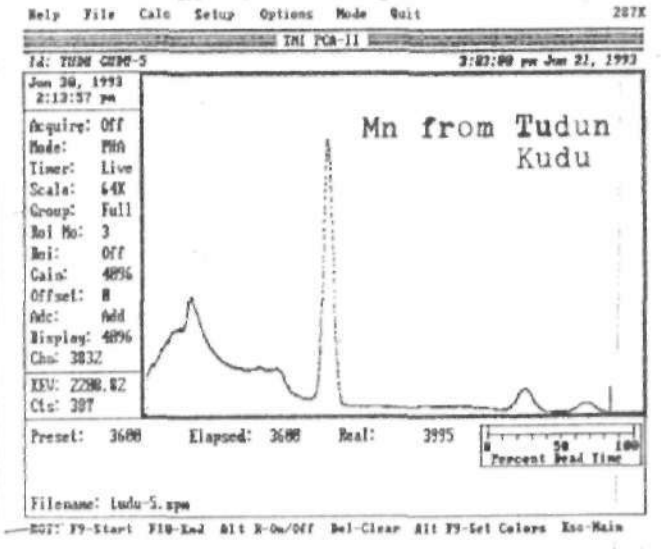






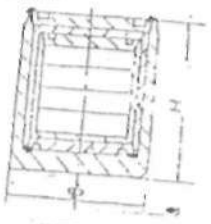






Specification
of Am-241/Be Neutron Source
I. A. E. of China

1. Serial number: AD-88/2031
2. Nuclide: Am-241 Half-life 433Y
Nominal activity: 185 GBq (5Ci)
Target material: Be
Form of active zone: Compacted mixture of americium oxide with beryllium metal.
3. neutron emission: 1.29×10^7 n/s ± 10%
Measurement date: 14 April, 1988
4. Encapsulation
Outside dimension: φ30×48 (mm)
Material: Stainless steel (1Cr18Ni9Ti)
Encapsulation: Doubly encapsulated in stainless steel sealed by argon arc welding (See Figure)
5. Quality Control:
Classification ISO 2919/C56535
Wipe test A
Bubble test B
Immersion test L
6. Transportation container:
U. S. A /DOE/3HU
Refrence No: BGRNLE-099/GN-710
7. Attention:
The source is strictly forbidden to be opened. If there is any qustion,please contact with I. A. E of China



放射性物品安全运输证明书
Certificate of Radioactive Package Type

位名称 ationtype	镅一铍中子源 Am-Be neutron Sources	强度（活度） Activity	1.29×10⁷ (中子/秒) (n/sec)
态 ate	固体 液体 气体 Solid, Liquid, Gas		
射线类型 diation Type	γ射线、中子 γ-ray, neutron		
剂量率 ose Rate	货包表面剂量 On the Surface of Package	2.5mrem/h	
	距一米处剂量 At the Distance of 1 Meter		
编号 mber			
型 of Package	I	型 号 Type of Packaging	II

此产品经辐射安全检验合格，符合国际原子能机构1984年修订的《放射性物质安全运输规程》有关要求。

These packages have been checked for its radiation safety according to " Regulations for the Safe Transport of Radioactive Materials " revised by IAEA in 1984. It meets all requirements.

检查机关（盖章）
Inspection Institution:

检查人员 Gan Li Jun
Signature

签发日期 1989.3.18
Date

Fig. Ap 8 The Manufacturers Specification for the 5Ci Am-Be Neutron Source.